



*2017-2018 Undergraduate Team Engine*

*Candidate Engines for a Next Generation Supersonic Transport*



*ETU – V TULPAR*



TEAM MEMBERS

Veli Can ÜSTÜNDAĞ - 921399

Çağdaş Cem ERGİN - 920976







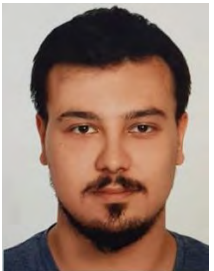



Baran İPER - 921398

Onur TAN - 921395

Faculty Advisor

Asst. Prof. Sıtkı USLU

## SIGNATURES

	<p><b>Faculty Advisor</b> Asst. Prof. Sıtkı USLU TOBB University of Economics and Technology</p>	
	<p><b>Team Leader</b> Cagdas Cem ERGIN TOBB University of Economics and Technology Department of Mechanical Engineering AIAA Member Number: 920976</p>	
	<p><b>Team Member</b> Veli Can USTUNDAG TOBB University of Economics and Technology Department of Mechanical Engineering AIAA Member Number: 921399</p>	
	<p><b>Team Member</b> Baran IPER TOBB University of Economics and Technology Department of Mechanical Engineering AIAA Member Number: 921398</p>	
	<p><b>Team Member</b> Onur TAN TOBB University of Economics and Technology Department of Mechanical Engineering AIAA Member Number: 921395</p>	

## TABLE OF CONTENT

LIST OF TABLES .....	v
LIST OF FIGURES .....	vi
NOMENCLATURE.....	ix
1. INTRODUCTION.....	1
2. STATE OF THE ART.....	2
3. DESIGN OF THE ENGINE.....	3
3.1. ENGINE CYCLE ANALYSIS AND DESIGN.....	3
3.1.1. Baseline Engine Validation and Cycle Analysis .....	3
3.1.1.1. On-Desing Analysis of Baseline Engine .....	3
3.1.1.2. Off-Desing Analysis of Baseline Engine .....	4
3.1.2. Alternatives Engine Cycle and New Concept Designs for ETU-V TULPAR.....	5
3.1.2.1. Engine Spool Selection .....	5
3.1.2.2. Variable Bypass Technology.....	6
3.1.2.3. Afterburner Investigation .....	7
3.1.2.4. Nozzle Concept .....	8
3.1.3. Engine Compenents and Diagram of ETU-V TULPAR.....	9
3.1.4. Cycle Analysis and Optimization of the New Engine TULPAR.....	10
3.1.4.1. Design Analysis of the TULPAR .....	10
3.1.4.2. Off-Design Analysis of the TULPAR .....	11
3.1.5. Comparison between TULPAR and Baseline Engine .....	12
4. DETAILED DESIGN OF THE COMPONENTS.....	14
4.1. SUPERSONIC INLET (SUPIN) DESIGN.....	14
4.2. DETAILED TURBOMACHINERY DESIGN (AXIAL FAN - HPC).....	18
4.2.1. Compressor Design.....	18
4.2.1.1. Guidelines of Compressor Design Parameters .....	19
4.2.2. Fan (LPC) Design.....	20
4.2.3. Axial High Pressure Compressor Design .....	27
4.3. COMBUSTION CHAMBER .....	31
4.4. DETAILED TURBOMACHINERY DESIGN (HPT - LPT).....	36
4.4.1. Axial High-Pressure Turbine Design.....	37
4.4.2. Axial Low-Pressure Turbine Design .....	43
4.5. STRESS CALCULATIONS FOR TURBOMACHINERY BLADES .....	46
4.6. NOZZLE GUIDE VANE COOLING.....	47
4.7. MIXER DESIGN .....	51
4.8. FULLY VARIABLE AREA NOZZLE .....	53
4.8.1. Nozzle Type Selection.....	53
4.8.2. Nozzle Geometry Calculations .....	54
4.8.3. Analysis and Configurations.....	55
4.9. THRUST REVERSERS .....	56

4.10.	SHAFT DESIGN .....	59
5.	EMISSIONS.....	62
5.1.	Rich Quick Quench Lean (RQL) Technology .....	62
5.2.	Emission Standards .....	63
6.	ENGINE SUBSYSTEMS .....	64
6.1.	Lubrication Systems.....	64
6.2.	Engine Starter.....	66
6.3.	Anti-Icing System .....	67
6.4.	Fire Detection and Extinguishing System.....	67
6.5.	Cooling and Ventilation Systems.....	68
7.	MATERIAL SELECTION.....	68
7.1.	Inlet Materials .....	69
7.2.	Fan (LPC) Materials .....	70
7.3.	HP Compressor Materials .....	70
7.4.	Combustion Chamber Materials .....	71
7.5.	Turbine Materials.....	71
7.6.	Mixer-Nozzle Materials .....	73
7.7.	Shaft Materials .....	73
8.	CONCLUSION .....	74
	REFERENCES.....	75

## LIST OF TABLES

Table 1: General Aircraft Technical Specifications [2] .....	1
Table 2: General Aircraft Performance Specifications [2] .....	1
Table 3: Design Features of the Baseline Engine [2] .....	1
Table 4: Installed Engine Requirements [2] .....	2
Table 5: Similar Engine Specifications .....	2
Table 6: Under Development Engines and Concorde Specifications [3] .....	3
Table 7: Comparison of GasTurb and NPSS Results .....	4
Table 8: Baseline Engine Performance at Off-Design Points .....	5
Table 9: Comparison of 2-Spool and 3-Spool Engine Performance .....	6
Table 10: Fuel Consumption at Different Bypass Ratio .....	7
Table 11: Comparison between using Afterburner and without using Afterburner for Hot Day Take-off Condition .....	8
Table 12: Stations of ETU-V TULPAR .....	9
Table 13: Comparison of Baseline and TULPAR Engine Design Parameters .....	11
Table 14: TULPAR Engine Performance at Off-Design Points .....	12
Table 15: Comparison of Performance Results .....	13
Table 16: Engine Size and Weight for Baseline and TULPAR Engines .....	13
Table 17: Supersonic Inlet MATLAB Input Values [17-18-19] .....	15
Table 18: Supersonic Inlet –Design Point Conditions .....	15
Table 19: TULPAR Supersonic Inlet Result Comparison .....	16
Table 20: Supersonic Inlet – Mach number results on design point .....	16
Table 21: Supersonic Inlet – Oblique shock and ramp angle results on design point .....	16
Table 22: Supersonic Inlet – Geometrical results on design point .....	16
Table 23: Supersonic Inlet – Total pressure recovery results on design point .....	17
Table 24: Comparison between the axial and centrifugal compressor [7] .....	19
Table 25: Range and typical values of each design parameters for compression systems [5] .....	19
Table 26: Thermodynamic Properties and Geometrical Dimensions obtained from GasTurb .....	20
Table 27: Fan Preliminary Design Properties .....	21
Table 28: Detail Design Parameters of Axial Fan .....	26
Table 29: Preliminary Design Properties .....	27
Table 30: Detail Design Parameters of HPC .....	29
Table 31: Combustion Chamber Design Parameter Assumptions [23-26-27-28] .....	33
Table 32: Combustion Chamber Design Assumptions .....	33
Table 33: Combustion chamber on design conditions .....	34
Table 34: Combustion Chamber - Geometrical results on-design point .....	34
Table 35: Combustion Chamber performance results on-design point .....	35
Table 36: Combustion Chamber flame tube hole results .....	35
Table 37: Range of axial flow turbine design parameters for HPT [4] .....	36
Table 38: Range of axial flow turbine design parameters for LPT [4] .....	37

Table 39: Preliminary Design Properties .....	37
Table 40: Detailed Design Parameters of HPT .....	42
Table 41: Preliminary Design Properties .....	43
Table 42: Detailed Design Parameters of LPT.....	45
Table 43: Blade Structural Analysis of 1 <sup>st</sup> Stage Rotor in LPC (Fan) .....	46
Table 44: Blade Structural Analysis of 1 <sup>st</sup> Stage Rotor in HPC .....	46
Table 45: Blade Structural Analysis of Last Stage Rotor in HPT .....	47
Table 46: Blade Structural Analysis of Last Stage Rotor in LPT.....	47
Table 47: Cooling hole parameters for the suction and pressure side cooling rows. [36].....	51
Table 48: Geometric dimensions of the designed mixer .....	52
Table 49: Nozzle on design condition (Inputs and Outputs).....	54
Table 50: Input Parameters of Each Mission Profile.....	55
Table 51: Calculated Nozzle Parameters for Mission Profiles.....	55
Table 52: Geometric dimensions for each mission profile.....	56
Table 53: The material properties of Super CMV [56-57].....	60
Table 54: Input values of MATLAB Code for each shaft.....	61
Table 55: The MATLAB critical speed results for each shaft .....	61
Table 56: LTO Cycle for supersonic engines and comparison between TULPAR engine NOx emission and emission standarts [2].....	63
Table 57: The typical characteristics of BP Turbo Oil 2197 [71] .....	66
Table 58: Inlet Material Mechanical Properties [80] .....	69
Table 59: Fan Coating Material Mechanical Properties [81-82].....	70
Table 60: Compressor Material Mechanical Properties [83-84].....	70
Table 61: Combustion Chamber Materials Mechanical Properties [89-90].....	71
Table 62: Frequently used nozzle materials by GE, P&W, RR [77].....	73
Table 63: Selected materials for designed components .....	73

## LIST OF FIGURES

Figure 1: Typical Turbofan Engine Components [1] .....	1
Figure 2: Baseline Engine Performance at Cruise Condition.....	4
Figure 3: The bypass flap design which is used in the SR-71 [12] .....	7
Figure 4: Overall Engine Configuration of ETU-V TULPAR.....	9
Figure 5: TULPAR Engine Optimized Performance at Cruise Condition .....	11
Figure 6: Inlet Recovery Factor [2].....	12
Figure 7: The sketch of the whole mixed compression inlet system [16].....	15
Figure 8: Supersonic Inlet – Pressure recovery standarts for different mach number [8] .....	16
Figure 9: Supersonic Inlet – 3D geometry of intake system in CAD.....	17
Figure 10: Supersonic Inlet – Cross sectional area of intake system in CAD.....	17
Figure 11: Development of Pressure Ratio [21].....	20
Figure 12: Polytropic Efficiency as a function of Work and Flow Coefficients .....	21

Figure 13: Preliminary Design of Fan Rotor and Stator.....	21
Figure 14: Velocity Triangles of The First Stage from Hub Section .....	22
Figure 15: Velocity Triangles of The First Stage from Mean Section .....	22
Figure 16: Velocity Triangles of The First Stage from Tip Section.....	23
Figure 17: Total Pressure Variation throughout the Axial Fan .....	23
Figure 18: Total Temperature Variation throughout the Axial Fan .....	24
Figure 19: Relative Mach Number Distribution at Tip Section of the First Rotor Blade.....	24
Figure 20: Rotor (left) and Stator (right) Blade Profiles .....	25
Figure 21: Rotor (left) and Stator (right) Design of The First Stage .....	25
Figure 22: Side view and whole 3D desing of Axial Fan.....	25
Figure 23: LPC Characteristics Map .....	26
Figure 24: Velocity Triangles of The First Stage from Hub Section .....	28
Figure 25: Velocity Triangles of The First Stage from Mean Section .....	28
Figure 26: Velocity Triangles of The First Stage fromTip Section.....	28
Figure 27: HPC Characteristics Map .....	30
Figure 28: Rotor (left) and Stator (right) Design of The First Stage .....	30
Figure 29: 3D Design of the First 5-Stages of the Compressor.....	30
Figure 30: Main components and geometry of annular combustion chamber [23].....	31
Figure 31: Airblast atomizer which has same direction flow ducts [28].....	31
Figure 32: Liner cooling technologies [4] .....	32
Figure 33: Air flow through the liner hole [23].....	33
Figure 34: 3D model of combustor chamber, front view (left) and back view (right) .....	35
Figure 35: Primary swirler (left), whole swirler (middle), secondary swirler (right).....	36
Figure 36: A cross-sectional view of the combustion chamber.....	36
Figure 37: Preliminary Design of HPT Rotor and Stator .....	37
Figure 38: Velocity Triangles of The First Stage from Hub Section .....	38
Figure 39: Velocity Triangles of The First Stage from Mean Section .....	38
Figure 40: Velocity Triangles of The First Stage from Tip Section.....	39
Figure 41: Stator Blade Mach Number Distribution .....	39
Figure 42: Stator Blade Total Pressure Distribution .....	40
Figure 43: Rotor Blade Mach Number Distribution.....	40
Figure 44: Rotor Blade Total Pressure Distribution.....	40
Figure 45: Rotor (right) and Stator (leftt) Design of The Last Stage .....	41
Figure 46: 3D Design of the HPT .....	41
Figure 47: Smith Chart for Turbine Efficiency .....	42
Figure 48: Velocity Triangles of The First Stage from Hub Section .....	43
Figure 49: Velocity Triangles of The First Stage from Mean Section .....	44
Figure 50: Velocity Triangles of The First Stage from Tip Section.....	44
Figure 51: Rotor (right) and Stator (leftt) Design of The Last Stage .....	45
Figure 52: 3D Design of the LPT .....	45

Figure 53: Schematic of air-cooled turbine [30] .....	47
Figure 54: Turbine cooling methods a) convection cooling, b) impingement cooling, c) film cooling, d) full-coverage film cooling, e) transpiration cooling [30] .....	48
Figure 55: Relevant cooling systems for ranges of turbine inlet temperatures [5] .....	49
Figure 56: The material improvements and cooling effects of film cooling and TBC [34] .....	50
Figure 57: The types of shaped film holes [37] .....	50
Figure 58: The nozzle guide vane geometry [36] .....	51
Figure 59: Schematic representation of geometrical dimensions [38] .....	52
Figure 60: 3D model of the mixer .....	52
Figure 61: Cross sectional view of the mixer .....	53
Figure 62: Schematic representation of the opening and closing mechanism of nozzle [44] .....	54
Figure 63: Geometric Parameters of the Nozzle .....	56
Figure 64: 3D model of the cruise condition convergent-divergent nozzle .....	56
Figure 65: Comparative landing runs with and without thrust reversers [47] .....	57
Figure 66: Bucket target type thrust reverser system using deflector doors [48] .....	58
Figure 67: Thrust reverser control volume [49] .....	58
Figure 68: Shaft structure and bearing locations (two spool) [52] .....	60
Figure 69: 3D model of HP Spool and LP Spool shafts .....	62
Figure 70: RQL Combustor Sections [59] .....	62
Figure 71: The typical dry-sump lubrication system [70] .....	65
Figure 72: The typical lubrication system for an engine with three bearing compartments [46] .....	65
Figure 73: Pneumatic System Architecture [72] .....	66
Figure 74: Hot air anti-icing system [73] .....	67
Figure 75: Fire Extinguishing System [74] .....	68
Figure 76: Common materials used in engine structure [77] .....	69
Figure 77: Cyclic Oxidation Tests (left) and Results of Hot-Corrosion Tests (right) .....	72
Figure 78: Comparisons among alloys in terms of a combination of creep and oxidation [46] .....	72



## NOMENCLATURE

AC	: Inlet Capture Area	MFP	: Mass Flow Parameter
ALR	: Air-Liquid ratio	NACA	: National Advisory Committee for Aeronautics
AIA	: Aircraft Industries Association	NGV	: Nozzle Guide Vane
APU	: Auxiliary Power Unit	NOx	: Nitric Oxides
AR	: Aspect Ratio	OPR	: Overall Pressure Ratio
BPR	: By-Pass Ratio	PR	: Pressure Recovery
CAD	: Computer-Aided Design	PF	: Pattern Factor
CC	: Combustion Chamber	PM	: Powder Metallurgy
CD	: Convergent - Divergent	RES	: Residence Time
CFD	: Computational Fluid Dynamics	RFP	: Request for Proposal
CFRP	: Carbon Fiber Reinforced Polymer	RPM	: Revolutions per Minute
CRV	: Central Recirculation Vortex	RQL	: Rich-Burn Quick-Quench Lean-Burn
CMC	: Ceramic Matrix Composite	SLS	: Sea Level Static
CMV	: Chrome Molybdenum Vanadium	SN	: Swirl Number
CO	: Carbon Monoxide	SUPIN	: Supersonic Inlet
D	: D Factor	TBC	: Thermal Barrier Coating
DI	: Direct Injection	TET	: Turbine Entry Temperature
DC	: Discharge coefficient	TO	: Take-Off
DCA	: Double Circular Arc	TPR	: Total Pressure Recovery
EEC	: Electronic Engine Controller	TSFC	: Thrust Specific Fuel Consumption
EI	: Emission Index	UHC	: Unburned Hydrocarbons
ER	: Equivalence Ratio	YSZ	: Yttrium-Stabilized Zirconium
ES	: Emission Standart		
FAR	: Fuel-Air Ratio		
FOD	: Foreign Object Damage		
FPR	: Fan Pressure Ratio		
FRP	: Fiber Reinforced Polymer		
GE	: General Electric		
HPC	: High Pressure Compressor		
HPT	: High Pressure Turbine		
HTS	: High Thermal Stability		
IGV	: Inlet Guide Vane		
IPC	: Intermediate Pressure Compressor		
IPT	: Intermediate Pressure Turbine		
LA	: Liquid atomization		
LHV	: Lower heating value		
LPC	: Low Pressure Compressor		
LPP	: Lean-Premixed-Prevaporized Combuster		
LPT	: Low Pressure Turbine		

# 1. INTRODUCTION

AIAA Undergraduate Team Engine Design Competition 2017/18 Project “Candidate Engines for a Next Generation Supersonic Transport” is about designing a new turbofan engine that is developed version of a base engine given in the RFP. The new engine design is required to carry 100-passenger at supersonic speed, with and entry-into-service date of 2025. The turbofan engine components are shown in Figure 1.

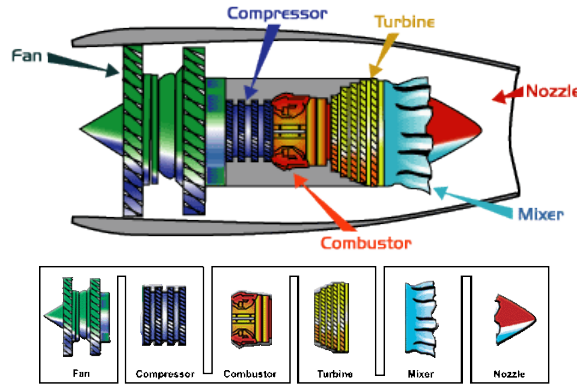


Figure 1: Typical Turbofan Engine Components [1]

The general characteristics of aircraft (Technical and Performance Specifications) that will carry 100 passengers in 2025 are given in the Table 1 and Table 2 below, respectively.

Table 1: General Aircraft Technical Specifications [2]

Technical Specifications	
Max. take-off weight	317,499 lb
Payload weight	21,000 lb
Operating empty weight	146,420 lb
Wing loading (takeoff)	77.5 psf
Power plant	2 × mixed-flow turbofans; 61,000 lbf each @ SLS

Table 2: General Aircraft Performance Specifications [2]

Performance Specifications	
Maximum speed	Mach 1.8 at 55,000 feet
Cruise speed	Mach 1.6 at 50,000-55,000 feet
Range	4000 nmi
Cruise L/D	9.2

The base engine specifications that is given in Table 3 could be used as a starting point and the engine weight and fuel consumption should be minimized in the new engine design.

Table 3: Design Features of the Baseline Engine [2]

Design Features	Specifications
Engine Type	Mixed-flow turbofan
FPR	2.25
OPR @max. Power	35.0
BPR @max. Power	1.71
Maximum net thrust @sea level	69,600 lbf
SFC @max. Power	0.51 lbm/hr/lbf
Fan diameter	89 inches
Number of fan stages	2
Number of compressor stages	11
Number of HP turbine stages	2
Number of LP turbine stages	4

When designing the new engine, the best combination of design parameters such as OPR, BPR, FPR and TET should be determined.

The baseline engine is a 2-spool mixed-flow turbofan, its fan diameter is 89 inches and the bare engine weight, excluding the inlet, is estimated to be 13,000 pounds. The future flight envelope ranges from take-off at static sea-level conditions to supersonic cruise at up to 55,000 feet/Mach 1.8. It is hoped that the range might be extended by reducing the thrust specific fuel consumption and minimizing engine mass. In addition, the thrust specific fuel consumption (TSFC) at each condition should be improved at least %5 lower than the values shown in the Table 4.

Table 4: Installed Engine Requirements [2]

Flight Condition	Altitude (ft) & Mach Number	Thrust (lbf)	TSFC (lbm/lbf.hr)
SLS	0 feet & Mach 0	64,625	0.520
Hot Day Take-off	0 feet & Mach 0.25 (+27°F dTamb)	56,570	0.652
Transonic Pinch	40550 feet & Mach 1.129	14,278	0.950
Supersonic Cruise	52500 feet & Mach 1,6	14,685	1.091

## 2. STATE OF THE ART

Extensive literature search was done before the starting of the new design to see what was done so far and to benefit from the experiences. Approximately, 80 turbofan engines are listed according to their characteristics such as thrust, OPR, BPR and engine weight. The all (more than 60) turbofan engines which are evaluated are given in Appendix B. The engines with low bypass ratio and close to desired thrust are listed in the Table 5 below.

Table 5: Similar Engine Specifications

Engine	Number of Spool	Maximum Thrust	SFC	BPR	OPR	TET	Weight	Lenght	Diameter
Kuznetsov NK-321	3 Spool	Take-off (wet): 55,077 lbf	Subsonic: 1.58 lb/hr	1.4	28.4	1630K	3,442 kg	5,994 mm	1,461 mm
		Supersonic Cruise (dry): 31,000 lbf	Supersonic: 3.75 lb/hr			2934 R	7,588 lb	236 in	57.5 in
NK-144	2 Spool	Take-off (wet): 38,580 lbf	Supersonic: 4.92 lb/hr	0.6	14.2	-	-	5,200 mm	1,500 mm
		Supersonic Cruise (dry): 28660 lbf				-	-	204.72 in	59.05 in
NK-144-22	2 Spool	Take-off (wet): 40,000 lbf	Subsonic: 2.03 lb/hr	0.53	14.2	-	-	5,200 mm	1,500 mm
		Supersonic Cruise (dry): 33,070 lbf	Supersonic: 4 lb/hr			-	-	204.72 in	59.05 in
Pratt & Whitney F135	2 Spool	Take-off (wet): 43,000 lbf	Wet: 2.0 lb/lbf/hr	0.57	28	-	-	5,590 mm	1,170 mm
		Supersonic Cruise(dry): 28,000 lbf	Dry: 0.7 lb/lbf/hr			-	-	220 in	46 in

In addition, supersonic aircrafts are carried out and evaluated separately. According to literature surveys, the aircrafts and their specifications are taken as a guideline during the engine design process.

In Table 6, specifications of Concorde, one of the first supersonic transportation aircraft, and under-development supersonic aircrafts are shown.

Table 6: Under Development Engines and Concorde Specifications [3]

<b>Model</b>	<b>Passengers</b>	<b>Cruise</b>	<b>Range</b>	<b>MTOW</b>	<b>Total Thrust</b>	<b>Thrust / Weight</b>
Concorde	120	Mach 2.02	3900 nmi	408000 lb	152000 lbf	0.37
Boom Technology	55	Mach 2.2	4500 nmi	17000 lb	45000-60000 lbf	0.26-0.35
Aerion AS2	12	Mach1.5	4500 nmi	120000 lb	45000 -51000 lbf	0.38-0.43
Spike S-512	18	Mach 1.6	6200 nmi	115000 lb	26500 lbf	0.35

The ETU-V TULPAR engine, which has been designed with literature researches and baseline motor developments, is described in full details with this report.

### **3. DESIGN OF THE ENGINE**

#### **3.1. ENGINE CYCLE ANALYSIS AND DESIGN**

This section includes baseline engine validation which is the first step of new engine design, selection of the optimum engine cycle, concept design and technologies that can be used in the new design, and also thermodynamic analysis and optimization of the ETU-V TULPAR. As stated in the project, a good literature review was carried out and the technological developments to be realized until 2025 have been taken into consideration for the design. As a result of the review, the best combination of cost, reliability and feasibility concepts has been chosen and new engine, “TULPAR”, has been designed in accordance with performance requirements and geometrical constraints. Validation of baseline engine and new engine optimization were performed using gas turbine simulation software GasTurb [2].

##### **3.1.1. Baseline Engine Validation and Cycle Analysis**

As a first step in the project, it is very important to be able to replicate the baseline engine performance results for validation purpose. The baseline engine was used as a starting point for TULPAR engine. In this section, design and off design cycle analysis of the baseline engine are performed by GasTurb 13.

###### **3.1.1.1. On-Desing Analysis of Baseline Engine**

As stated in the RFP (Request for Proposal), in engine with supersonic capabilities, the cruise is taken as a design point. For this reason, 1.6 Mach and 52500ft altitude cruise conditions of the baseline engine are specified as a design point. In Figure 2, the analysis results of the baseline engine at cruise condition obtained using the GasTurb are given in detail.

Performance analysis of the base engine at cruise condition in RFP was created by using NPSS software. The baseline engine output given in RFP is well validated by the results obtained from GasTurb calculations.

Station	W lb/s	T R	P psia	WRstd lb/s	FN	=	14684,73 lb
amb		389,97	1,492				
1	616,060	589,81	6,343		TSFC	=	1,0929 lb/(lb*h)
2	616,060	589,81	5,993	1610,933	WF Burner	=	4,45801 lb/s
13	404,385	763,65	13,639	528,716	s NOX	=	1,9921
21	211,675	769,97	13,503	280,700	BPR	=	1,9104
25	211,675	769,97	13,503	280,700	Core Eff	=	0,6057
3	207,706	1780,45	220,612	25,635	Prop Eff	=	0,8034
31	169,340	1780,45	220,612		P3/P2	=	36,811
4	173,798	3273,60	211,891	30,283	NGV	=	2 Stage HPT
40	173,798	3273,60	211,891		P16/P6	=	1,00650
41	190,732	3151,03	211,891	32,605	A63	=	3266,63 in <sup>2</sup>
43	190,732	2199,79	36,490		A163	=	3800,40 in <sup>2</sup>
44	208,725	2165,69	36,490		A64	=	7067,03 in <sup>2</sup>
45	212,164	2159,80	36,490	174,362	XM63	=	0,24476
49	212,164	1726,72	13,003		XM163	=	0,25783
5	214,017	1723,15	13,003	440,877	XM64	=	0,25990
6	214,017	1723,15	12,873		P63/P6	=	0,99890
16	404,385	763,65	12,956		P163/P16	=	0,99890
64	618,401	1114,91	12,871		A8	=	3151,77 in <sup>2</sup>
8	618,401	1114,91	12,871	1035,218	CD8	=	0,96300
Bleed	2,117	1290,22	70,555		Ang8	=	18,50 °
Efficiencies:	isen	poly	RNI	P/P	P8/Pamb	=	8,62896
Outer LPC	0,8923	0,9039	0,350	2,276	WLkBy/w25	=	0,00000
Inner LPC	0,8490	0,8650	0,350	2,253	WCHN/w25	=	0,08000
HP Compressor	0,8533	0,8957	0,574	16,338	WCHR/w25	=	0,08500
Burner	0,9970			0,960	Loading	=	100,00 %
HP Turbine	0,9138	0,8960	1,755	5,807	WCLN/w25	=	0,01625
LP Turbine	0,9121	0,9014	0,467	2,806	WCLR/w25	=	0,00875
Mixer	0,9900				WBHD/w21	=	0,00000
HP Spool mech Eff	0,9987	Nom Spd	6358 rpm		far7	=	0,00726
LP Spool mech Eff	1,0000	Nom Spd	6361 rpm		WBLD/w25	=	0,01000
P2/P1=	0,9448	P25/P21=	1,0000	P45/P44=	PWX	=	100,0 hp
Con-Di Nozzle:					P16/P13	=	0,9500
A9*(Ps9-Pamb)	564,233				P6/P5	=	0,9900
hum [%]	0,0	war0	FHV	Fuel	A9/A8	=	1,72316
	0,00000	18400,0	Generic		CFG1d	=	0,92493

Figure 2: Baseline Engine Performance at Cruise Condition

In Table 7, the comparison of the baseline engine performance results given in RFP and the results obtained from GasTurb at cruise condition are given.

Table 7: Comparison of GasTurb and NPSS Results

Design Parameters	Baseline Engine Results given in RFP by NPSS	Baseline Engine Results obtained by GasTurb
Installed Thrust (Fn)	14684.7 lbf	14684.73 lbf
TSFC	1.0914 lbm/(lb.f.h)	1.0929 lbm/(lb.f.h)
Total Mass Flow Rate	616.06 lbm/s	616.06 lbm/s
TET	3273.6 °R	3273.6 °R
Overall Pressure Ratio	36.813	36.811
Fan Pressure Ratio	2.275	2.276
HPC Pressure Ratio	16.34	16.34
HPT Pressure Ratio	5.78	5.80
LPT Pressure Ratio	2.79	2.80
Nozzle Exit Mach Number	2.06	2.02
Fuel-Air Ratio	0.0262	0.0263

### 3.1.1.2. Off-Desing Analysis of Baseline Engine

Apart from the design point for the new engine, the desired thrust and fuel consumption values must also be achieved at off-design points. For this reason, performance analysis should be carried out to obtain the required performance criteria at each off-design point specified in the RFP. As given in RFP, SLS (Sea Level Static) condition, Hot Day Take-off at 0.25 Mach condition and Transonic Pinch at Mach number of 1.129 at 40550 ft altitude condition are off-design points of the baseline engine. In order to obtain the required thrust and specific fuel consumption values at each point, the turbine entry temperature (TET) is changed and also inlet pressure recovery value, which depends on the flight Mach number is determined at each point using the charts given in the RFP [2].

The key parameters of the baseline engine off-design performance are shown in Table 8. After performing the performance analysis of the off-design points and obtaining desired performance criteria such as thrust (FN) and TSFC (Thrust Specific Fuel Consumption), validation of the baseline engine is now completed.

Table 8: Baseline Engine Performance at Off-Design Points

Key Parameters	SLS (Sea Level Static)	Hot Day Take-off	Transonic Pinch
Mach Number	0	0.25	1.129
Altitude	0	0	40550
TET(T <sub>4</sub> )	2910 °R	3130 ° R	2875 °R
Inlet Recovery Factor	0.95	0.9588	0.945
Fn	65117.6 lbf	56883.7 lbf	14968 lbf
Fn <sub>Required</sub>	64625 lbf	56570 lbf	14278 lbf
TSFC	0.52 lbm/(lbf.h)	0.653 lbm/(lbf.h)	0.95lbm/(lbf.h)

### 3.1.2. Alternatives Engine Cycle and New Concept Designs for ETU-V TULPAR

Once the validation of the baseline engine is completed, design and optimization of the new engine calculations are performed. A good literature review was carried out primarily to determine alternative engine cycles and new technologies that can be used for supersonic passenger transport. The cost, reliability, feasibility and safety criteria were the most important constraints in designing the new engine. In this section, different engine cycles and innovative design concepts which are planned to be used in “TULPAR” will be introduced. Among different engine cycles and concept designs, the new design will be chosen to optimize fuel consumption and weight reduction.

#### 3.1.2.1. Engine Spool Selection

As stated in the RFP, baseline engine is low bypass, 2-spool mixed flow turbofan engine, but different engine architecture is permitted [2]. Among the alternative engine cycles, geared 2-spool, 3-spool and 2-spool mixed flow turbofan engine cycles are considered. Each engine cycle is investigated for its advantages, disadvantages, and whether it meets required performance criteria.

It is well known that 2-spool geared and 3-spool turbofan engines are more advantages than 2-spool engines for the engine start up. However, 2-spool engines have a simpler architecture, cheaper and lighter than the other two alternative engine cycles. Although 2-spool geared turbofan engines have more advantage than 2-spool turbofan engines in terms of starting up engine, it is eliminated from the alternatives because of not being efficient and suitable for the supersonic flight [8].

Today, 2-spool engines are more widely used for their simplicity reasons. However, in 2-spool engines limiting the rotation speed of the fan blade tip speed causes the low-pressure compressor and the turbine rotating slower than optimal [8]. In order to solve this problem, a 3-spool engine design is compared with 2-spool engine cycle. It is clearly seen that the 3-spool engine has a higher weight and complexity compared to the 2-spool engine. In order to sum up, 2- spool design has the following advantages compared to 3-spool engine: [8-9]

- Less Complicated
- Lighter
- Lower Manufacturing Cost
- Require Less Maintenance

During the validation, the performance results of 2-spool mixed flow turbofan engine at 1.6 Mach and 52500 ft altitude cruise condition were obtained using the GasTurb. To clearly see the difference between the 2-spool and the 3-spool engine cycles, thermodynamic analysis was performed in the GasTurb program and the results are summarized in Table 9 for 1.6 Mach number and 52500 ft altitude cruise condition.

Table 9: Comparison of 2-Spool and 3-Spool Engine Performance

Inputs		Design Parameters	2-Spool Engine	3-Spool Engine
Mach	1.6	Fn (lbf)	14684.7	14684.7
Altitude (ft)	52500	TSFC ( lbm/(lbf.h)	1.0929	1.0914
Intake PR	0.9448	W <sub>fuel</sub> (lbm/s)	4.458	4.452
Overall PR	36.81	NOx	1.9921	2.004
Bypass Ratio	1.91	W <sub>engine</sub> (lbm)	15022.9	17017.5
Mass Flow Rate (lbm/s)	616	L <sub>engine</sub> ( in)	337	351.2
TET (R)	3273.6	<b>Stage Number</b>		
Nozzle Area Ratio	1.723			
HPC PolyEff (%)	89.6	Fan = 2 stage	Fan = 2 stage	
LPT PolyEff (%)	90.14	HPC = 11 stage	IPC = 5 stage HPC = 6 stage	
HPT PolyEff (%)	89.6	HPT = 2 stage	HPT = 2 stage IPT = 2 stage	
IPC/IPT PolyEff (%)	90	LPT = 4 stage	LPT = 2 stage	

As a result of the literature researches and thermodynamic analysis performed in Gasturb, 2 spool engine cycle design is selected for TULPAR.

### 3.1.2.2. Variable Bypass Technology

Bypass ratio (BPR) is defined as the ratio of the mass flow rate in the bypass stream to mass flow rate passing through the core of the turbofan engine. In turbofan engines, there are two basic flows called as “Primary Flow” and “Secondary Flow”. The air entering to the engine is divided into two parts at the point called the “splitter” after the fan stage. The air passing through the core of the engine is called “Primary Flow” or “Hot Stream” and the air which does not enter to the core and passes through the bypass channel is called “Secondary Flow” or “Cold Stream”.

Turbofan Engines can be classified as low, medium, high bypass and ultra-high bypass according to their bypass ratio [11]. These are;

- Low-Bypass Turbofan Engine BPR < 2
- Medium-Bypass Turbofan Engine  $2 \leq \text{BPR} < 5$
- High-Bypass Turbofan Engine  $5 \leq \text{BPR} < 9$
- Ultra-High-Bypass Turbofan Engine BPR  $\geq 9$

Turbofan engines can produce higher thrust while consuming lower fuel consumption compared to turbojet engines using bypass technology. Most of the thrust is generated by bypass air. This ratio could go up to 80% for high bypass ratio engines. In addition, the speed of the air taken from the engine core is high and causes the exhaust noise. The speed of the air in the bypass channel is lower than speed of the hot gases exiting the turbine in the core. For this reason, high bypass ratio engines are preferred in commercial aviation since the increase in bypass ratio results in reduced fuel consumption and exhaust noise. Although engines with higher bypass ratios produce higher thrust, the increase in bypass ratio causes the engine size and the engine weight to increase. This causes the engine to become more complex and more expensive [12].

In the RFP, it is stated that accommodation within the existing nacelle envelope is preferred and also fan diameter to be 87.5 inches. The way to reduce fuel consumption by increasing the bypass ratio so as not to affect the engine fan size and engine weight is investigated. As a result of the investigations, the bypass flaps design used before in the SR-71 combat aircraft is found. These bypass flaps provide variable BPR for a given engine. A similar design is chosen to use in the TULPAR engine. In this design, changing the flap angle by controller when needed, some of the air passing through the core is transferred to the bypass channel by keeping the total mass flow rate which

enters to the engine constant. In this way, fuel consumption is improved by increasing bypass ratio without increasing the fan diameter and engine dimensions. In Figure 3, the bypass flap design used in the SR-71 is shown [12].

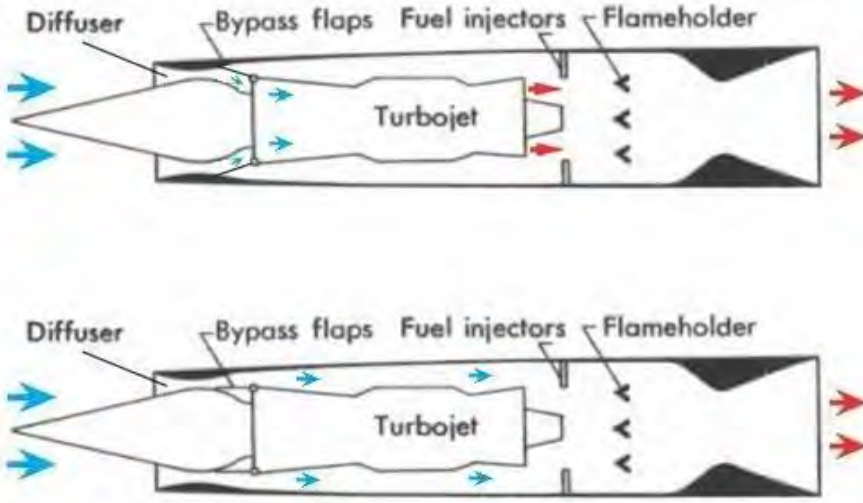


Figure 3: The bypass flap design which is used in the SR-71 [12]

In order to understand the effect of the bypass flap design on fuel consumption better, results are obtained at different bypass ratios using baseline engine data. During the analysis, the total air flow entering the engine is kept constant. Firstly, 5% of the air passing through the core is transferred to the bypass section. Then analyzes are performed for 10% and 15% respectively and the results are summarized in Table 10.

Table 10: Fuel Consumption at Different Bypass Ratio

Parameters	Condition 1 Baseline Engine	Condition 2 %5 Core to Bypass	Condition 3 %10 Core to Bypass	Condition 4 %15 Core to Bypass
BPR	1.91	2.06	2.23	2.42
Total Mass Flow Rate (lbm/s)	616.06	616.06	616.06	616.06
Cold Stream Mass Flow Rate (lbm/s)	404.37	414.95	425.56	436.14
Hot Stream Mass Flow Rate (lbm/s)	211.66	201.08	190.50	179.92
TET (R)	3273.6	3335.8	3405.2	3482.5
$W_{fuel}$ (lbm/s)	4.45	4.43	4.41	4.37
TSFC (lbm/(lbf.h))	1.095	1.089	1.085	1.081

**3.1.2.3. Afterburner Investigation**

In this project, many engine cycles and design concepts are considered before starting the new engine design and optimization. Several new designs are identified and analyzed in order to minimize fuel consumption, reduce engine weight and size which are the main goals of the project. As a result of these analyzes, the most optimum engine cycle and design concept that meet the performance criteria and the required constraints were tested. For this reason, inspired by literature studies and the Concorde aircraft used in supersonic passenger transport in the past, afterburner technology especially used for supersonic flight and take-off condition is considered to be used in TULPAR engine. The main purpose for considering to use an afterburner (AB) in TULPAR engine is to provide the required thrust by reducing the fan and engine diameters. In this case, for same thrust, it is considered that the



engine fan diameter and engine total weight will be reduced by decreasing the total mass flow entering the engine. However, since it is known that thrust specific fuel consumption will increase by using Afterburner, performance analysis on Hot Day Take-off for two different designs using afterburner and without using afterburner are performed in GasTurb to get detailed results and to make a healthier comparison. In the Table 11, comparison of these two cases are given.

Table 11: Comparison between using Afterburner and without using Afterburner for Hot Day Take-off Condition

Design Parameters	With Afterburner	Without Afterburner
Thrust (lbf)	57312.1	57312
TSFC (lbm/(lbf.h))	0.721	0.606
Total Mass Flow Rate (lbm) (lb/s)	1451.5	1538.9
Engine Fan Diameter (inches)	84.62	87.12
Engine Length (inches)	348.4	308
Engine Weight (lbm)	12889.7	13320

Compared with the results obtained from GasTurb, as expected, the use of afterburner provides some improvement in engine fan diameter and engine weight. However, the use of afterburner has a negative impact on the TULPAR engine because it causes an increase in thrust fuel consumption of close to 20 percent for the same thrust and cannot meet the required fuel consumption values, and also causes an increase in total engine length of up to 13 percent. For this reason it is decided that the use of an afterburner is not needed in the TULPAR engine.

**3.1.2.4. Nozzle Concept**

In preliminary design of the aircraft engine with supersonic conditions, it is very important to select the appropriate nozzle concept and design the nozzle that can meet the required performance criteria. Specific fuel consumption and thrust strongly depend on nozzle performance and also the nozzle which provides more thrust by increasing the speed of the exhaust gases that has an important effect on the engine performance [4].

In modern jet engines, design criteria to be considered when designing the nozzle are summarized as follows:

- Nozzle exit static pressure should be as close as possible to atmospheric pressure,
- Accelerate the flow with minimum pressure loss,
- Low cooling requirements and noise,
- Allow mixing core and bypass stream when needed,
- Low manufacturing cost,
- Allow for thrust reversing when it is necessary,
- Nozzle should be light and have simple system [4-14].

As given in the RFP, it is stated that an appropriate convergent-divergent noise-attenuating nozzle should be designed to be efficient in the supersonic cruise condition and meet the noise standards at take-off. Also, in the nozzle concept to be selected, it is tried to determine the design that best provides on-design and off-design performance conditions and minimizes the nozzle propulsion system drags. Considering all these design criteria and performance requirements, fully-variable convergent-divergent nozzle design is selected to use in TULPAR engine for optimum nozzle performance. In this configuration, using fully controlling divergent flaps provide A9 variation and thrust vector control and also this nozzle configuration performs ideal performance at all flight conditions without using Afterburner. These two factors have an important effect on the selection of the fully-variable convergent-divergent nozzle. Using this selected nozzle concept, the TULPAR engine is analyzed and optimized in GasTurb. The performance results are shown in detail in the nozzle design section.

### 3.1.3. Engine Components and Diagram of ETU-V TULPAR

ETU-V TULPAR is low bypass, 2-spool mixed flow turbofan engine. TULPAR consists of Air Intake System, 2 stage Fan, 10 stage HPC (high pressure compressor), Combuster and Fuel System, 2 stage HPT (high pressure turbine), 3 stage LPT (low pressure turbine), Mixer and Exhaust System. In addition to these systems and components, subsystems such as Lubrication System, Anti-Icing System, Auxiliary Power Unit and Starting System are designed detailed. TULPAR is designed to be used for supersonic passenger transportation. Therefore, bypass duct technology and Convergent-Divergent Nozzle (CD) which has variable nozzle area are used to obtain desired thrust and thrust specific fuel consumption. As given below, engine configuration of TULPAR is shown in the Figure 4.

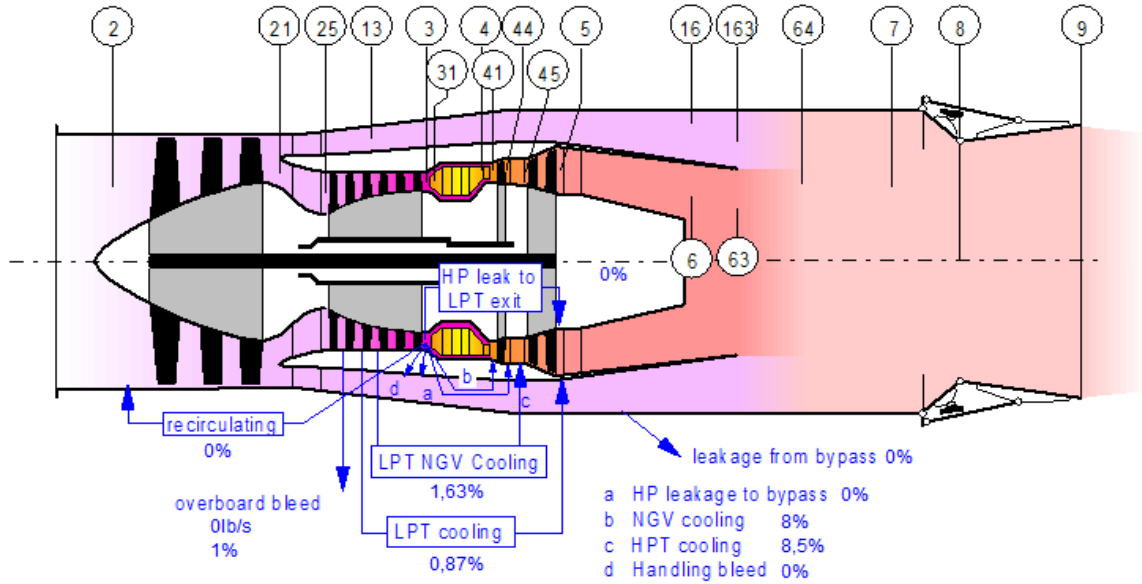


Figure 4: Overall Engine Configuration of ETU-V TULPAR

In engine configuration of TULPAR which is given in Figure 4, there are station numbers which are created automatically by GasTurb. Explanation of these numbers are given in Table 12.

Table 12: Stations of ETU-V TULPAR

Stations	Station Numbers
Fan Inlet	2
Fan Exit to Core	21
HP Compressor Inlet	25
HP Compressor Exit	3
Burner Exit	4
HP Turbine Exit	44
LP Turbine Inlet	45
LP Turbine Exit	5
Exit Guide Vane Exit	6
Bypass Inlet	13
Bypass Exit	16
Nozzle Throat	8
Nozzle Exit	9

### **3.1.4. Cycle Analysis and Optimization of the New Engine TULPAR**

Within the scope of the project, the performance data for the baseline engine was first validated for each flight condition by using GasTurb. New engine cycles and technologies were searched and concept designs were developed for the new engine design to meet desired performance criteria and to best provide the specified standards. As a result of these studies and researches, 2-spool low bypass mixed flow turbofan engine concept was determined to use in the TULPAR engine. In addition, variable bypass technology to increase the bypass ratio by using bypass flaps without significantly changing fan diameter and engine overall size and fully variable convergent-divergent nozzle to provide desired thrust at each flight condition were decided to use in TULPAR engine. After making the engine cycle selection and deciding on the concept designs to be used in the new engine, performance analysis and optimization for the TULPAR engine is now started.

As mentioned in RFP, the main purpose of the cycle analysis and optimization for the TULPAR engine is to minimize the fuel consumption at all flight conditions and increase the range of the aircraft by decreasing the engine weight and fuel consumption. In order to minimize fuel consumption, the best combination of the main design parameters which are the fan pressure ratio, overall pressure ratio, bypass ratio and turbine entry temperature are tried to be created by considering the new component design technologies, material development and advanced manufacturing techniques that can be used until 2025. For this reason, based on the entry into service date, development of new material and especially potential application of the carbon matrix composite has an important effect on determination of mechanical and thermodynamic properties for components to be used in TULPAR engine [2].

#### **3.1.4.1. Design Analysis of the TULPAR**

Generally, an engine with supersonic capabilities is designed at the beginning of the cruise (top of the climb) conditions rather than takeoff. When designing the TULPAR engine, 1.6 Mach and 52500 Altitude cruise condition is selected as on-designing point to follow this criteria.

Before the analysis is started, limit points for some design parameters are determined. Firstly, since it is known that the NO<sub>x</sub> emission increases exponentially with increasing turbine entry temperature, 3600°R (2000K) is set as the upper limit for turbine entry temperature in order to keep the NO<sub>x</sub> emission in line with the standards. Secondly, In RFP, it is specified that accommodation within the existing nacelle envelope is preferred. For this reason, corrected mass flow rate at each flight condition is tried to keep constant to not increase the fan diameter (87.5 inches) and engine size and weight. As a result of literature review, it is clearly seen that as the overall pressure ratio increases, the thrust specific fuel consumption decreases, as the turbine entry temperature increases, the produced thrust increases and the thrust specific fuel consumption decreases and also the increase in the bypass ratio has a positive effect on fuel consumption.

TULPAR engine optimization is performed using the GasTurb optimization tool. The main objective of the optimization is to determine the best combination of the 4 main design parameters which are the overall pressure ratio, bypass ratio, turbine entry temperature and fan pressure ratio so as to achieve the required thrust and meet the desired constraints. For this reason, these 4 main design parameters are selected as design variables and the upper and lower limits are set for each variable. Corrected mass flow rate to keep engine fan diameter and overall size constant and NO<sub>x</sub> emission in order to meet standards are selected as constraints. The main function is to minimize thrust specific fuel consumption. As a result of approximately 5000 cycles in GasTurb optimization, for design point of beginning of the cruise in TULPAR engine, performance results obtained by using GasTurb are summarized in the following Figure 5 and also, the comparison of the 4 main design parameters is given in the following Table 13.

Station	W lb/s	T R	P psia	WRstd lb/s	FN	= 15022,79 lb	
amb		389,97	1,492				
1	616,036	589,81	6,343		TSFC	= 0,9795 lb/(lb*h)	
2	616,036	589,81	5,993	1610,870	WF Burner	= 4,08750 lb/s	
13	432,353	763,65	13,639	565,284	s NOX	= 4,2678	
21	183,683	779,06	13,999	236,320	BPR	= 2,3538	
25	183,683	779,06	13,999	236,320	Core Eff	= 0,6249	
3	180,239	1991,11	328,984	15,775	Prop Eff	= 0,7997	
31	146,947	1991,11	328,984		P3/P2	= 54,893	
4	151,034	3535,20	315,980	18,339	NGV	2 Stage HPT	
40	151,034	3535,20	315,980		P16/P6	= 1,00901	
41	165,729	3408,77	315,980	19,760	A63	= 2909,40 in <sup>2</sup>	
43	165,729	2267,04	42,092		A163	= 4025,34 in <sup>2</sup>	
44	181,342	2244,47	42,092		A64	= 6934,75 in <sup>2</sup>	
45	184,327	2240,57	42,092	133,756	XM63	= 0,24002	
49	184,327	1738,50	12,971		XM163	= 0,26047	
5	185,934	1735,77	12,971	385,383	XM64	= 0,25990	
6	185,934	1735,77	12,841		P63/P6	= 0,99890	
16	432,353	763,65	12,956		P163/P16	= 0,99890	
64	618,287	1074,84	12,862	1016,978	A8	= 3094,64 in <sup>2</sup>	
8	618,287	1074,84	12,862		CD8	= 0,96300	
Bleed	1,837	1405,86	93,725		Ang8	= 18,50 °	
-----							
Efficiencies:	isent	polytr	RNI	P/P	P8/Pamb	= 8,62285	
Outer LPC	0,8923	0,9039	0,350	2,276	WLkBy/w25	= 0,00000	
Inner LPC	0,8483	0,8650	0,350	2,336	WCHN/w25	= 0,08000	
HP Compressor	0,8480	0,8957	0,587	23,500	WCHR/w25	= 0,08500	
Burner	0,9970			0,960	Loading	= 100,00 %	
HP Turbine	0,9161	0,8960	2,386	7,507	WCLN/w25	= 0,01625	
LP Turbine	0,9135	0,9014	0,516	3,245	WCLR/w25	= 0,00875	
Mixer	0,9900				WBHD/w21	= 0,00000	
-----							
HP Spool mech Eff	0,9987	Nom Spd	6358 rpm		far7	= 0,00666	
LP Spool mech Eff	1,0000	Nom Spd	6361 rpm		WBLD/w25	= 0,01000	
-----							
P2/P1=	0,9448	P25/P21=	1,0000	P45/P44=	1,0000	PWX	= 100,0 hp
Con-Di Nozzle:						P16/P13	= 0,9500
A9*(Ps9-Pamb)	717,708					P6/P5	= 0,9900
-----							
hum [%]	war0	FHV	Fuel		A9/A8	= 1,70131	
0.0	0.00000	18400.0	Generic		CFGid	= 0,95014	

Figure 5: TULPAR Engine Optimized Performance at Cruise Condition

Table 13: Comparison of Baseline and TULPAR Engine Design Parameters

Design Parameters	Baseline Engine: Supersonic Cruise	TULPAR Engine: Supersonic Cruise
Flight Mach Number	1.6	1.6
Altitude (ft)	52500	52500
TET (°R)	3273.6	3273.6
Overall Pressure Ratio	36.8	55
Fan Pressure Ratio	2.27	2.34
Bypass Ratio	1.91	2.35
Fn (lbf)	14684.7	15023.9
TSFC (lbm/lbf.h)	1.0929	0.9795

When the performance results and Table 13 are examined, it is seen that significant changes are made in the main design parameters of the TULPAR engine compared to the baseline engine. The main purpose in these changes is to obtain the lowest fuel consumption that provides the required thrust. For this reason, using GasTurb optimization tool, the best combination of the design parameters to meet the determined constraints and requirements has been established. For the turbine inlet temperature, 3600 Rankine is determined as upper limit considering the NOx emission standards. For overall pressure ratio, 50 is determined as the lower limit and 60 is determined as the upper limit considering the overall pressure ratio (OPR) values currently used in the turbofan engines.

### 3.1.4.2. Off-Design Analysis of the TULPAR

After the on-design performance analysis of TULPAR engine is completed, the desired thrust and the targeted specific fuel consumption values for each off-design point must also be achieved. For this reason, performance analysis should be performed to obtain the desired performance criteria at each off-design point specified in the RFP. Performance analysis are performed for SLS (Sea Level Static) condition, Hot Day Take-off (TO) at 0.25 Mach condition and Transonic Pinch at 1.129 Mach at 40550 ft Altitude condition respectively by using GasTurb.

For each off-design condition, the turbine entry temperature is changed and the inlet pressure recovery value is determined using the following figure which is given in RFP to reduce fuel consumption and provide the required thrust value. The Figure 6 given below shows the change in inlet recovery factor according to the flight mach number and the ratio of inlet throat area (A0) to inlet capture area (AC).

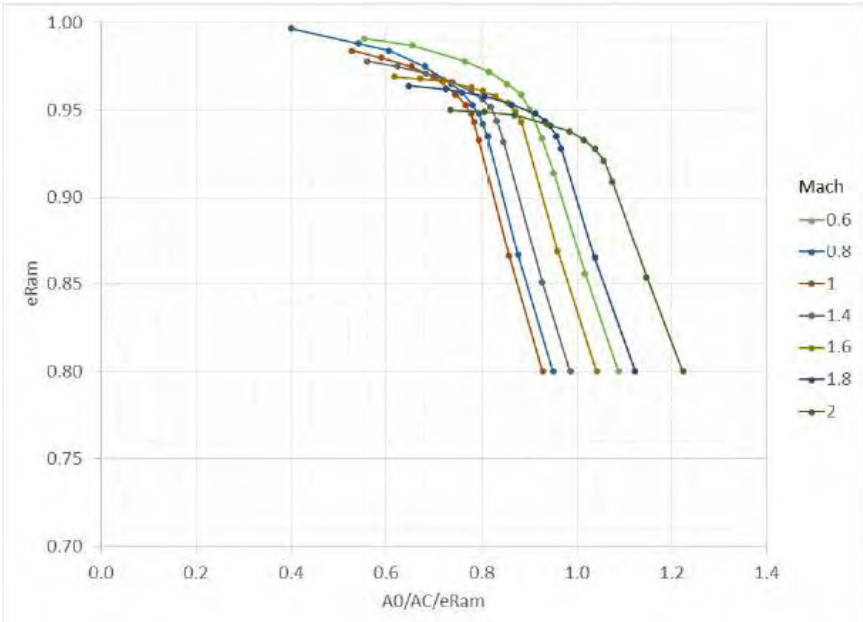


Figure 6: Inlet Recovery Factor [2]

In addition, the optimum nozzle area ( $A_9/A_8$ ) ratio for each off-design condition is calculated using the GasTurb optimization tool. An iterative process is followed for the off-design performance analysis of the TULPAR engine and nozzle area ratio ( $A_9/A_8$ ), turbine entry temperature and overall pressure ratio values are determined to best achieve the desired performance criteria and constraints as a result of this iterative process. The results of key parameters of the TULPAR, engine off-design performance are shown in Table 14.

Table 14: TULPAR Engine Performance at Off-Design Points

Key Parameters	SLS (Sea Level Static)	Hot Day Take-off	Transonic Pinch
Mach Number	0	0.25	1.129
Altitude (ft)	0	0	40550
TET( $T_4$ ) ( $^{\circ}$ R)	3139.9	3412.6	3100.1
Inlet Recovery Factor	0.95	0.9588	0.945
$A_9/A_8$	1.02	1.04	1.21
$F_n$ (lbf)	65131.65	57288.06	15062.20
TSFC (lbm/(lbf.h))	0.4778	0.6071	0.8685

The performance analysis results for off-design conditions are obtained by changing the turbine entry temperature, nozzle area ratio, entry recovery factor, flight mach number and altitude as given in Table 14. The optimal values for these design variables are determined using the GasTurb optimization tool. Compared to the baseline motor, the performance results and the improvements of TULPAR engine are given in more detail in the next section.

### 3.1.5. Comparison between TULPAR and Baseline Engine

After baseline engine validation and performance analysis and optimization for the new engine, significant improvement in fuel consumption is achieved in each flight condition in TULPAR engine compared to the baseline engine. In particular with variable bypass ratio technology, fuel consumption is reduced, and by using of fully variable convergent-divergent nozzle, the desired thrust values are provided. In addition, improvements in fuel

consumption as well as improvements in engine weight and size are provided. In the following table, thrust specific fuel consumption, thrust, fuel mass flow rate values for both the TULPAR and Baseline engine are summarized at each flight condition. The performance results for each condition are given in the comparison Table 15 of the TULPAR and Baseline Engine

When the results are examined, significant improvements are made in the fuel consumption by obtaining the desired thrust value for each condition. For Sea Level Static condition, TSFC and amount of the fuel per second consumed during the flight are improved by %8.1. For Hot Day Take-off, the amount of the fuel is decreased by %6.3, while the TSFC is improved nearly %7 and also TSFC is decreased by %8.6 and mass fuel rate is improved by %8.1 for Transonic Pinch. The greatest improvements for TSFC and the amount of fuel per second are achieved in the Supersonic Cruise Condition. In this condition, the mass fuel rate is reduced by 8.3% while the TSFC is improved by 10.3%.

Table 15: Comparison of Performance Results

Flight Condition	Design Parameters	Baseline Engine	TULPAR Engine	% Improvements
Sea Level Static	TSFC lbm/(lbf.h)	0.520	0.478	8.1
	$F_{Required}$ (lbf)	64625	65127	Provided
	$W_{fuel}$ (lbf/s)	9.39	8.64	8.0
Hot Day Take-Off	TSFC lbm/(lbf.h)	0.652	0.607	7.0
	$F_{Required}$ (lbf)	56570	57286	Provided
	$W_{fuel}$ (lbf/s)	10.32	9.65	6.5
Transonic Pinch	TSFC lbm/(lbf.h)	0.950	0.868	8.6
	$F_{Required}$ (lbf)	14278	15062	Provided
	$W_{fuel}$ (lbf/s)	3.95	3.64	7.9
Supersonic Cruise	TSFC lbm/(lbf.h)	1.0929	0.979	10.4
	$F_{Required}$ (lbf)	14685	15024	Provided
	$W_{fuel}$ (lbf/s)	4.45	4.10	7.9

In addition to improvements in the performance of the new engine, improvements in engine geometry and engine weight are also provided compared to the baseline engine as a result of optimization. All these improvements are achieved by creating the best combination of main design parameters and using new technologies for TULPAR engine.

In this process up to 2025, technological developments are considered and the TULPAR engine is designed as a result of these improvements. Comparison of the geometrical properties between TULPAR engine and Baseline engine is given in Table 16.

Table 16: Engine Size and Weight for Baseline and TULPAR Engines

Geometric Parameter	Baseline Engine	TULPAR Engine	Improvement [%]
Fan Diameter	87.5 inches	87.1 inches	0.5
Engine Length	337.13 inches	308 inches	9
Engine Weight	15023 lbf	13320 lbf	11

When the values in Table 15 and Table 16 are examined, both the performance increase and the geometric improvements are provided in the TULPAR engine compared to the baseline engine.

## 4. DETAILED DESIGN OF THE COMPONENTS

### 4.1. SUPERSONIC INLET (SUPIN) DESIGN

Depending on technological developments, increased aircraft performance levels and more demanding working conditions have increased the complexity of gas turbine engines, which has resulted in a significant increase in cost and time spent to improve engine performance. The investigation on improving engine performance begins with the appropriate inlet design. The main purpose of using inlet system is providing the proper quantity and uniformity of air to the engine face with minimum total pressure loss. The quality of the airflow (especially total pressure loss) affect the engine performance (engine thrust and the fuel consumption) significantly. Total pressure recovery is the main design parameter for inlet systems. [4]

The intake system of each aircraft must be designed according to the task profile of the aircraft, and intake design depends on many parameters. These are;

- It should provide sufficient mass flow to the engine with an appropriate mach number on the engine face,
- The design should be as light as possible and the production cost should be low,
- It should provide spatially and temporally smooth flow into the engine compressor,
- It should provide acoustic absorption of fan noise for quiet engine,
- It should integrate to fuselage well for low installation drag [5].

The performance should be assessed not only at design point but also at all flight conditions. Inlet performance is usually determined by three different parameters. These are;

- Delivered engine airflow,
- Total pressure recovery (the ratio of the total pressure of the airflow at the engine face to that of the freestream),
- Aerodynamic drag coefficient [15].

There are different inlet types for subsonic and supersonic flight conditions. Internal compression, external compression and mixed compression inlets are the types of supersonic inlets (SUPIN). Mixed Compression Inlet was selected for TULPAR depending upon RFP.

Supersonic inlets can also be classified as two-dimensional (rectangular) and axisymmetric. When axisymmetric inlets are compared to two-dimensional inlets, axisymmetric inlets are more advantageous in terms of weight and total pressure ratio. However, two-dimensional inlets have advantages in terms of achieving the necessary air flow conditions and ease of design [16].

The advantages of using two-dimensional supersonic inlet are listed below. These are;

- Presenting lower risk of surge in asymmetric flow conditions,
- Less distortion at high angle of attack,
- Better geometry variation possibilities. [10]

Besides, safety is the paramount consideration for transportation aircrafts. [16] So, two-dimensional inlet was selected for TULPAR. This inlet type was also used in Concorde, one of the first supersonic passenger transportation aircraft in the world and has been used by America as an inlet type of supersonic aircraft.

Also, the ramp number is determined as a two because it is suggested in RFP. Because high total pressure recovery can be obtained with mixed compression inlets by means of multiple ramps without thinking on a cowl wave drag penalty much. [20]

As mentioned before, 2 ramps two-dimensional mixed compression inlet system was selected. It is economical at flight Mach numbers below approximately 2.5 Mach [16]. Two external oblique shocks, one internal oblique shock and one normal shock compression system was designed. The sketch of the whole TULPAR inlet system is shown in Figure 7 [16].

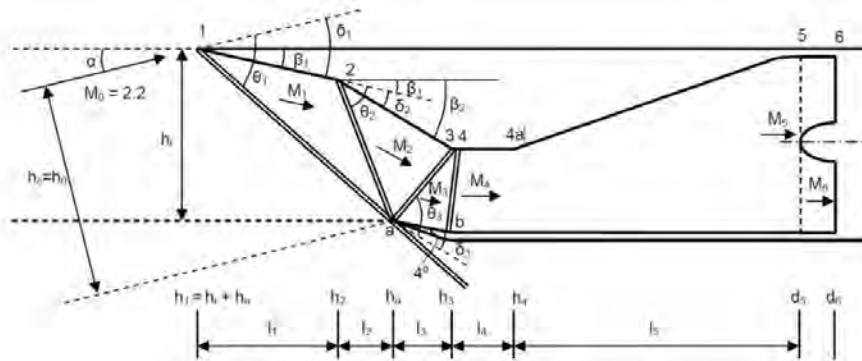


Figure 7: The sketch of the whole mixed compression inlet system [16]

As seen in Figure 7, the inlet system consists of external supersonic diffuser, throat and subsonic diffuser. In this figure,  $\theta$  and  $\delta$  symbolize the shock wave angles and ramp angles, respectively. Also, point 1, 2, 3 and 4 represent oblique or normal shocks.

Ramp angles, shock wave angles and all geometrical dimensions were calculated by using newly developed MATLAB code. In addition, temperature, pressure, density, speed and mach number values of each station were calculated separately (both static and stagnation values) in MATLAB code. This code was validated by using previous experimental results. The input variables and their values are shown in Table 17. These values are obtained from GasTurb and literature surveys.

Table 17: Supersonic Inlet MATLAB Input Values [17-18-19]

Variables	Value	Source
Hub to tip ratio ( $h/t$ )	0.33	GasTurb
Freestream mach number ( $M_0$ )	1.6 for cruise	RFP
Fan entry mach number ( $M_6$ )	0.3898	GasTurb
Face mass flow rate (Weng)	616.015 lb/s	GasTurb
Engine face diameter ( $D_{fan}$ )	87 inches	GasTurb
Up stream mach number of normal shock ( $M_{4 up}$ )	1.1	Literature Survey
Diffuser duct angle	6-12	Literature Survey
Cowl lip angle (degree)	2-5	Literature Survey
Subsonic diffuser efficiency	0.93	Literature Survey

Cruise was selected as an on-design condition. These flight condition values are calculated for cruise depending upon altitude and mach number of flight condition. The on-design conditions are shown in Table 18.

Table 18: Supersonic Inlet –Design Point Conditions

Parameters	Value
Static temperature of freestream air	390.06 R
Static pressure of freestream air	1.492 psi
Static density of freestream air	$5.9740 \times 10^{-6}$ lb/in <sup>3</sup>
Gas constant	53.3533 ft.lbf/lb.R
Specific Heat Ratio	1.3898

At the end of the calculations, it has been observed that the MATLAB results were consistent with GasTurb results. These thermodynamic results are shown in Table 19 and the percentage error values were determined for each parameter.



Table 19: TULPAR Supersonic Inlet Result Comparison

Parameters	MATLAB Value	GasTurb Value	Percentage error %
Total Pressure (psi)	6.09	6.00	1.57
Static Pressure (psi)	5.48	5.40	1.56
Total Temperature (R)	588.6	589.806	2.34
Static Temperature (R)	571.338	572.49	0.2
Velocity (ft/s)	456.36	457.05	0.15
Density (lb/in <sup>3</sup> )	1.4487 x 10 <sup>-5</sup>	1.4725 x 10 <sup>-5</sup>	1.64
Mass Flow (lb/s)	616.015	616.015	-

Moreover, Mach number results on design point, oblique shock angle and ramp angle results of intake geometry and geometrical results on design point are shown in Table 20, Table 21 and Table 22, respectively.

Table 20: Supersonic Inlet – Mach number results on design point

M0	M1	M2	M3	M4	M5	M6
1.6	1.4424	1.2771	1.1	0.9118	0.3898	0.3898

Table 21: Supersonic Inlet – Oblique shock and ramp angle results on design point

θ1	θ2	θ3	δ1	δ2	δ3
43.65°	49.97°	59.86°	4.6237°	4.6417°	4.2062°

Table 22: Supersonic Inlet – Geometrical results on design point

Geometrical Parameters	Value (inches)
First Ramp Length (L1)	27.78
Second Ramp Length (L2+L3)	120.16
Throat Length (L4)	65.43
Subsonic Diffuser Length (L5)	129.75
Throat Height (H4)	65.43
Cowl Lip Diameter (Ha)	1.9738
Engine Diameter (D5)	98.42
Engine Face Diameter (D6)	87.40
Total Intake Length (top)	342.913
Total Intake Length (bottom)	261.81

In addition, the total pressure recovery value of intake system was calculated. There are some standarts for supersonic inlet recovery. These standarts are AIA (Aircraft Industries Association) and Department of Defense (MIL-E-5008B) standarts. These standarts are classified depending upon free stream mach number and shown in Figure 8.

$$\begin{array}{lll}
 \pi_d = 1 - 0.1(M_0 - 1)^{1.5} & 1 < M_0 & \text{AIA-Standard} \\
 \pi_d = 1 - 0.075(M_0 - 1)^{1.35} & 1 < M_0 < 5 & \text{MIL-E-5008B} \\
 \pi_d = 800/(M_0^4 + 935) & 5 < M_0 & \text{MIL-E-5008B}
 \end{array}$$

Figure 8: Supersonic Inlet – Pressure recovery standarts for different mach number [8]

So, specific value of the total pressure recovery was calculated by using Equation 1. Results are shown in Table 23. It is seen that the values are close to each other. In addition to this, these values are acceptable depending upon the literature surveys. (approximately > 0.94) [4]

$$\eta_{Rspec} = 1 - 0.075(M_0 - 1)^{1.35} \quad (4.1)$$

Table 23: Supersonic Inlet – Total pressure recovery results on design point

Total pressure recovery (MATLAB)	Specific value of the total pressure recovery	Percentage error %
0.9609	0.9624	0.15

The intake geometry for on-design point conditions was prepared in Siemens NX software. The on design intake geometry is shown in Figure 9. Also, technical drawing of intake system is given in Appendix A section. Furthermore, Carbon fiber reinforced polymer was selected as a suitable material for intake system depending upon operational conditions. The selected material is described in Material Selection section in detail.

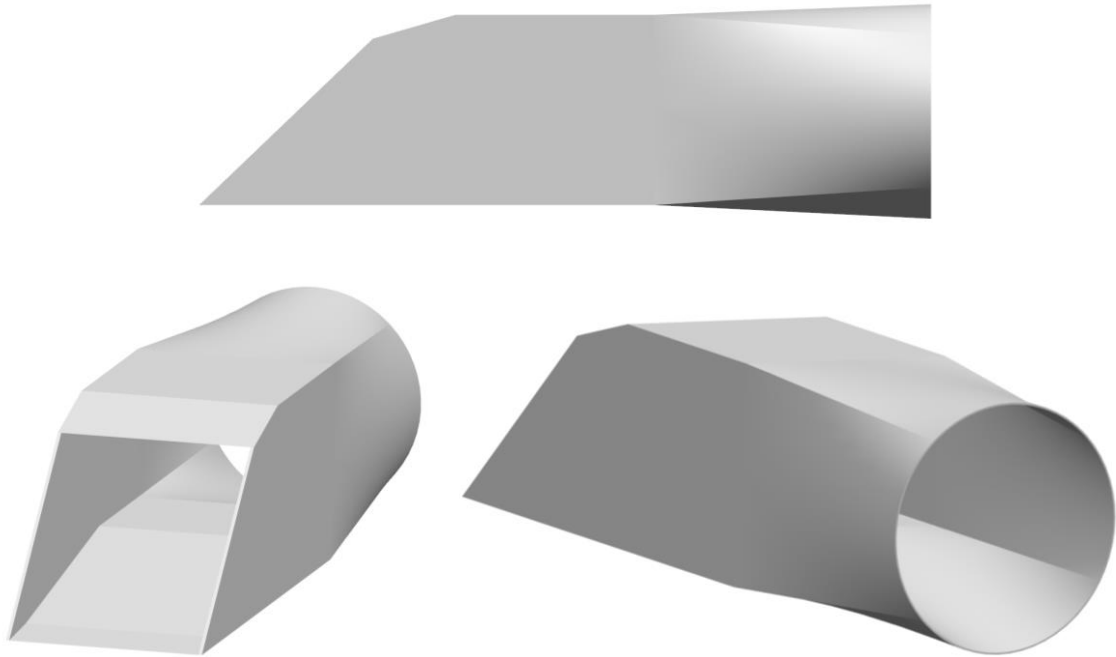


Figure 9: Supersonic Inlet – 3D geometry of intake system in CAD

Also, the cross-sectional area of intake system is shown in Figure 10 so that the cross-sectional area can be better explained.



Figure 10: Supersonic Inlet – Cross sectional area of intake system in CAD

In general, total pressure recovery at off-design points is higher when compared to on-design points. The most important thing in off-design is matching the captured mass flow with the mass flow need of the engine. There are different methods used to provide the required air flow. These are; [16]

- Adjusting second ramp angle (between 0 and on-design value),
- Opening a bypass door to dump extra air,
- Opening an auxiliary door to provide more air [16].

So, TULPAR engine has a variable ramp angle technology for off-design conditions. This type intake system is mandatory to obtain high efficiency and to provide enough amount of air to the engine face. What's more, variable ramp angle technology was used in Concorde aircraft. Also, total inlet drag value was calculated by using the equations in RFP and tables. The inlet drag value was calculated as a 2328.40 lbf for transonic pinch.

## **4.2. DETAILED TURBOMACHINERY DESIGN (AXIAL FAN - HPC)**

In this section, a detailed turbomachinery design for the optimum engine TULPAR whose thermodynamic and geometrical dimensions are determined will be explained. In detailed design, an iterative process is followed using the GasTurb and AxSTREAM Turbomachinery programs. Thermodynamic properties and geometrical constraints obtained from the GasTurb are determined as boundary conditions for the AxSTREAM calculations. 1D and 2D analyzes are carried out by using design parameters such as total pressure, temperature, mass flow rate.

In fact, each component's length and diameter are calculated by GasTurb's one dimensional calculation. But it is necessary to perform more detailed design analysis for turbomachinery with a program such as AxSTREAM. Averaged flow and work coefficients, De-Haller Number and diffusion factor which are the most important design criteria for compressor. Zweifel coefficient for turbine design, aspect ratios as blade height to chord, solidity, pitch and chord values for each stage of turbomachinery. By using 1D and 2D streamline calculation in AxSTREAM, temperature, pressure, and mach number distribution for each stage can be obtained and also 3D blade design of each stage can be created. In summary, the geometric properties of the 1D turbomachinery components obtained from the GasTurb are used as a reference for detailed design in the AxSTREAM. The detailed design properties of the turbomachinery are determined as a result of the analysis to be performed on AxSTREAM.

TULPAR is the 2-spool mixed flow turbofan engine and it consists of 2-stage Fan, 10-stage High Pressure Compressor, 2-stage High Pressure Turbine and 3-stage Low Pressure Turbine. In the RFP, it is stated that accommodation within the existing nacelle envelope is preferred and fan diameter is determined in baseline engine as 87.5 inches. In addition, the new engine weight to be designed excluding the inlet is stated to be approximately 13000 pounds. For this reason, in TULPAR engine design, it is tried to meet these geometric constraints stated in baseline engine. After the thermodynamic and geometrical dimensions determined for the TULPAR engine, the detailed design process for the turbomachinery components is started. All turbomachinery components are designed according to performance analysis results on supersonic cruise condition. Because the maximum pressures and temperatures for the turbomachinery parts are obtained at supersonic cruise condition.

### **4.2.1. Compressor Design**

This section includes detailed information about detailed design of the compressor system of the ETU-V TULPAR. Detailed information about compressor selection, preliminary design properties, the design parameters and criteria, the performance characteristics, analysis results will be explained in this part.

In gas turbine engines, air is compressed before the expansion through the turbine using two types of compressors depending on the compression of the air, desired pressure ratio and efficiency values, flow rate through the compressor and the amount of thrust to be obtained, one giving axial flow compressor and the other centrifugal flow compressor. The centrifugal flow compressor is a single or two stage unit that uses a propeller to accelerate the air and a diffuser to achieve the required pressure rise. The axial flow compressor is a multi-stage unit that includes rotor blades and stator blades to accelerate and distribute the air until a desired pressure rise is achieved [4-6]. By using a centrifugal flow compressor, higher pressure ratios per stage can be achieved. However, especially in large engines, compared to centrifugal flow compressor with the same frontal area, axial flow compressor is preferred to use. Because in axial flow compressor, more mass flow rate can be passed, higher

isotropic efficiency can be reached and higher overall pressure ratio can be obtained. In Table 24, comparison between the axial and centrifugal compressor according to flow rate, pressure ratios and efficiency is given.

Table 24: Comparison between the axial and centrifugal compressor [7]

Variables	Centrifugal Compressor	Axial Compressor
Pressure Ratio per Stage-Efficiency	$\approx 10$ – low efficiency $<5$ – high efficiency	$<1.5$ – high efficiency
Mass Flow Rate	Low	High
Overall Pressure Ratio	Moderate	High

Considering the overall pressure ratio of the new engine to be designed and the required mass flow rate, the axial compressor design is chosen as the compressor type.

The first step to start detailed engine design and optimization of the new engine is the compressor design. Designing the compressor to the most appropriate conditions and constraints is a difficult and complicated process for having more design parameters than the other gas turbine components. For this reason, an iterative process is needed to be followed, in particular using theoretical calculations based on some assumptions, to simplify the preliminary design process [4-5-7].

#### 4.2.1.1. Guidelines of Compressor Design Parameters

Guiding criteria of any compression system design parameters are listed in Table 25, which includes range and typical values of each parameters. [5] Also, in Figure 11, development of overall pressure ratio over past fifty years is shown.

Table 25: Range and typical values of each design parameters for compression systems [5]

Parameter	Range of Values	Typical Value
Flow Coefficient, $\phi$	$0.3 \leq \phi \leq 0.9$	0.6
Axial Mach Number, $M_z$	$0.3 \leq M_z \leq 0.6$	0.55
Degree of Reaction, $^\circ R$	$0.1 \leq ^\circ R \leq 0.90$	0.5 (for $M < 1$ )
D-Factor, D	$D \leq 0.6$	0.45
Tip Tangential Mach Number, $M_T$	1.0-1.5	1.3
Reynolds Number Based on chord, $Re_c$	$300,000 \leq Re_c$	$>500,000$
Stage Average Aspect Ratio, AR	$1.0 \leq AR \leq 4.0$	$< 2.0$
Stage Average Solidity, $\sigma$	$1.0 \leq \sigma \leq 2.0$	1.4
Loading Coefficient, $\psi$	$0.2 \leq \psi \leq 0.5$	0.35
Polytropic Efficiency, $e_c$	$0.85 \leq e_c \leq 0.92$	0.9
Tip Relative Mach Number (1 <sup>st</sup> Rotor), $(M_{1r})_{tip}$	$(M_{1r})_{tip} \leq 1.7$	1.3-1.5
Hub rotational speed, $\omega_{rh}$	$\omega_{rh} \leq 380$ m/s	300 m/s
Tip rotational speed, $\omega_{rt}$	$450 \leq \omega_{rt} \leq 500$ m/s	500 m/s
De Haller Criterion, $W_2 / W_1$	$W_2 / W_1 \geq 0.72$	0.75
Compressor Pressure Ratio per Spool	$\Pi_c < 20$	up to 20
Aspect Ratio, Fan	$\sim 2- 5$	$< 1.5$
Aspect Ratio, Compressor	$\sim 1- 4$	$\sim 2$
DCA Blade (Range)	$0.8 \leq M \leq 1.2$	Same
Axial Gap Between Blade Rows	$0.23c_z$ to $0.25c_z$	$0.25c_z$
NACA-65 Series (Range)	$M \leq 0.8$	Same
Taper Ratio	$\sim 0.8- 1.0$	0.8

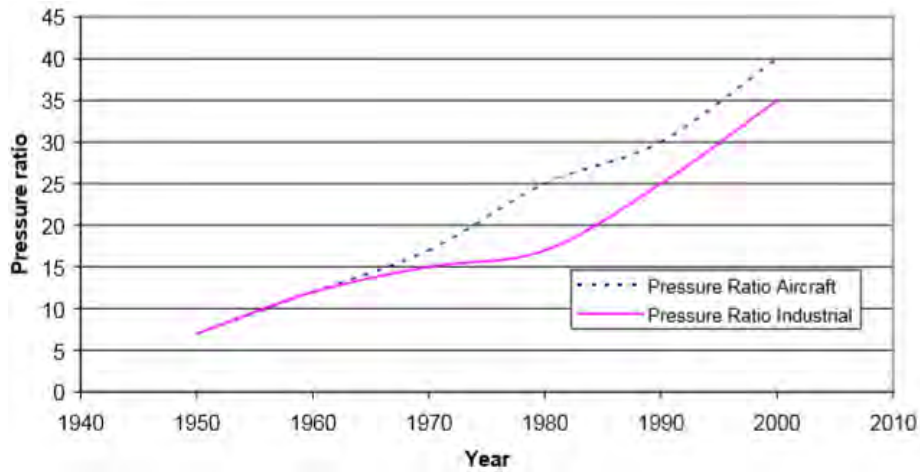


Figure 11: Development of Pressure Ratio [21]

Since complete design of the aircraft is expected to be on service in 2025, in the detailed design process, it is necessary to take into consideration the technological developments in pressure ratios and the development of materials which will resistant to higher temperature as a result of today's work [21]. For this reason, considering the graph given in Figure 11 and technological developments until 2025, 55 overall pressure ratio of the compressor system is quite suitable for TULPAR engine.

#### 4.2.2. Fan (LPC) Design

Since the AxSTREAM license does not allow access to the fan design tool, the fan of the TULPAR engine is designed as a low pressure axial compressor in the AxSTREAM. TULPAR engine has 2-stage axial fan. In the following Table 26, the thermodynamic properties and geometrical dimensions of the fan obtained by using the GasTurb to be used as boundary conditions for the detailed compressor design in AxSTREAM are given.

Table 26: Thermodynamic Properties and Geometrical Dimensions obtained from GasTurb

Thermodynamic Properties		Geometrical Properties	
Total pressure at inlet	5.95 psi	Isentropic Efficiency	0.876
Total temperature at inlet	589.9 °R	Tip diameter	87.5 in
Total pressure at outlet	13.98 psi	1 <sup>st</sup> stage blade height	29.5 in
Total temperature at outlet	779.1 °R	Min. blade height	29.5 in
Mass Flow Rate	616.04 lbm/s	Number of stages	2
Shaft Rotational Speed	6361 rpm	Min hub diameter	20.6 in
Polytropic Efficiency	0.90	Max hub diameter	33.5 in

These results obtained as a result of the performance analysis and optimization for the TULPAR engine are used to determine the lower and upper limits of these parameters required for detailed design in AxSTREAM. After specifying upper and lower limits for these parameters, some conceptual design options are created for preliminary design in AxSTREAM and shown in Figure 12.

In Figure 12, distribution of the polytropic efficiency according to average work coefficient and average flow coefficient is given. The color scale given alongside the graph shows the polytropic efficiency value. One of these design options, which has the best efficiency value and meets all specific design criteria such as De-Haller Number and equivalent diffusion factor determined as a result of literature research is chosen for the optimization and 1D/2D calculations. Some design parameters for the selected point are shown in the Table 27.

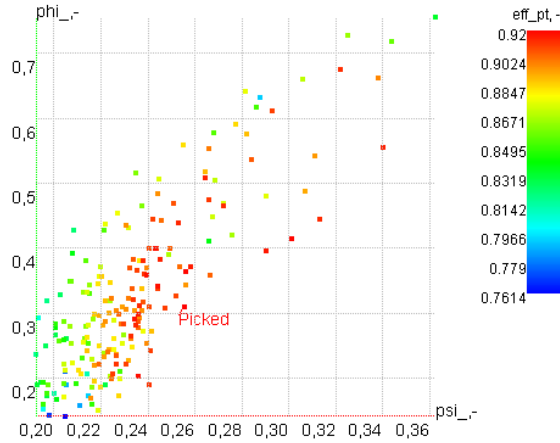


Figure 12: Polytopic Efficiency as a function of Work and Flow Coefficients

Table 27: Fan Preliminary Design Properties

Thermodynamic Properties and Geometrical Dimensions			
Total pressure at inlet	5.90 psi	Polytropic Efficiency	0.897
Total temperature at inlet	589.8 °R	Tip diameter	87.1 in
Total pressure at outlet	13.89 psi	1 <sup>st</sup> stage blade height	33.3 in
Total temperature at outlet	767.3 °R	Min. blade height	20.3 in
Mass Flow Rate	616 lbm/s	Number of stages	2
Shaft Rotational Speed	6524 rpm	Min hub diameter	20.5 in

The preliminary design of the rotor and stator created by using the values given in Table 27 is shown in Figure 13.

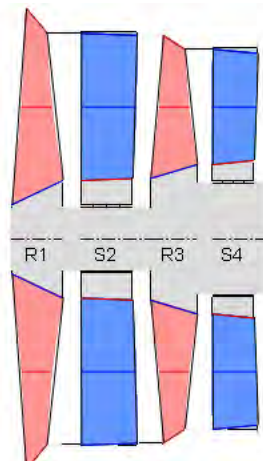


Figure 13: Preliminary Design of Fan Rotor and Stator

Since the diameter of the fan is given as 87.5 in RFP, tip diameter is selected as the specific diameter while designing in AxSTREAM and this value specified in RFP is chosen as the reference for maximum fan diameter.

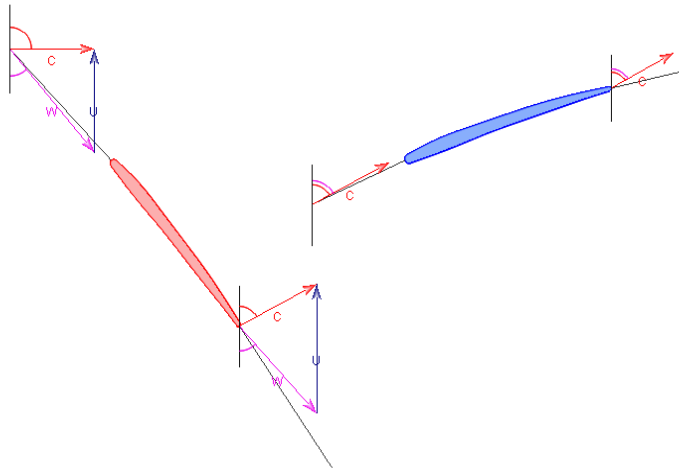
The velocity triangles for each stage are obtained, but only the velocity triangles of the first stage are shown in Figure 14, 15 and 16. For each rotor and stator, the velocity triangles are obtained from three different sections: hub, mean and tip section.

Calc section\_1 In solve Rotor\_1-1

C = 892.386843 ft/s  
W = 1368.480709 ft/s  
U = 1037.489842 ft/s  
B = 40.700152 tan. deg  
A = 90.000000 tan. deg  
K1 = 43.700152 tan. deg

Calc section\_1 In solve Stator\_2-1

C = 920.080920 ft/s  
B = 62.697669 tan. deg  
A = 62.697669 tan. deg  
K1 = 65.697669 tan. deg



K2 = 34.521138 tan. deg  
A = 62.697669 tan. deg  
B = 42.953069 tan. deg  
U = 1300.219342 ft/s  
W = 1199.858904 ft/s  
C = 920.080920 ft/s

K2 = 77.423132 tan. deg  
A = 61.871191 tan. deg  
B = 61.871191 tan. deg  
C = 754.222509 ft/s

Calc section\_1 Out solve Rotor\_1-1

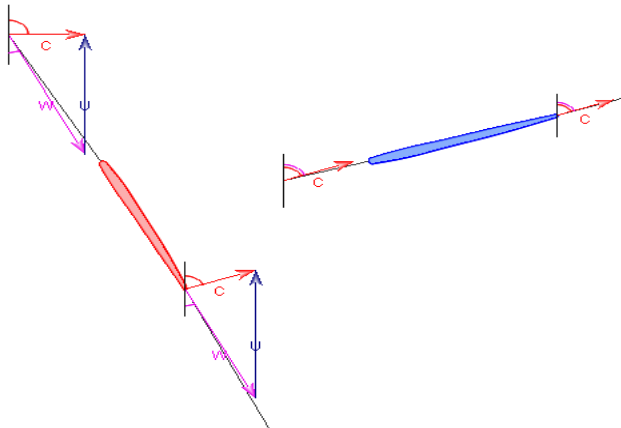
Calc section\_1 Out solve Stator\_2-1

Figure 14: Velocity Triangles of The First Stage from Hub Section

Calc section\_2 In solve Rotor\_1-1- Calc section\_2 In solve Stator\_2-1

C = 892.386843 ft/s  
W = 1999.656822 ft/s  
U = 1789.489628 ft/s  
B = 26.504621 tan. deg  
A = 90.000000 tan. deg  
K1 = 29.504621 tan. deg

C = 866.053222 ft/s  
B = 70.740221 tan. deg  
A = 70.740221 tan. deg  
K1 = 73.740221 tan. deg



K2 = 24.966016 tan. deg  
A = 70.740221 tan. deg  
B = 26.564771 tan. deg  
U = 1920.854378 ft/s  
W = 1828.188142 ft/s  
C = 866.053222 ft/s

K2 = 71.396767 tan. deg  
A = 70.488870 tan. deg  
B = 70.488870 tan. deg  
C = 705.662762 ft/s

Calc section\_2 Out solve Rotor\_1-1

Calc section\_2 Out solve Stator\_2-1

Figure 15: Velocity Triangles of The First Stage from Mean Section

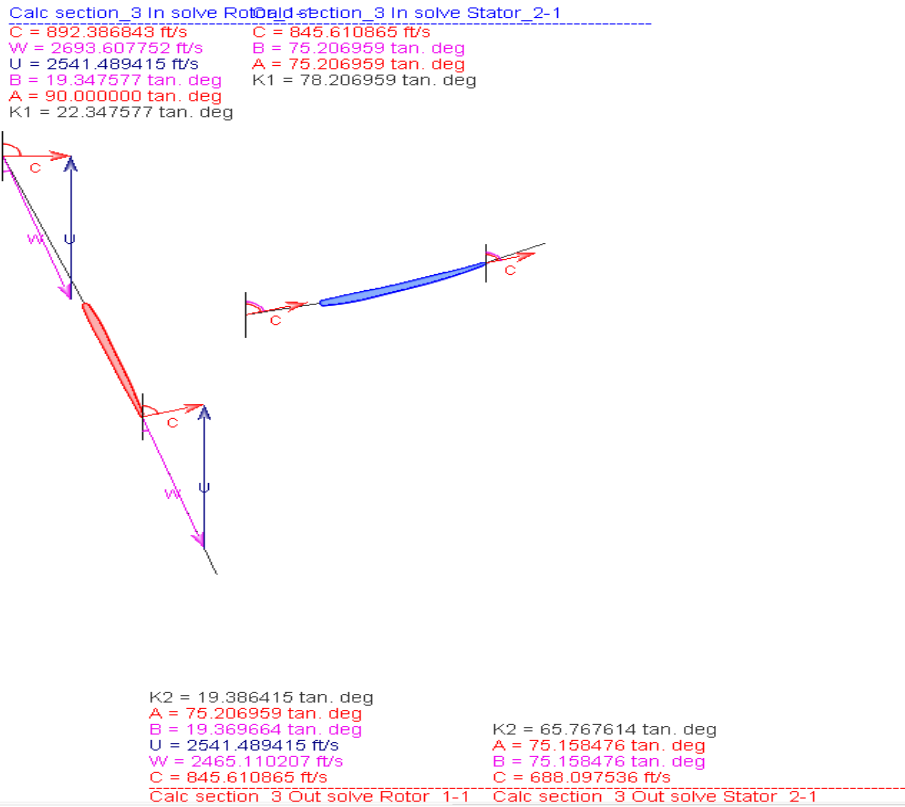


Figure 16: Velocity Triangles of The First Stage from Tip Section

After the preliminary design of the 2-stage fan is completed, 1D/2D streamline calculation is started to obtain temperature, pressure and mach number distribution in each stage. Streamline analysis is performed to determine the course of the flow through the fan stages and critical points are determined by finding pressure and temperature increases in each stage. The distribution of total temperature, total pressure and relative mach number distribution in tip section of first blade is given in Figure 17, 18 and 19 below.

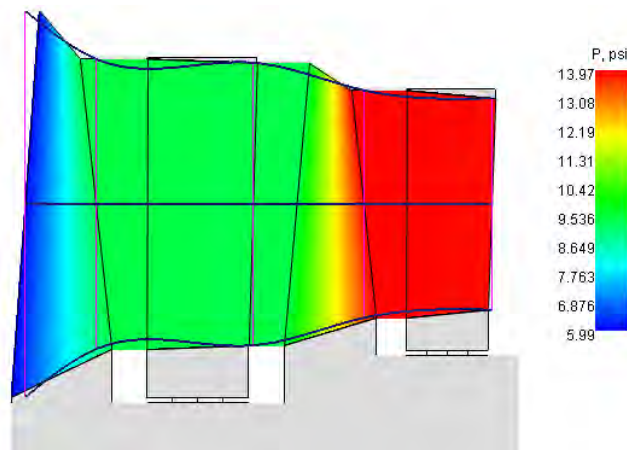


Figure 17: Total Pressure Variation throughout the Axial Fan

As can be seen in the Figure 17, the total pressure increases throughout the fan stages. Total pressure in last the stage is almost 13.9 psi.



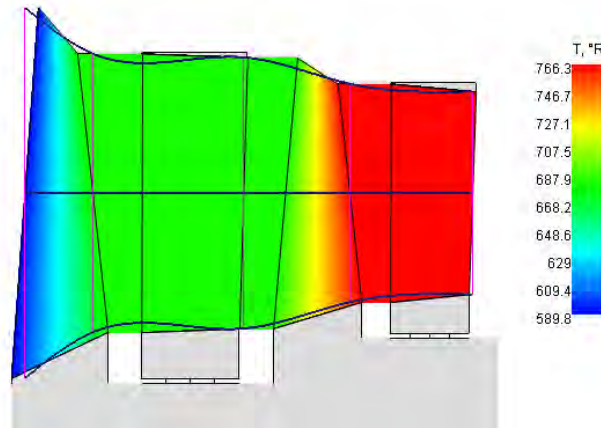


Figure 18: Total Temperature Variation throughout the Axial Fan

As can be seen in the Figure 18, the total temperature increases with increasing total pressure. In the last stage of fan, total temperature reaches approximately 809 °R. Especially for material selection to be used in fan production, this temperature distribution has a significant effect.

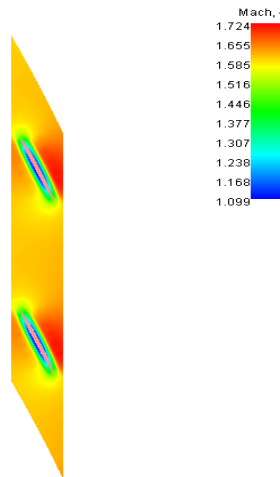


Figure 19: Relative Mach Number Distribution at Tip Section of the First Rotor Blade

When Mach number distribution is examined, it is seen that mach number increases throughout tip section and mach number values decrease to 1.1-1.2 values as going through the hub section of the axial fan. However, mach number in tip section of the first stage where the maximum mach number is reached is up to 1.7. When compared with the typical mach number values which is given in Table 25, it appears to be very close to the upper limit of the relative mach number specified in Aircraft Propulsion-Saeed Farokhi [5].

Blade profile has a significant effect on the temperature, pressure and mach number distribution on the blade. For this reason, the most optimal blade design that meets the compressor design criteria and satisfies the desired performance criteria is required. This principle describes the variety of the swirl velocity profile in the downstream of the rotor anchored at the pitchline [5]. Among these blade principles “free-vortex blade design” where the irrational flow around the vortex is zero is selected to be applied to the detailed blade design in axial fan design.

Also when the mach number distribution on the fan stages is examined, the camber profile is chosen because the mach values on the fan are in accordance with the range given in Table 25 for the camber profile and this profile provides the optimal pressure and mach number distribution for blade on the fan. In the following Figure 20, the rotor and stator blade designs are given for the first stage of the fan respectively.



Figure 20: Rotor (left) and Stator (right) Blade Profiles

After the blade design is completed, the 3D rotor and stator designs of the first stage of the fan are shown in Figure 21 and also 3D design of whole fan geometry is shown in Figure 22 below.

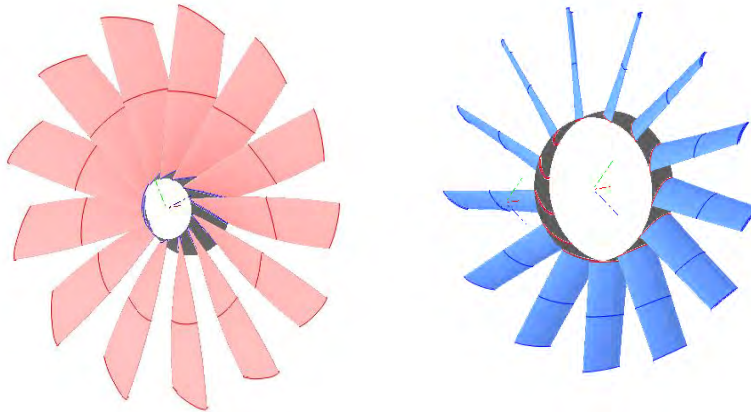


Figure 21: Rotor (left) and Stator (right) Design of The First Stage

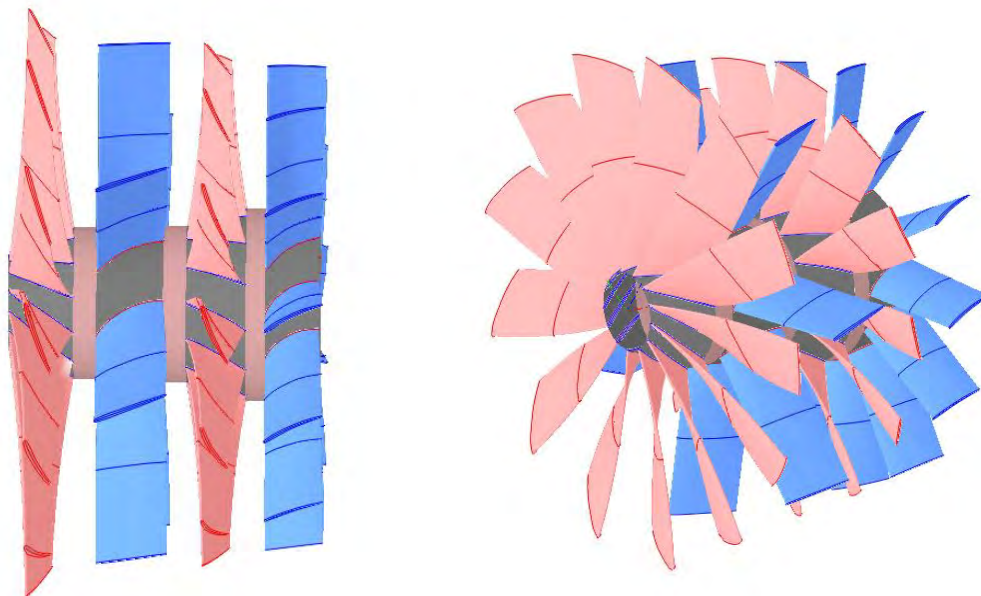


Figure 22: Side view and whole 3D desing of Axial Fan

Detailed Design Parameters obtained from AxSTREAM for each stage in Axial Fan are given in Table 28. When each parameter is compared with typical values, it is seen that the results are consistent with typical values.

Table 28: Detail Design Parameters of Axial Fan

Variables	STAGE 1		STAGE 2	
	Rotor	Stator	Rotor	Stator
De Haller Number	0.81	0.78	0.75	0.78
Flow Coefficient	0.443	0.396	0.447	0.385
Aspect Ratio	3.2	2.5	2.8	2.3
Solidity	1.1	1.22	1.24	1.32
Loading Coefficient	0.24	0.22	0.25	0.23
Number of Blades	13	10	12	13
Stagger Angle	31.63	30.45	23.77	34.02
Inlet Metal Angle	58.5	35.2	73.5	83.8
Outlet Metal Angle	58.2	83.8	58.9	34.1
Degree of Reaction	0.85	0.78	0.82	0.73
Blade Chord (in)	11.2	11.22	9.56	9.36
Leading Edge Radius (in)	0.232	0.225	0.197	0.183
Trailing Edge Radius (in)	0.1	0.11	0.09	0.09
Absolute Max Mach Number	1.38	0.78	1.15	0.62
Mean Radius	26.9	26.9	26.9	26.9
Hub to Tip Ratio	0.24	0.36	0.36	0.44
Stage Pressure Ratio	1.62		1.46	

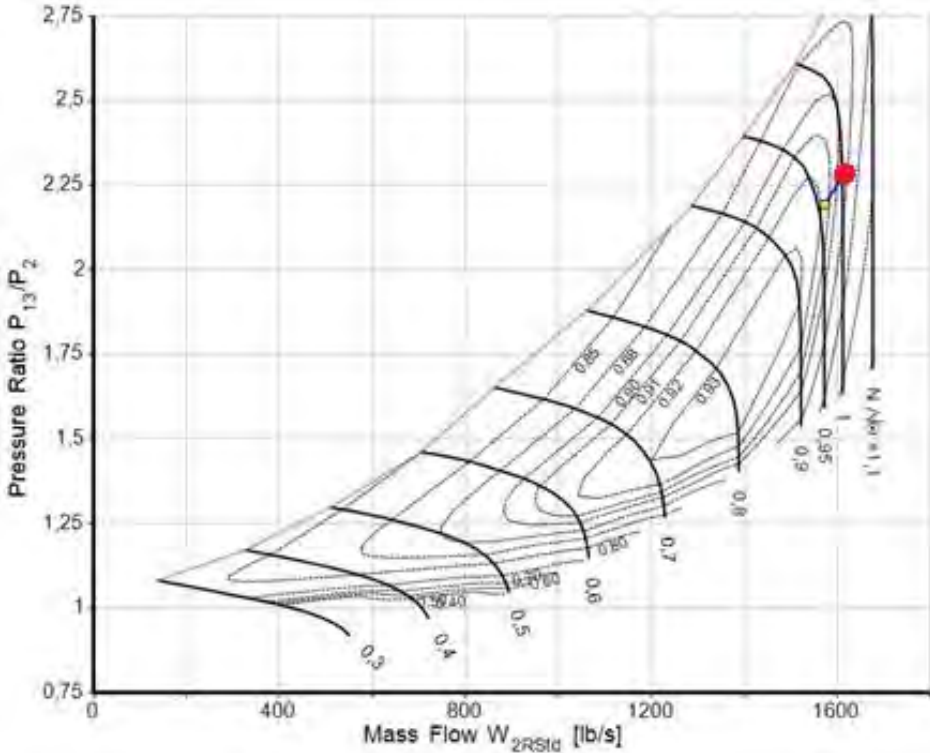


Figure 23: LPC Characteristics Map

The change in compressor efficiency depending on pressure ratio and corrected mass flow rate is given in Figure 23 for LPC. In this map, the red point indicates the compressor design point and the red line indicates the surge

line. As in HPC, since the surge margin is above the critical range determined for the compressor design, LPT works efficiently without stall for TULPAR engine.

#### 4.2.3. Axial High Pressure Compressor Design

In the baseline engine, high pressure compressor has 11-stages. Some studies are examined to see if the reduction can be made in compressor stages to provide weight reduction resulting in more compact engine design. In this process, by creating compressor maps for both 10-stages and 11-stages, it is tried to determine whether the stage reduction has negatively affected and the compressor has exceeded surge line. As a result of the researches and analyzes, it is determined that 10-stage compressor works as efficiently as 11-stage compressor for the same performance criteria and also 10-stages compressor provides weight reduction. Because of these reasons, 10-stage axial compressor design is selected to be used in TULPAR engine.

In baseline engine, LP Shaft Speed and HP Shaft Speed are very close to each other. The new engine to be designed has 2-spool engine configuration and it has been determined that the spool shaft speeds are quite different from each other in 2-spool turbofan engines. Therefore, as a result of literature review, range and typical values of each design parameters for compression systems are given in Table 25. These values are obtained from Aircraft Propulsion-Saeed Farokhi. [5]

Firstly analyzes are performed by using the same shaft speeds given in baseline engine and the maximum relative tip mach number values for each component (LPC, HPC, HPT and LPT) are calculated.

As a result of these calculations, it is determined that the maximum tip relative mach number given in Table 25 and the maximum tip relative mach number calculated by using AxSTREAM for the fan (LPC) are consistent. However, it is seen that the maximum relative tip mach number value calculated for HPC and HPT is out of the mach number range given in Table 25 and is inconsistent with upper and lower limits. For this reason, HP shaft speed is calculated by taking the upper limit given in Table 25 for maximum tip relative mach number as a reference ( $(M_{1r})_{tip} \sim 1.5$ ).

As a result of calculation, HP shaft speed is determined as 8850 rpm, and also it is seen that maximum tip relative mach number is in the range obtained as a result of literature review.

The same process followed in fan design is applied to the axial high pressure compressor design. TULPAR engine has 10-stage axial high pressure compressor. In Table 29, thermodynamic and geometrical dimensions for the selected point as a result of preliminary design are given.

Table 29: Preliminary Design Properties

<b>Thermodynamic Properties and Geometrical Dimensions</b>			
Total pressure at inlet	13.92 psi	Polytropic Efficiency	0.91
Total temperature at inlet	779.04 R	Tip diameter	42.87 in
Total pressure at outlet	334.46 psi	1 <sup>st</sup> stage blade height	9.97 in
Total temperature at outlet	2043.2 R	Min. blade height	2.9 in
Mass Flow Rate	183.7 lbm/s	Number of stages	10
Shaft Rotational Speed	8850 rpm	Min hub diameter	22.75 in

TULPAR engine has 10-stage HPC. The velocity triangles for each stage are obtained, but only the velocity triangles of the first stage are shown in Figure 24, 25 and 26. For each rotor and stator, the velocity triangles are obtained from three different sections: hub, mean, and tip section.

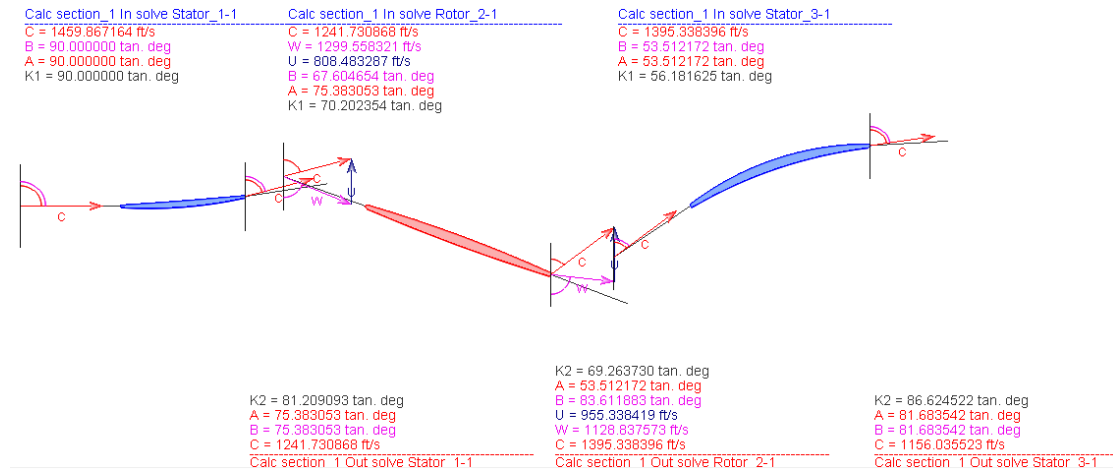


Figure 24: Velocity Triangles of The First Stage from Hub Section

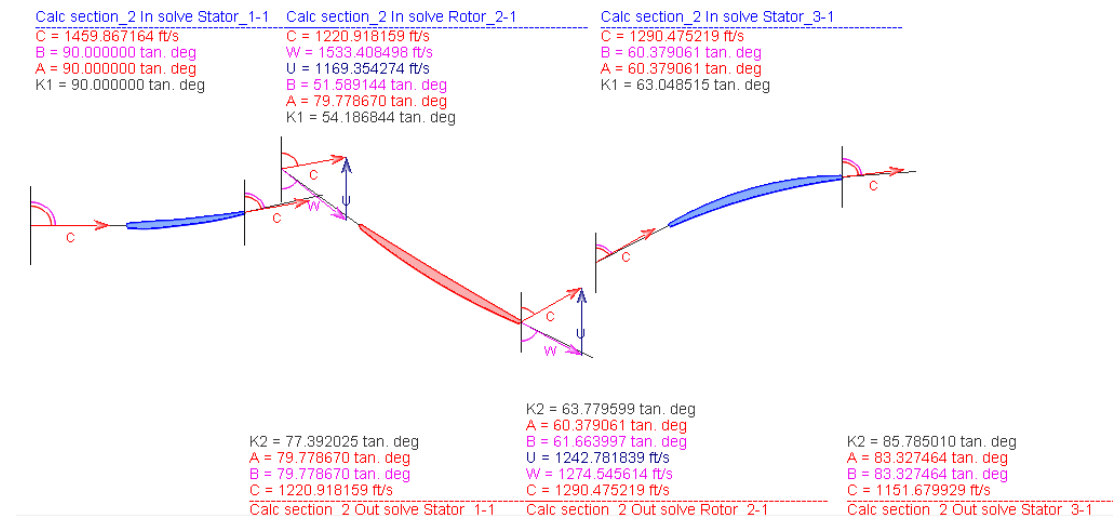


Figure 25: Velocity Triangles of The First Stage from Mean Section

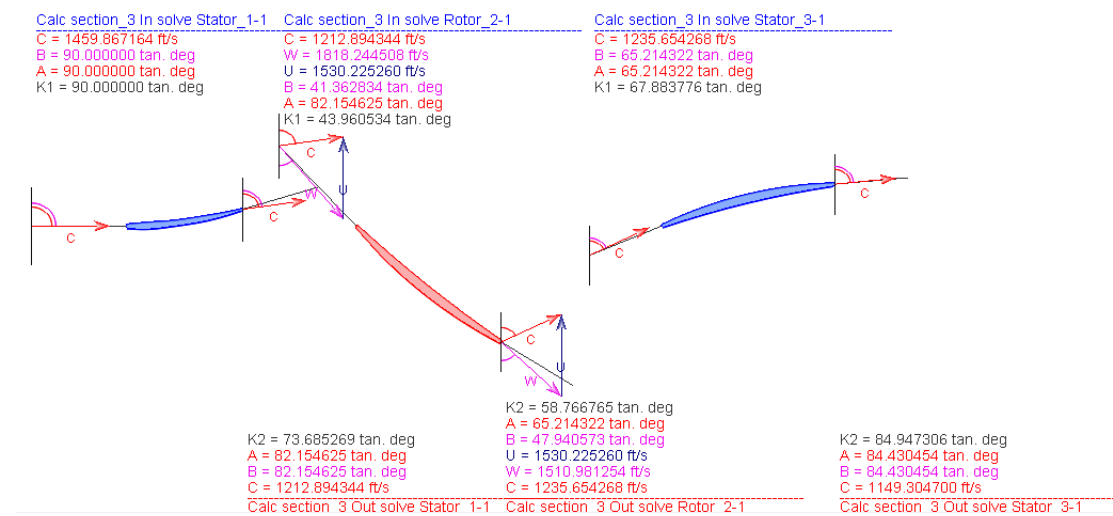


Figure 26: Velocity Triangles of The First Stage from Tip Section

As a result of analysis in AxSTREAM, detailed design parameters obtained from AxSTREAM for first 5 stage in High Pressure Compressor are given in the Table 30. When each parameter is compared with typical values, it is seen that the results are consistent with typical values.

Table 30: Detail Design Parameters of HPC

Variables	STAGE 1		STAGE 2		STAGE 3		STAGE 4		STAGE 5	
	Rotor	Stator	Rotor	Stator	Rotor	Stator	Rotor	Stator	Rotor	Stator
De Haller Number	0.731	0.728	0.732	0.725	0.726	0.724	0.728	0.724	0.730	0.727
Flow Coefficient	0.58	0.48	0.54	0.43	0.52	0.42	0.51	0.38	0.49	0.34
Aspect Ratio	2.14	1.78	1.73	1.51	1.51	1.34	1.36	1.23	1.27	1.14
Solidity	1.60	1.98	1.58	1.82	1.52	1.67	1.44	1.55	1.37	1.45
Loading Coefficient	0.53	0.51	0.47	0.44	0.43	0.39	0.40	0.37	0.38	0.34
Number of Blades	35	48	43	54	50	59	56	64	62	68
Stagger Angle	30.42	27.35	38.75	26.13	43.36	25.37	46.33	24.80	48.44	24.34
Inlet Metal Angle	49.88	38.67	41.16	41.19	36.87	42.64	34.31	43.63	32.52	44.39
Outlet Metal Angle	69.26	86.62	61.33	86.55	56.39	86.63	53.04	86.76	50.59	86.92
Degree of Reaction	0.63	0.37	0.68	0.32	0.7	0.3	0.72	0.28	0.74	0.26
Blade Chord (in)	4.65	4.44	4.05	3.86	3.50	3.07	3.07	2.91	2.68	2.64
Leading Edge Radius (in)	0.047	0.039	0.039	0.035	0.035	0.031	0.027	0.027	0.024	0.024
Trailing Edge Radius (in)	0.047	0.043	0.039	0.001	0.035	0.031	0.027	0.027	0.024	0.024
Absolute Max Mach Number	1.34	0.87	1.14	0.75	1.03	0.68	0.95	0.63	0.89	0.61
Mean Radius	16.24	17.26	17.71	18.33	18.58	19.0	19.14	19.44	19.53	19.74
Hub to Tip Ratio	0.53	0.62	0.67	0.73	0.75	0.79	0.80	0.83	0.84	0.86
Stage Pressure Ratio	1.43		1.42		1.38		1.34		1.29	

In Figure 27, compressor characteristics map is shown. This map shows the change in compressor efficiency depending on pressure ratio and corrected mass flow rate. In this map, the red point indicates the compressor design point and the red line indicates the surge line.

Surge Margin is distance of the design (operating) point from the surge line. For an ideal design, surge margin should exceed %10 limit. The 0-10% surge margin range is assumed as a critical range for compressor design [5].

When the compressor map for TULPAR engine is examined, it is clearly seen that the decrease in the number of stages does not have any negative effect on the operation of the compressor and compressor surge margin exceeds %10 range.

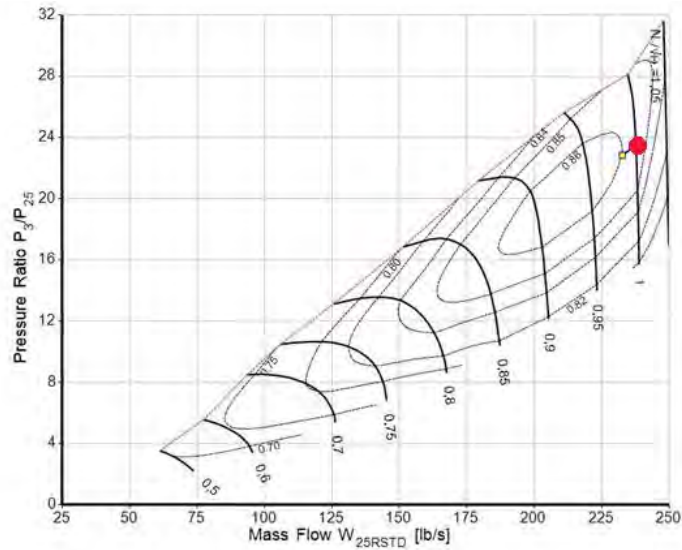


Figure 27: HPC Characteristics Map

The rotor and stator 3D designs of the first stage created in AxSTREAM and the 3D design of first 5-stages are as shown in Figure 28 and 29 below, respectively.

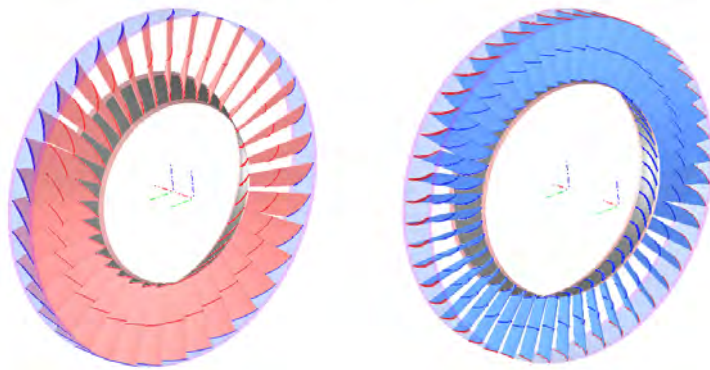


Figure 28: Rotor (left) and Stator (right) Design of The First Stage

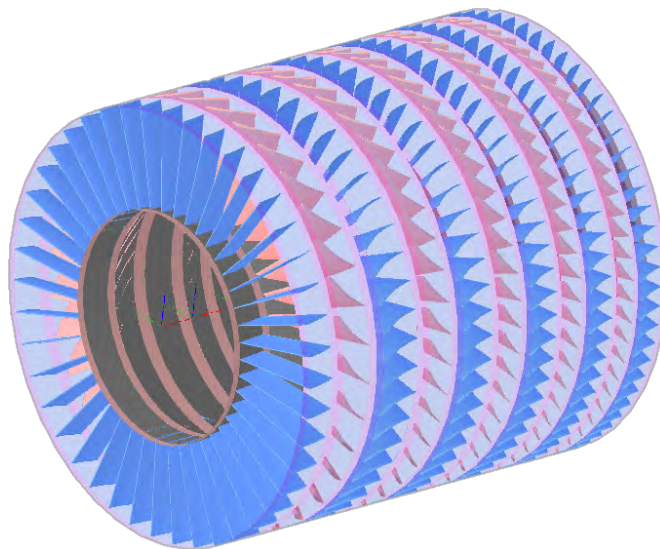


Figure 29: 3D Design of the First 5-Stages of the Compressor

### 4.3. COMBUSTION CHAMBER

Combustion chamber (CC) is the component of an Aero engine where the fuel and air mixture is burned. Good mixing of air and fuel is vital to obtain a high combustion efficiency. Liquid fuel should be well and fast atomized into droplets as small as possible for high combustion efficiency with the help of swirlers. When designing a highly efficient combustion chamber, many parameters need to be considered and combustor must satisfy a wide range of requirements [22-23].

There are three different types of combustion chambers. These are can combustor (tubular), annular combustor and can-annular (tuboannular) combustor. Fully annular combustion type of combustor is the most commonly used type because of the clean aerodynamic layout. Annular combustor has many advantages when compared to other types of combustor. These advantages are including more uniform combustion, less surface area and shorter size compared to other types, tending to have very uniform exit temperatures, having the lowest pressure drop (approximately %5 of combustor inlet total pressure) and simpler design. [22-24]

So, annular type of combustor was selected and designed for TULPAR. Besides, main components of annular combustion and geometry of combustion chamber are shown in Figure 30.

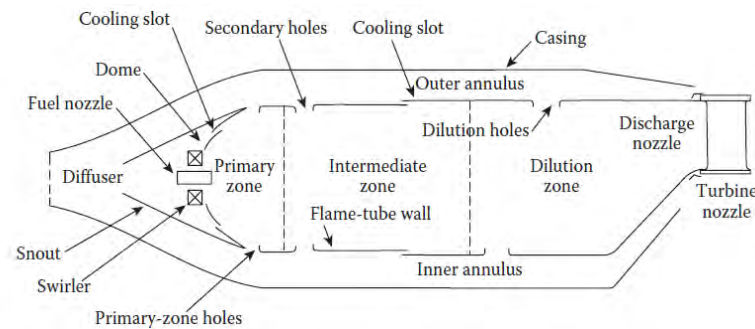


Figure 30: Main components and geometry of annular combustion chamber [23]

Liquid atomization (LA) and evaporation processes are important for the performance of a gas turbine combustion system. So, liquid fuel should be atomized into a large number of droplets (smaller the droplet size, the faster evaporation). There are many trends of atomizer design for this purpose. Pre-filming radial airblast swirler type atomizer was selected for ETU-V TULPAR. Atomizer gives a rotary motion to the air entering the atomization with the help of ducts. The number of atomizer should be increased as much as possible to obtain high mixing efficiency. The two channel airblast atomizers have very significant advantages. These are relatively cool liner walls, minimizing exhaust smoke and protecting inner line from overheating because it allows the formation of Central Recirculation Vortex (CRV) structures [23-28]. Primary swirler has eight holes, secondary swirler has twelve holes in our design. The used airblast atomizer is shown in Figure 31.

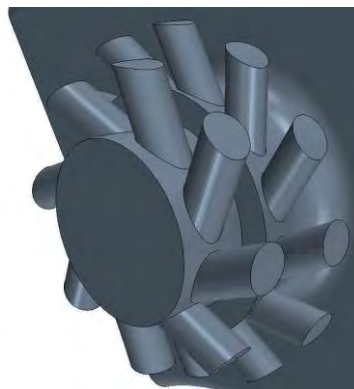


Figure 31: Airblast atomizer which has same direction flow ducts [28]



Another important parameter in the combustion chamber design is NO<sub>x</sub> emissions. The design of a low emission comprises of a balance providing enough time and temperatures to complete the reactions. For this purpose, three different design modeling is emphasized. These are Lean-Premixed-Prevaporized Combuster (LPP), Rich-Burn Quick-Quench Lean-Burn (RQL) and Direct Injection (DI) [25].

Rich-Burn Quick-Quench Lean-Burn (RQL) concept was selected for TULPAR. This concept has some advantages of good stability because of its rich zone in which NO<sub>x</sub> formation rates are low due to combined effects of oxygen depletion and low temperature, followed by quick mixing with rest of combustion air in the quick quench zone. [23-25]. RQL combustion concept has an equivalence ratio (ER) around 1.5 in primary zone and 0.7 in secondary zone. The primary zone equivalence ratio should not be very rich (higher than 1.6) to minimize amount of smoke, carbon monoxide (CO) and unburned hydrocarbons (UHC) [26]. Equivalence ratio is defined in Equation 4.2.

$$\Phi = \frac{m_{fuel}/m_{air}}{(m_{fuel}/m_{air})_{stoic}} \quad (4.2)$$

Liners are used to contain the combustion process and to facilitate distribution of the air to all different combustion zones in sufficient quantities. The liner must have sufficient thermal resistance to withstand continuous and cyclic high temperature operation and to withstand the buckling load created by differential pressure. This is accomplished by the effective use of cooling air and the use of appropriate materials [23]. The liner cooling technologies are shown in Figure 32. [4]

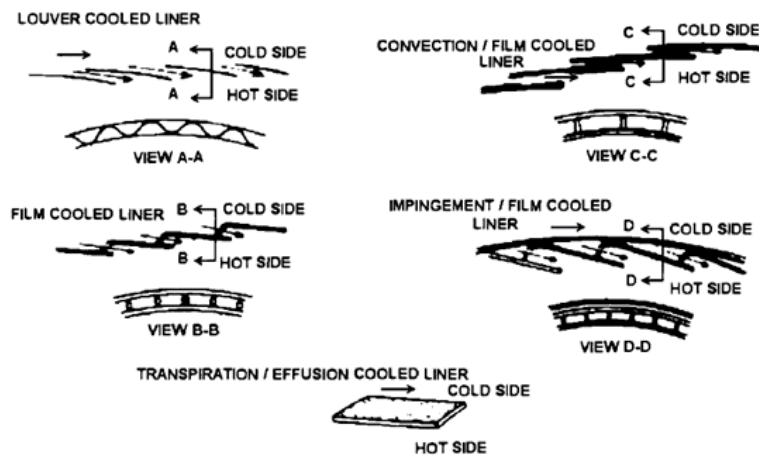


Figure 32: Liner cooling technologies [4]

The most common way to protect the combustion chamber and the undercoat is film cooling. In the film cooling method, the cooling flow be destroyed by turbulence and the cooling effect reduces. Large amounts of air are used to prevent this situation, which causes the cooling air to waste. So, the film cooling method is combined with other cooling forms to increase the cooling efficiency. Multiholed walls method was an one of the effective ways. This cooling method is used in dome section of combustor in our design. Other method is transpiration cooling method, but there are no porous materials in the market. [4] Also, clogged pores are the big problem. So, the film cooling method was selected for TULPAR.

Geometrical dimensions of combustor and important combustion performance parameters were calculated by using newly developed MATLAB code. These calculations were performed for cruise conditions. The input values used in the prepared MATLAB code are mentioned below. While some of these values were taken from GasTurb, other values were assumed according to literature surveys. The values were modified to achieve high performance relative to some constraints [24-26]. These assumptions are shown in Table 31.

Table 31: Combustion Chamber Design Parameter Assumptions [23-26-27-28]

Design Parameters	Value
Reference velocity (ft/s)	16.40 - 98.42
Passage Mach number	0.1 - 0.15
Pattern factor (PF)	0.2 – 0.3
Stoichiometric FAR (fuel to air ratio)	0.0685
Snout discharge coefficient	1
Equivalence ratio in the primary zone	1.2 – 1.6
Equivalence ratio in the secondary zone	0.4 – 0.8
The ratio of primary zone length to flame tube height	1
The ratio of secondary zone length to flame tube height	1.2
Atomizer ALR (Air liquid ratio)	>8
Total pressure loss ( $\Delta P$ ) in diffuser	% 1

It has been assumed that the pressure distribution in the secondary air channels has a constant behavior.

Also, the similar behavior is observed in the flame tube after liner pressure drop. So, it is accepted that the average velocity of air entering each hole is the same regardless of diameter and position. The mass flow rates, discharge coefficients and hole diameters were iteratively calculated using the Kaddah correlation. In Figure 33, flow through the liner hole is shown [23].

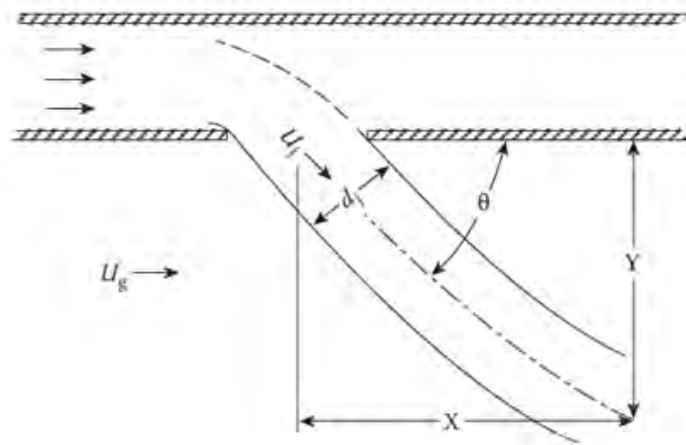


Figure 33: Air flow through the liner hole [23]

The geometric dimensions of the combustion chamber were determined by using the GasTurb results and assumptions mentioned above. As a result of comprehensive literature studies, the validity of these assumptions has been accepted. The assumptions which were used on design point in MATLAB code is shown in Table 32.

Table 32: Combustion Chamber Design Assumptions

Parameter	Value
Primary zone equivalence ratio	1.5
Secondary zone equivalence ratio	0.7
Pattern factor	0.25
Stoichiometric FAR ratio	0.06850
Mean flame tube temperature (R)	3960
Snout discharge coefficient	1
Reference velocity (ft/s)	91.86
Passage mach number	0.11
Diffuser pressure loss (% of total pressure loss in combustion)	1

The design conditions of combustion chamber are shown in Table 33. The calculations were completed by using these values. Most of these condition values were taken from GasTurb software for optimized engine. The calculated geometrical dimensions of combustor for cruise condition are shown in Table 34.

In addition to these, the other important performance parameters about combustion efficiency were calculated by using MATLAB and results are shown in Table 35.

Table 33: Combustion chamber on design conditions

Parameter	Value
Total air mass flow rate (lb/s)	146.94
Total fuel mass flow rate (lb/s)	4.087
Mach number at combustor inlet	0.1951
Mach number at combustor outlet	0.0995
Total temperature at combustor inlet (R)	1991.1
Static temperature at combustor inlet (R)	1978.75
Total temperature at combustor outlet (R)	3535.2
Static temperature at combustor outlet (R)	3530.3
Total pressure at combustor inlet (psi)	329
Total pressure at combustor outlet (psi)	316
Heating value of fuel (BTU/lbm)	18400
Compressor blade pitch radius (in)	21.26
Turbine blade pitch radius (in)	22.84
The number of fuel nozzle	24
Primary swirler hole number	8
Secondary swirler hole number	12
Primary hole number per nozzle	4
Secondary hole number per nozzle	4
Dilution hole number per nozzle	3

Table 34: Combustion Chamber - Geometrical results on-design point

Geometrical Parameters	Value	Geometrical Parameters	Value
Combustion chamber angle	6.35	Reference height (inch)	3.901
Diffuser inlet area (inch <sup>2</sup> )	116.71	Snout inner area (inch <sup>2</sup> )	53.78
Diffuser inlet height (inch)	0.8740	Snout inner height (inch)	0.4015
Diffuser angle (degree)	34.08	Snout outer area (inch <sup>2</sup> )	206.92
Diffuser area ratio	1.77	Snout outer height (inch)	1.5511
Diffuser length (inch)	2.2362	Swirler diameter (inch)	1.377
Dome area (inch <sup>2</sup> )	368.12	Swirler p. hole diameter (inch)	0.1771
Dome height (inch)	2.756	Swirler s. hole diameter (inch)	0.1378
Dome length (inch)	0.394	Total length of combustor (inch)	0.14.17
Dome diffuser angle (degree)	34.08	Number of fuel nozzle	24
Flame tube volume (inch <sup>3</sup> )	4387.6	Primary swirler hole number	16
Primary hole diameter (inch)	0.63	Secondary swirler hole number	24
Secondary hole diameter (inch)	0.8070	Primary hole number per nozzle	4
Dilution hole diameter (inch)	0.9921	Second. hole number per nozzle	4
Primary zone length (inch)	2.756	Dilution hole number per nozzle	3
Secondary zone length (inch)	3.3070	Liner length (inch)	11.913
Dilution zone length (inch)	3.6535	Liner inner radius (inch)	19.881
Passage area (inch <sup>2</sup> )	153.14	Liner outer radius (inch)	22.63
Passage height (inch)	1.145	Recirculation zone length (inch)	2.756
Combustion inner radius (inch)	19.307	Recirculation zone angle(degree)	60.25
Combustion outer radius (inch)	23.212	Reference area (inch <sup>2</sup> )	521.26

Table 35: Combustion Chamber performance results on-design point

Parameters	Value	Parameters	Value
Residence time (ms)	3.72	Air-liquid ratio	8.26
Loading factor (kg/bar <sup>1.8</sup> m <sup>3</sup> s)	0.2	Air-fuel ratio	35.94
Combustion intensity(MW/m <sup>3</sup> bar)	47.55	Global equivalence ratio	0.4060

When the MATLAB results are evaluated, it is found that the residence time is sufficient enough to obtain high combustion efficiency. In addition to this, according to literature survey, combustion intensity value is acceptable for typical combustion chamber and air-liquid ratio is sufficient enough to atomize the fuel particles. In other words, the calculated values are consistent with typical values. Other important parameter results for primary, secondary and dilution holes are shown in Table 36.

Table 36: Combustion Chamber flame tube hole results

Parameters	Value
Jet velocity (ft/s)	375.06
Primary hole discharge coefficient (DC)	0.47
Secondary hole discharge coefficient (DC)	0.54
Dilution hole discharge coefficient (DC)	0.61

When examined these results, it is seen that flame tube hole results are close enough to typical combustion chamber results. Also, discharge coefficient values are acceptable for typical annular combustion chamber. In general, the typical values of hole discharge coefficient (DC) are between 0.5 and 0.7.

Also, 3D model of combustor and 3D model of radial swirler and combustion chamber were prepared in Siemens NX and shown in Figure 34 and 35, respectively. In addition to these, a cross-sectional view of the whole combustion chamber is shown in Figure 36.

Besides, technical drawing of combustor is given in Appendix A section. Furthermore, C/SiC CMC and Yttrium-stabilized Zirconium coating were selected as suitable materials depending upon operational conditions. The selected material is described in Material Selection section in detail.



Figure 34: 3D model of combustor chamber, front view (left) and back view (right)



Figure 35: Primary swirler (left), whole swirler (middle), secondary swirler (right)

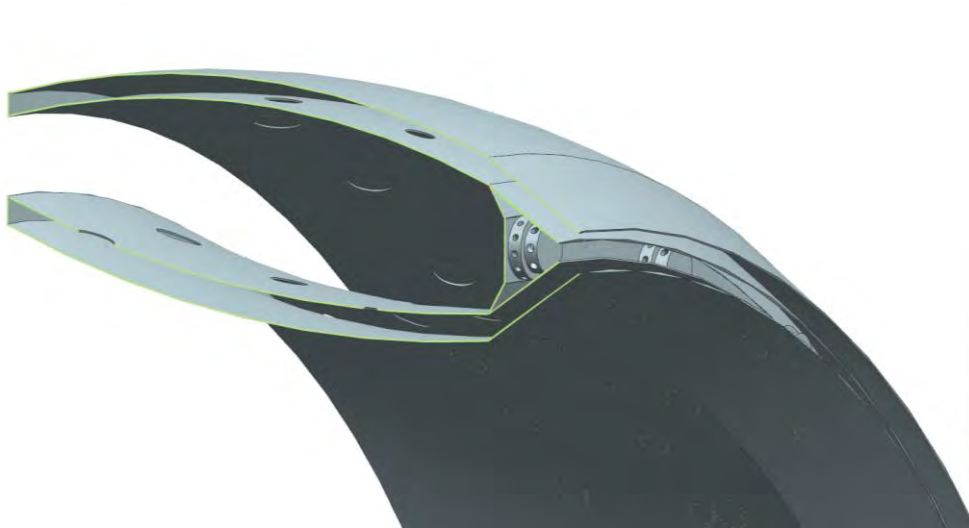


Figure 36: A cross-sectional view of the combustion chamber

#### 4.4. DETAILED TURBOMACHINERY DESIGN (HPT - LPT)

This section includes detailed information about detailed design of the turbine system of the ETU-V TULPAR. Detailed information about turbine selection, preliminary design properties, the design parameters and criteria, the performance characteristics, analysis results will be explained in this part. This candidate engine for a next generation supersonic transportation contains a high pressure (HPT) and low-pressure (LPT) turbine. In a 2-spool system, power is transferred to the HPT by the high-pressure compressor, and the fan transmits a power to the LPT. The efficiency, weight and length-width limits, the generated power, the rotor stress and the cost must be taken into account in the design of the turbine in which the energy required to rotate the compressor is generated.

In turbine design, compressibility and Mach number effects should be considered because the density of the air/fuel mixture in the turbine flow is variable. High inlet temperatures necessitate the required cooling. As in the compressor, there are no extensive rules for turbine flow and selection of airfoil geometry for the turbine [4] In Table 37, Range of axial flow turbine design parameters for HPT is shown [4].

Table 37: Range of axial flow turbine design parameters for HPT [4]

Parameters	Value
Maximum $AN^2$	$4 \times 10^{10} - 5 \times 10^{10} \text{ in}^2 \cdot \text{rpm}^2$
Stage Loading Coefficient ( $\psi$ )	1.4 – 2.0
Exit Mach Number	0.4 – 0.5
Exit Swirl Angle	0 – 40 deg

Range of axial flow turbine design parameters for LPT is shown in Table 38.

Table 38: Range of axial flow turbine design parameters for LPT [4]

Parameters	Value
Inlet corrected mass flow rate	40-44 lb/s
Hub/tip ratio at inlet	0.35 – 0.5
Maximum stage loading at hub	2.4
Exit Mach Number	0.4 – 0.5
Exit Swirl Angle	0 – 40 deg

In the process of developing turbine technology, HPT inlet temperature increase, cooling airflow and LPT stage loading coefficient should be considered. All of these parameters are important for increasing OPR and BPR and decreasing TSFC (accordingly efficiency).

Design methodology applied for compressor design in AxSTREAM is also applied for turbine design. In this process, the upper and lower limit values required for the detailed preliminary design in AxSTREAM are determined by using the design parameter values obtained from GasTurb. By using these parameters, some conceptual design options are created for preliminary design. Among these design points created in AxSTREAM, the point which meets the design criteria and has required maximum efficiency for the turbine is selected for detailed design. After that by using design parameters of selected design point, 3D design is created for rotor, stator and blade for each stage.

#### 4.4.1. Axial High-Pressure Turbine Design

The same process followed in compressor design is applied to the axial high pressure turbine design. TULPAR engine has 2-stage axial high pressure turbine. In the following Table 39, thermodynamic properties and geometrical dimensions for the selected point as a result of preliminary design are given.

Table 39: Preliminary Design Properties

Thermodynamic Properties and Geometrical Dimensions			
Parameters	Value	Parameters	Value
Total pressure at inlet	315.9 psi	Total Efficiency	0.89
Total temperature at inlet	3535.2 °R	Hub diameter	44.1 in
Total pressure at outlet	42.35 psi	1 <sup>st</sup> stage blade height	3.19 in
Total temperature at outlet	2227.9 °R	Max. blade height	6.42 m
Mass Flow Rate	151.0 lbm/s	Number of stages	2
Shaft Rotational Speed	8850 rpm	Max tip diameter	56.7 in

Rotor and stator geometries of each stage in the preliminary design which is created by using the values given in Table 39 is shown in Figure 37. High Pressure Turbine has 2-stage. By using AxSTREAM, Velocity triangles of the first stage are obtained for hub, mean and tip section and given in Figure 38, Figure 39 and Figure 40, respectively.

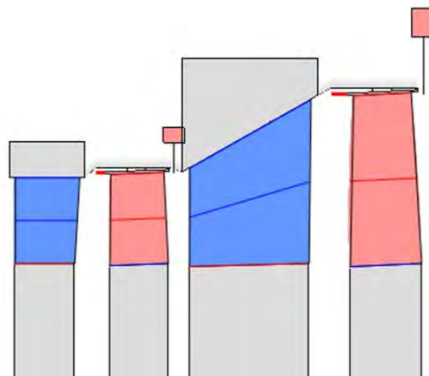


Figure 37: Preliminary Design of HPT Rotor and Stator

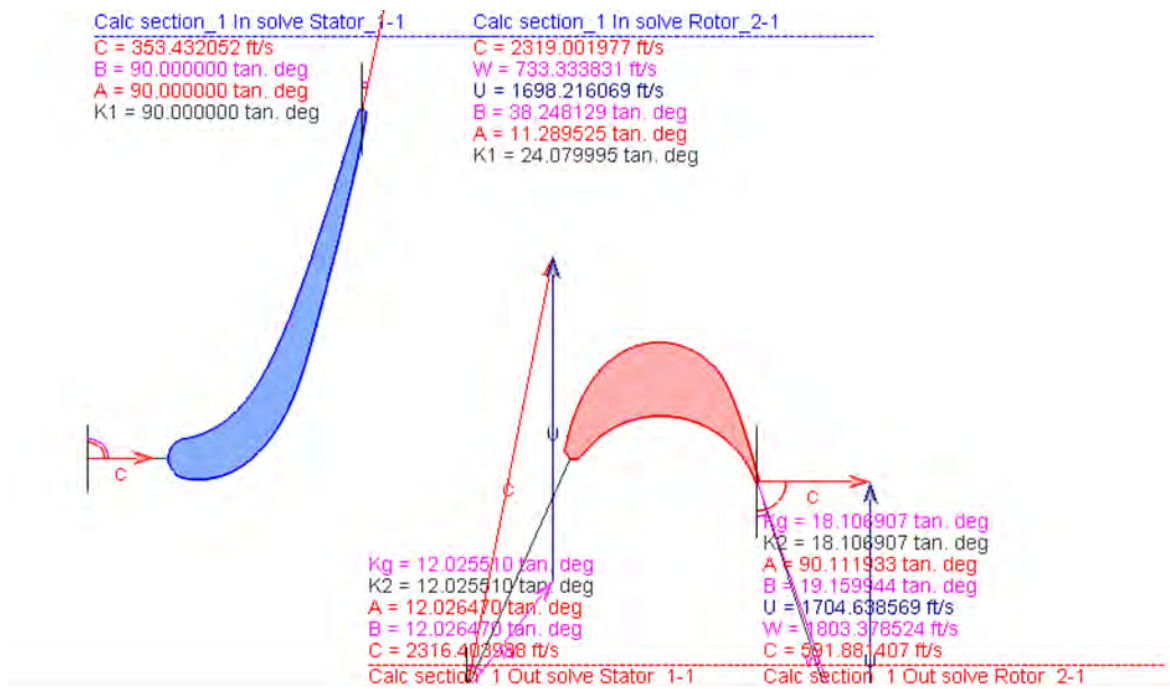


Figure 38: Velocity Triangles of The First Stage from Hub Section

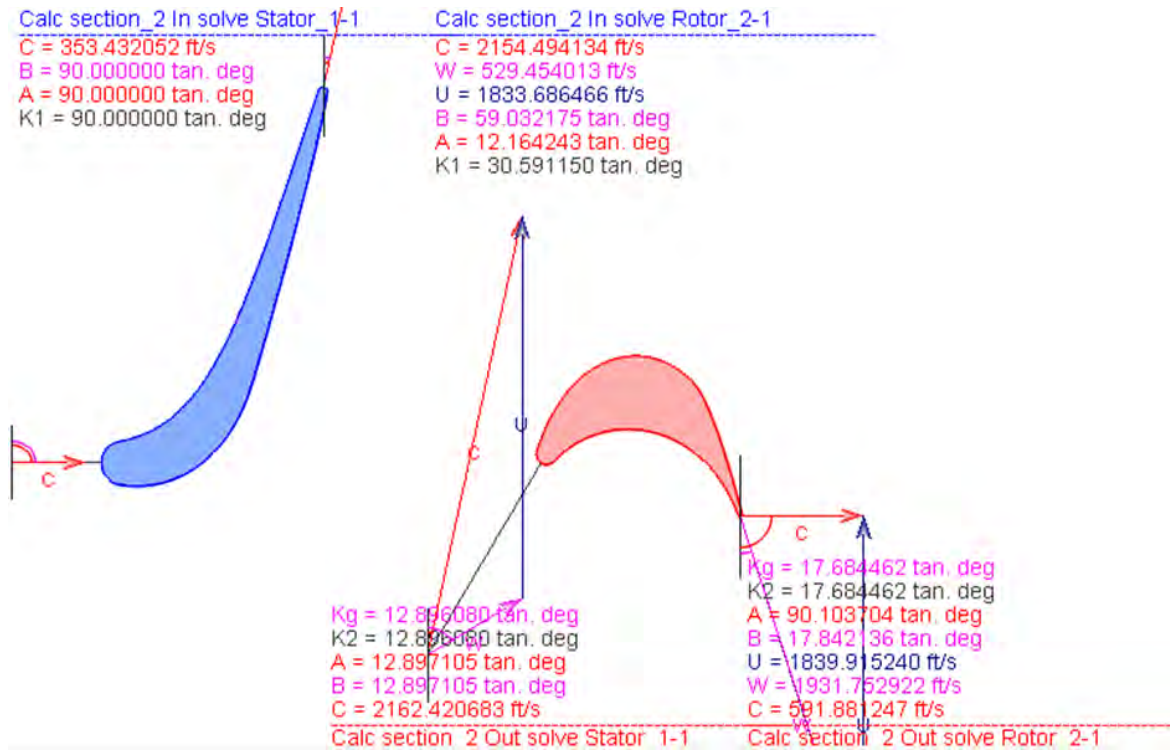


Figure 39: Velocity Triangles of The First Stage from Mean Section

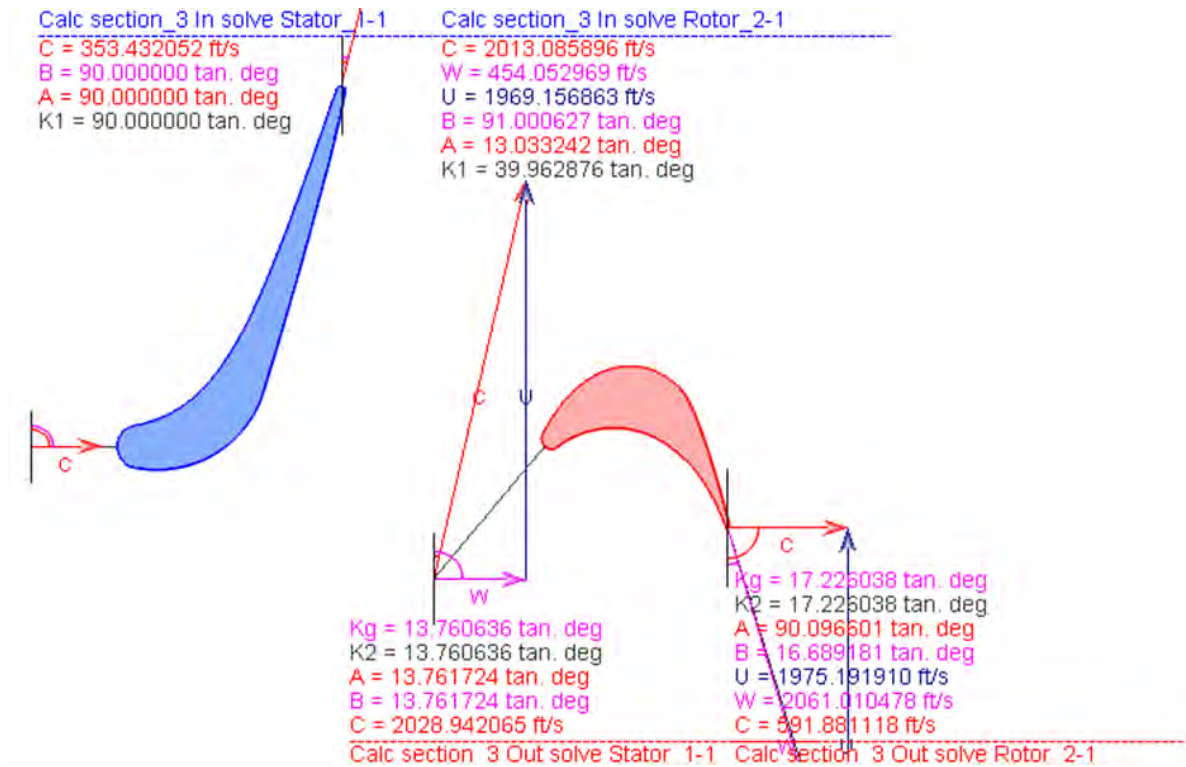


Figure 40: Velocity Triangles of The First Stage from Tip Section

The blade design has a significant effect on pressure, temperature and mach distribution in the turbine, just as in the compressor. For this reason, the most optimal blade design that meets the turbine design criteria and satisfies the desired performance criteria is required.

In the following Figures 41, 42, 43 and 44, mach number and total pressure distribution of the blades in the last stage of the HPT is given. In the blade design process, a blade profile that provides a smooth pressure and mach distribution by minimizing sudden pressure drops and flow separation is created.

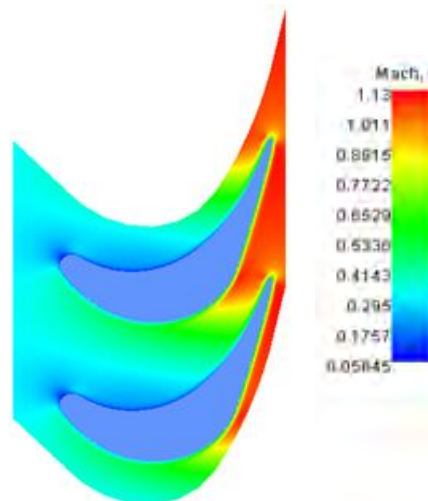


Figure 41: Stator Blade Mach Number Distribution

When the mach distribution of the stator is examined, it is seen that the distribution is smooth and the maximum mach number is in the ideal value range. Stator maximum tip mach number is about 1.1.



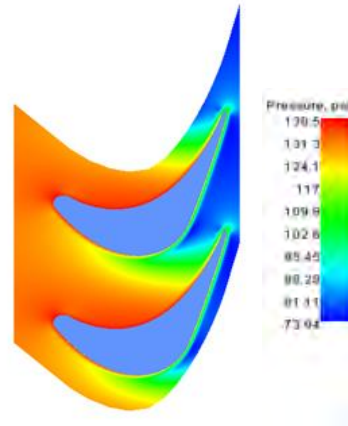


Figure 42: Stator Blade Total Pressure Distribution

It is shown that in the sections where the flow velocity decreases, the total pressure increases and also the desired pressure values are obtained throughout the stator.

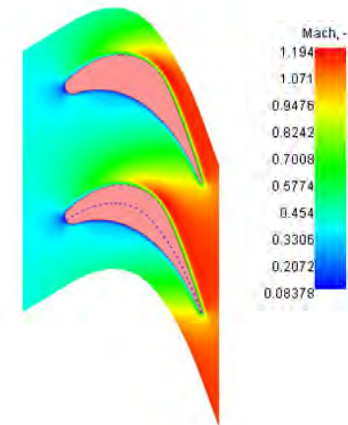


Figure 43: Rotor Blade Mach Number Distribution

When compared with the typical values found in the literature research, it is determined that mach number values is consistent with the typical value and also no seperation of flow on the blade is observed.

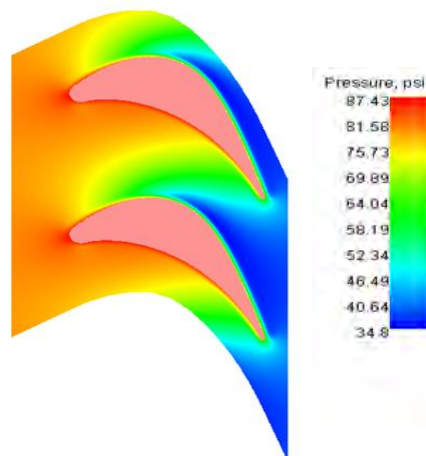


Figure 44: Rotor Blade Total Pressure Distribution

As can be seen, the total pressure in the last stage is in the range of 35-40 psi as expected. The pressure distribution throughout the blade is smooth and sudden pressure drops are minimized.

After the blade design is completed, the rotor and stator 3D designs of the last stage created in AxSTREAM and the 3D design of HPT are as shown in Figure 45 and 46 below, respectively.

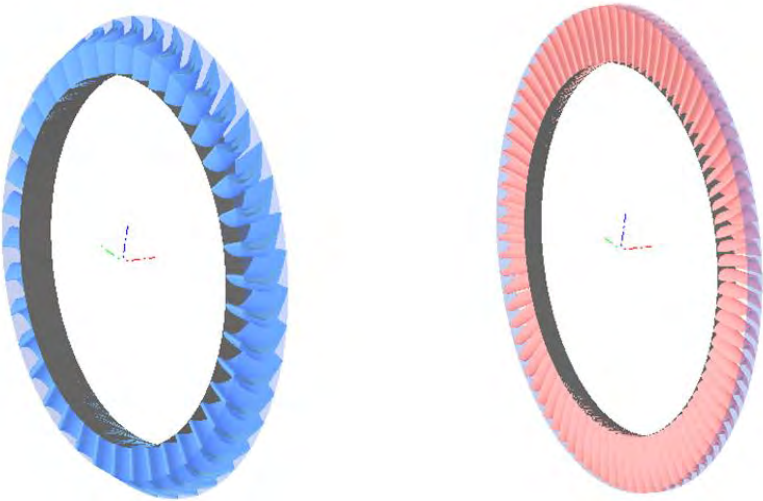


Figure 45: Rotor (right) and Stator (left) Design of The Last Stage

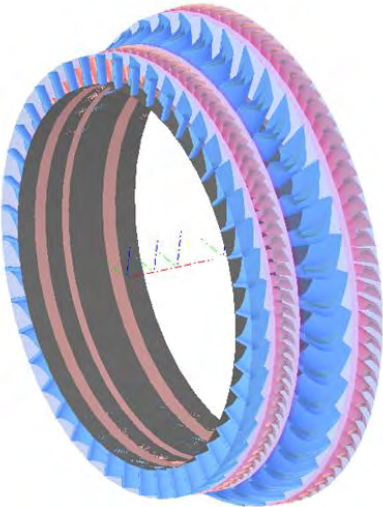


Figure 46: 3D Design of the HPT

In Table 40, detailed design parameter values are given. When these parameters are examined, it is clearly seen that performance and geometric results are consistent with typical value.

Both gas and steam turbines can be used to determine the average efficiency value for each stage using the Smith Chart given in Figure 47.

Table 40: Detailed Design Parameters of HPT

Variables	STAGE 1		STAGE 2	
	Stator	Rotor	Stator	Rotor
Aspect Ratio	0.72	1.61	1.17	2.48
Number of Blades	44	98	40	86
Solidity	1.36	1.43	1.35	1.43
Max Mach Number	0.93	0.91	1.1	1.18
Loading Coefficient	1.78	1.95	1.83	1.80
Zweifel Coefficient	0.78	0.80	0.79	0.79
Reaction	0.38	0.38	0.49	0.49
Flow Coefficient	0.48	0.45	0.61	0.55
Inlet Metal Angle	90	39.9	42.7	53.6
Outlet Metal Angle	12.0	17.2	12	19.8
Stagger Angle (tan.deg)	60.8	7.3	33.5	9.4
Stage Pressure Ratio	2.2		3.16	
Hub to Tip Ratio	0.87	0.86	0.85	0.77
Turbine Rotor Inlet Temperature [°R]	-	3535	-	2620
AN <sup>2</sup> (in <sup>2</sup> .rpm <sup>2</sup> )	3.85x10 <sup>10</sup>	4.1x10 <sup>10</sup>	4.43x10 <sup>10</sup>	8.15x10 <sup>10</sup>
Mean Radius (in)	23.72	23.74	23.84	25.24
Exit Mach Number	0.42			

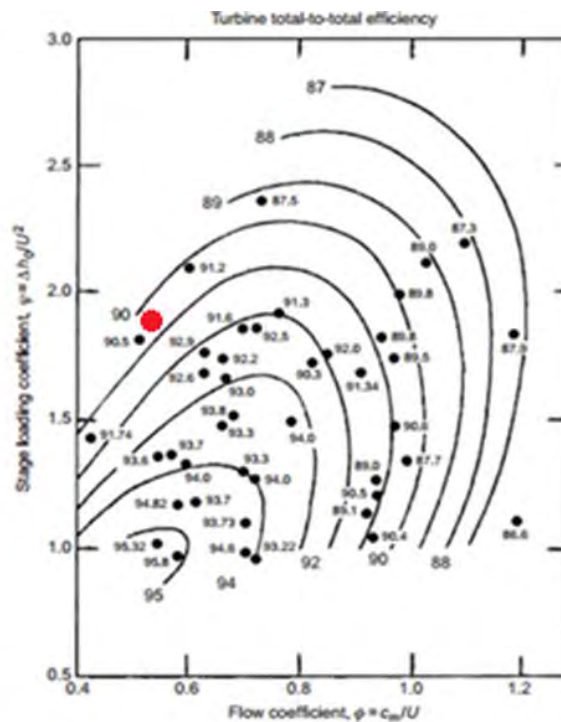


Figure 47: Smith Chart for Turbine Efficiency

In this chart, efficiency is calculated as a function of flow coefficient and stage loading factor. As a result of the performance analysis, it is seen that when the efficiency value calculated in AxSTREAM is compared with the efficiency value determined from the smith chart, these two values are very close to each other. In AxSTREAM average flow coefficient is approximately 0.57 and average loading factor is almost 1.92. As indicated by red point in Figure 47, average efficiency value is approximately 0.9 and efficiency value calculated from the AxSTREAM is 0.89 as given in Table 40.

#### 4.4.2. Axial Low-Pressure Turbine Design

In the baseline engine, low pressure turbine has 4-stages. As in the compressor design for a compact turbofan engine, some studies are examined to see if the reduction can be made in turbine stages. In this process, both 3-stage and 4-stage compressor design points are created for preliminary design using the same boundary condition values obtained from the GasTurb. The total efficiency values are compared for these design points and the optimal number of stages that provide the performance criteria for the turbine and meet the geometric constraints are selected. In addition, by examining the performance maps, it is tried to determine whether the stage reduction has negatively affected, especially on the pressure and the efficiency.

As a result of the researches and analyzes, it is determined that 3-stage turbine works more efficiently than 4-stage turbine for the same performance criteria. Furthermore, 3-stage turbine design provides weight reduction resulting in more compact engine design. Because of these reasons, 3-stage axial turbine design is selected to be used in TULPAR engine.

TULPAR engine has 3-stage axial low pressure turbine. The same process followed in HPT design is applied to the axial low pressure turbine design. Thermodynamic properties and geometrical dimensions for the selected point as a result of preliminary design are given in the Table 41.

Table 41: Preliminary Design Properties

Thermodynamic Properties and Geometrical Dimensions			
Parameters	Value	Parameters	Value
Total pressure at inlet	42.1 psi	Efficiency	0.88
Total temperature at inlet	2242.4 °R	Hub diameter	42.72 in
Total pressure at outlet	12.94 psi	1 <sup>st</sup> stage blade height	5.39 in
Total temperature at outlet	1704.9 °R	Max. blade height	10.71 in
Mass Flow Rate	181.1 lbm/s	Number of stages	3
Shaft Rotational Speed	6524 rpm	Max tip diameter	66.15 in

TULPAR engine has 3-stage LPT. The velocity triangles for each stage are obtained, but only the velocity triangles of the first stage are shown in Figure 48, 49 and 50. For each rotor and stator, the velocity triangles are obtained from three different sections: hub, mean, and tip section.

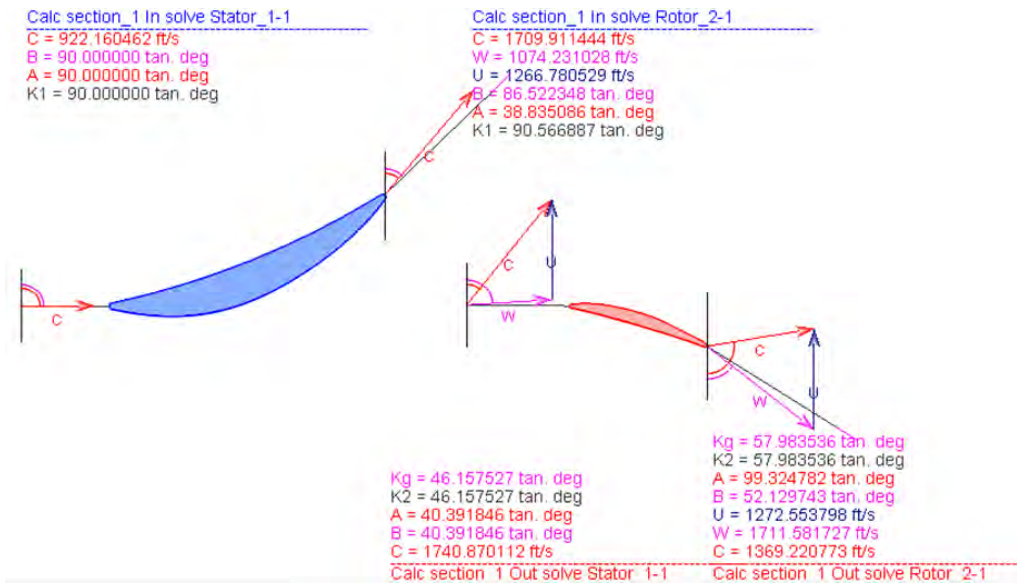


Figure 48: Velocity Triangles of The First Stage from Hub Section

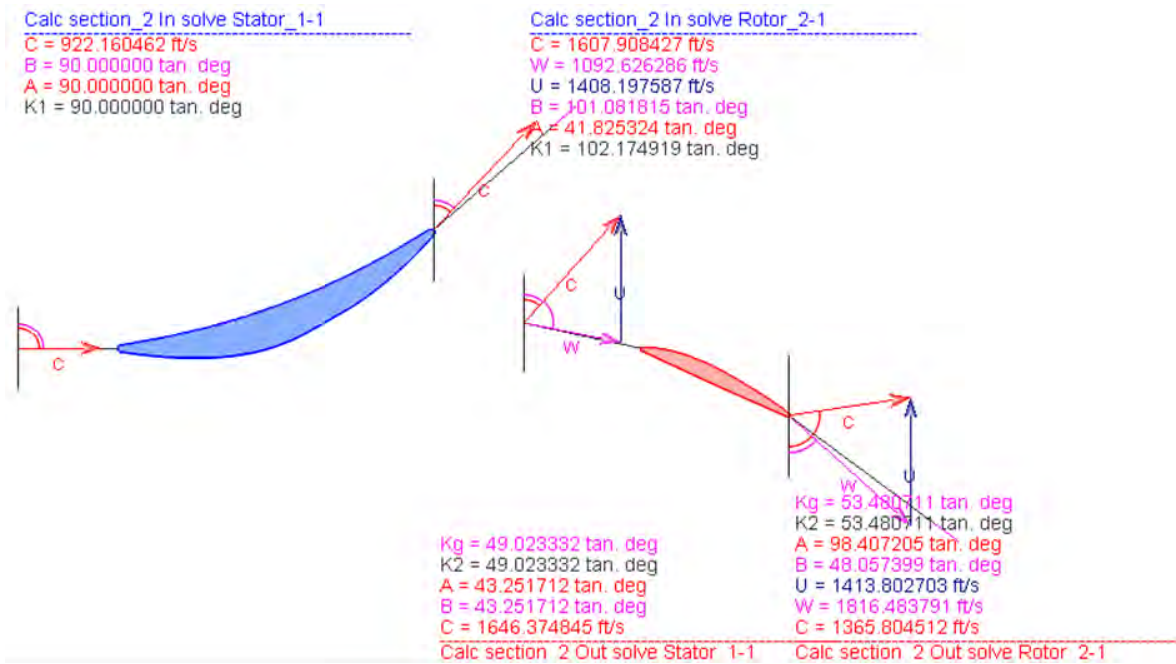


Figure 49: Velocity Triangles of The First Stage from Mean Section

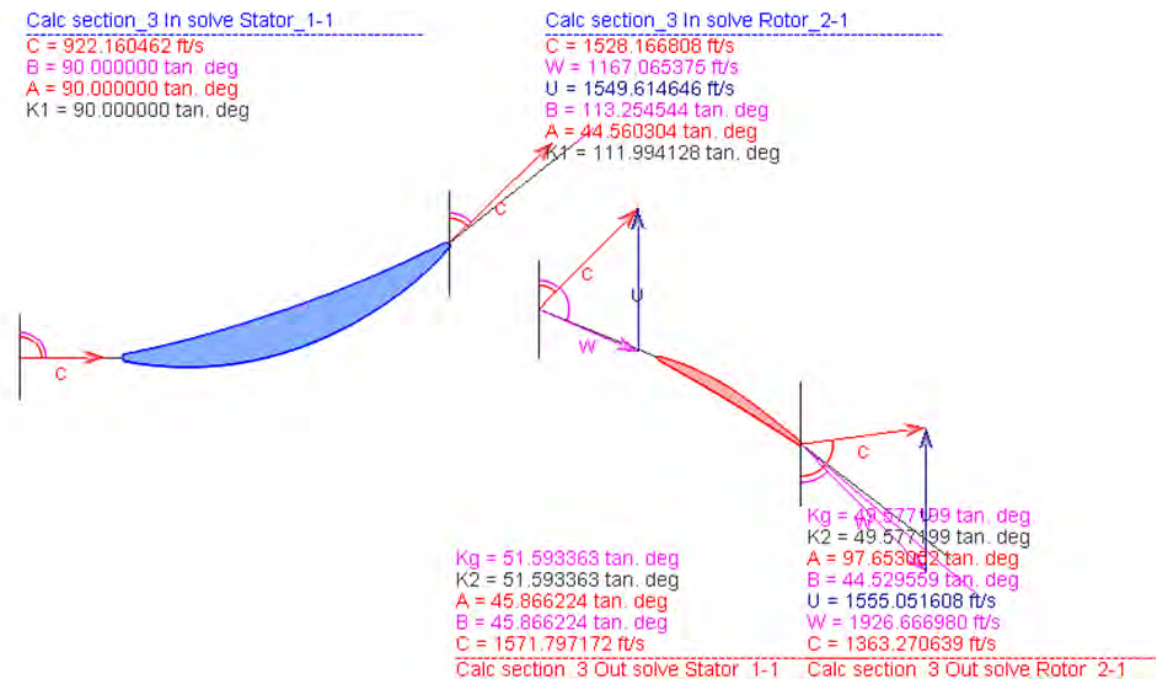


Figure 50: Velocity Triangles of The First Stage from Tip Section

As a result of analysis in AxSTREAM, detailed design parameters obtained from AxSTREAM for each stage in Low Pressure Turbine are given in the following table. When each parameter is compared with typical values shown in Table 42, it is seen that the results are consistent with typical values.

Table 42: Detailed Design Parameters of LPT

Variables	STAGE 1		STAGE 2		STAGE 3	
	Stator	Rotor	Stator	Rotor	Stator	Rotor
Aspect Ratio	0.91	1.98	1.19	2.51	1.53	3.13
Number of Blades	40	89	40	86	39	82
Solidity	1.33	1.43	1.35	1.43	1.34	1.43
Max Mach Number	0.98	1.06	0.99	1.1	1.03	1.13
Zweifel Coefficient	0.78	0.78	0.79	0.81	0.78	0.79
Reaction	0.43	0.43	0.40	0.40	0.36	0.36
Flow Coefficient	0.70	0.95	0.62	0.90	0.48	0.78
Inlet Metal Angle	90	87.8	90	82.41	88	80.48
Outlet Metal Angle	46.16	57.98	41.57	62.00	39.79	65.44
Stagger Angle (tan.deg)	21.9	16.3	30.4	10.2	33.6	7.5
Stage Pressure Ratio	1.51		1.47		1.40	
Hub to Tip Ratio	0.82	0.82	0.81	0.77	0.76	0.71
Turbine Rotor Inlet Temperature [°R]	-	2200	-	1972	-	1783
AN <sup>2</sup> (in <sup>2</sup> .rpm <sup>2</sup> )	3.12x10 <sup>10</sup>	3.28x10 <sup>10</sup>	3.48x10 <sup>10</sup>	4.62x10 <sup>10</sup>	4.88x10 <sup>10</sup>	6.61x10 <sup>10</sup>
Mean Radius (in)	24.70	24.73	24.85	25.60	25.73	26.80
Exit MachNumber	0.4					

The rotor and stator 3D designs of the last stage created in AxSTREAM and the 3D design of LPT are as shown in Figure 51 and 52, respectively.

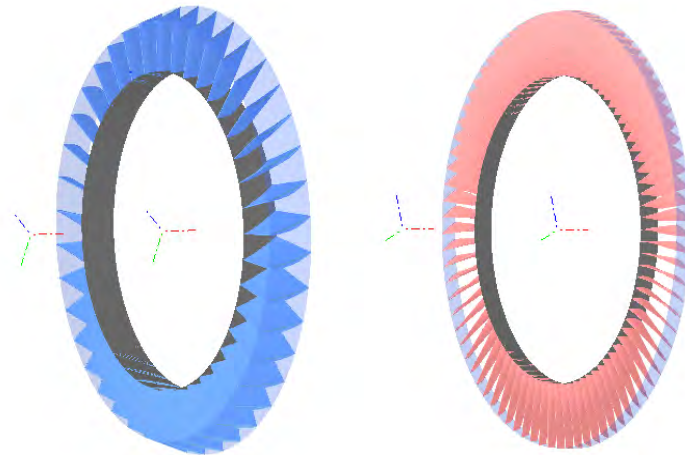


Figure 51: Rotor (right) and Stator (left) Design of The Last Stage

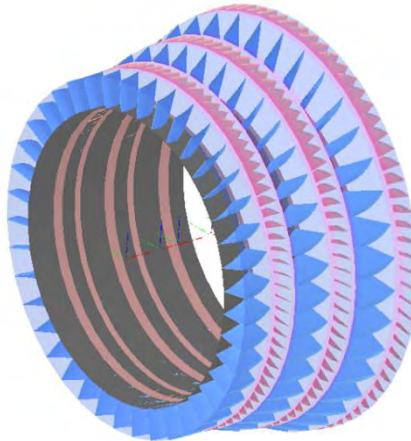


Figure 52: 3D Design of the LPT

#### 4.5. STRESS CALCULATIONS FOR TURBOMACHINERY BLADES

In the previous sections, streamline analyzes are performed for turbomachinery by considering aerodynamic design criteria and temperature, pressure, mach number distributions are obtained and blade designs are created. In addition to aerodynamic criteria, rotor and stator blades at each stage of the Compressor and also rotor blades at each stage of the Turbine are exposed to variety of stresses such as thermal, bending, vibrational and centrifugal because of high rotational speed and high temperature [5]. However, among these stresses, the most dominant and most critical stress for turbomachinery design is centrifugal stress caused by high rotational speed. Consequently, If the allowable stress value of the selected material for the blade is greater than the calculated stress value, rotor and stator blades are in safety margin under centrifugal loading [5]. Equation 4.3 is used for calculation allowable centrifugal stress on Turbomachinery blades. [13]

$$\sigma_c = \rho_{blade} \frac{\omega^2 A}{4\pi} \left(1 + \frac{A_t}{A_h}\right) \quad (4.3)$$

Where;

- $\sigma_c$ , Design Centrifugal Stress (psi),
- $\rho_{blade}$ , Blade material density (lbm/in<sup>3</sup>),
- $\omega$ , Angular Speed (rpm),
- A, Flow Area,
- $\frac{A_t}{A_h}$ , Blade Taper Ratio.

The taper ratio value is between 0.8 and 1 for turbomachinery component [5]. Taper Ratio for each blade is calculated by AxSTREAM. Material Selection for each component are given detailed in material section. CFRP is selected to be used in Fan Blade Design as a material to reduce the weight and increase the strength. The stress analysis results due to centrifugal loading and parameter specified in equation is given in Table 43.

Table 43: Blade Structural Analysis of 1<sup>st</sup> Stage Rotor in LPC (Fan)

Design Parameter- Rotor, 1 <sup>st</sup> Stage of Fan	Value
Material Density, $\rho_{blade}$	0.058 lbm/in <sup>3</sup>
Blade Taper Ratio	0.82
Flow Area	1550.0 in <sup>2</sup>
Fan Angular Speed, $\omega$	6524 rpm
Allowable Yield Strength	109793.6 psi
Design Centrifugal Stress, $\sigma_c$	57336.3 psi

Ti-45Al-8NB is selected to be used in HPC Blade Design as a material to reduce the weight and increase the strength. The stress analysis results due to centrifugal loading and parameter specified in equation is given in Table 44.

Table 44: Blade Structural Analysis of 1<sup>st</sup> Stage Rotor in HPC

Design Parameter- Rotor, 1 <sup>st</sup> Stage of HPC	Value
Material Density, $\rho_{blade}$	0.14 lbm/in <sup>3</sup>
Blade Taper Ratio	0.85
Flow Area	1023.0 in <sup>2</sup>
Fan Angular Speed, $\omega$	8850 rpm
Allowable Yield Strength	51865.5 psi
Design Centrifugal Stress, $\sigma_c$	27574.6 psi

As in the compressor, the critical stress value in the turbine is due to centrifugal loadings is caused by high rotational speed. Flow Area in Turbine is gradually increasing so that the flow can expand. For this reason, the rotor in the last stage has the largest flow area. The stress analysis results for last stage in HPT and LPT due to centrifugal loading is given in Table 45 and Table 46. TMS-238 is selected to be used in HPT and LPT Blade Design as a material to reduce the weight and increase the strength.

Table 45: Blade Structural Analysis of Last Stage Rotor in HPT

Design Parameter- Rotor, Last Stage of HPT	Value
Material Density, $\rho_{blade}$	0.33 lbm/in <sup>3</sup>
Blade Taper Ratio	0.84
Flow Area	1041.6 in <sup>2</sup>
Fan Angular Speed, $\omega$	8850 rpm
Allowable Yield Strength	150984.3 psi
Design Centrifugal Stress, $\sigma_c$	65300.3 psi

Table 46: Blade Structural Analysis of Last Stage Rotor in LPT

Design Parameter- Rotor, Last Stage of LPT	Value
Material Density, $\rho_{blade}$	0.33 lbm/in <sup>3</sup>
Blade Taper Ratio	0.85
Flow Area	1705 in <sup>2</sup>
Fan Angular Speed, $\omega$	6524 rpm
Allowable Yield Strength	150984.3 psi
Design Centrifugal Stress, $\sigma_c$	99983.3 psi

4.6. NOZZLE GUIDE VANE COOLING

Turbine inlet temperature (TET) is an important parameter for overall engine efficiency. Also, the thermal efficiency can be increased depending upon increasement of TET value. So, the ability to operate at high temperatures is very crucial in enhancing the performance of jet engines but high turbine inlet temperature values are not sustainable for long periods without enough amounts of cooling. So, the cooling of nozzle guide vane (NGV) is an important design problem [29].

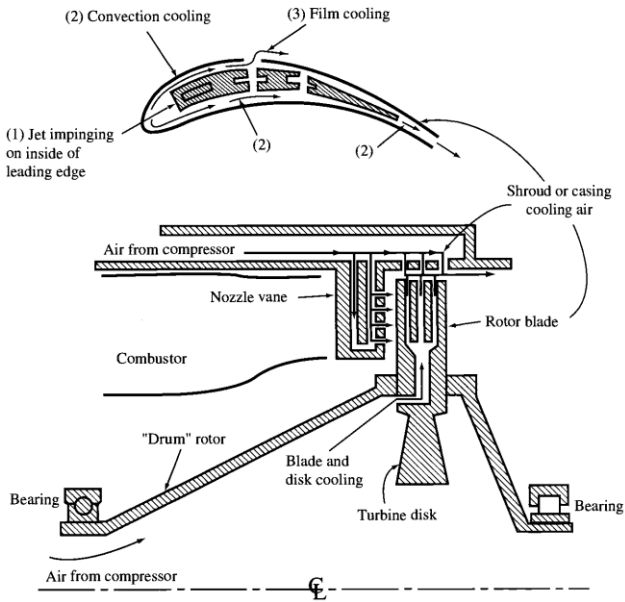


Figure 53: Schematic of air-cooled turbine [30]



The schematic of air-cooled turbine is shown in Figure 53. As seen in Figure 53, while first-stage stator blades are exposed to high temperature values which include hot spots from the combustor, first-stage rotor blades are colder due to dilution of hot gases with first-stage stator cooling air. Because distribution of the temperature is random in a circumferential direction at turbine inlet. So, this situation causes the first stator vanes to be designed for maximum temperature values (hot spots). The temperature gradually decreases in each stage, depending on the amount of cooling air. [31]

Approximately, 20% of the compressor discharge flow is used for cooling on new aircraft engines. The usage of large quantity of flow have two main disadvantages which lead to reduce advantages of high TET. These main disadvantages are reducing the capability of the turbine to drive the compressor and aerodynamic losses (mixing with the mainstream of turbine air flow). So, cooling air must be used as little as possible [31].

There are several cooling mechanisms which are used for fine blade cooling in the turbine. The cooling mechanisms which are illustrated in Figure 54 are;

- Convection cooling,
- Impingement cooling,
- Film cooling,
- Full-coverage film cooling,
- Transpiration cooling.

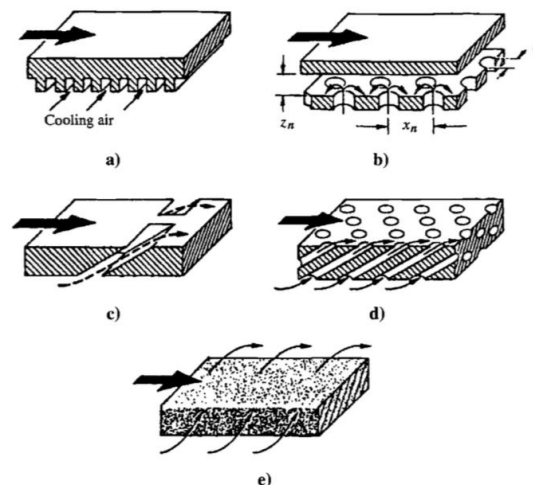


Figure 54: Turbine cooling methods a) convection cooling, b) impingement cooling, c) film cooling, d) full-coverage film cooling, e) transpiration cooling [30]

The life of hot blades are primarily limited by these design parameters [29]. These design parameters are creep, oxidation, corrosion, erosion and thermal fatigue [29-31]. Thus, choosing the suitable material for hot blades and determining the proper cooling method are vital so that the turbine inlet temperature can be kept as high as possible. Because TET exceeds melting temperature for many materials in general. So, materials are covered with special-high temperature coatings (TBC) because the blades can not retain their characteristics for very long time. [29-31] The most commonly used materials are nickel or cobalt based superalloys coated with yttria stabilized zirconia oxide ceramics (thermal barrier coating (TBC)). [34] The advantages of using TBC are reducing metal surface temperature, reducing heat transfer rate and providing protection of the metal against oxidation. As a result, the usage of TBC has allowed an increase approximately 100K in TET value [31-32-33]

Heat transfer mechanisms that should be considered for cooling systems can be divided 3 main headings. These mechanisms are very important to estimate blade surface operation temperature and corresponding material selection. These mechanisms are;

- Thermal conduction and absorption in the part,
- Convective cooling of the part inside by the cooler,
- Heat transfer to surface from the mainstream air by convection through a viscous boundary or a film cooling layer [31].

According to literature surveys, TMS-238 was selected as a suitable material for turbine blades depending upon operational conditions for TULPAR. Also, MCrAlY was used as a thermal barrier coating. The selected materials are described in Material Selection section in detail.

Other important parameter is selecting suitable cooling method for effective cooling. Relevant cooling systems for ranges of turbine-inlet temperatures are shown in Figure 55.

Temperature range, T	Cooling methods commonly used
$T < 1200\text{K}$	No cooling required
$1200\text{K} < T < 1450\text{K}$	Internal convective system
$1450\text{K} < T < 1600\text{K}$	Convective systems augmented by rows of film cooling holes
$1600\text{K} < T < 2000\text{K}$	Combinations of convection, impingement systems and film cooling
$T > 2000\text{K}$	Some kind of transpiration cooling

Figure 55: Relevant cooling systems for ranges of turbine inlet temperatures [5]

In our design, the turbine entry temperature value was calculated as an approximately 2000 K. As seen in Figure 55, transpiration cooling and the combinations of convection, impingement systems and film cooling methods can be suitable for TULPAR. So, these methods were evaluated in detail. Also, the transpiration and film cooling methods have good effectiveness when compared with other cooling methods. [35]

Film cooling is the application of internal cooling streams onto the outer skin of the components to provide a cooling layer that reduces a heat flow [33]. In this method, cooling air is passed through a series of small holes (The diameter of the film holes range  $\sim 0.5\text{--}1$  mm) inclined at an angle to the surface. This cooling system is widely used in contemporary military and civil turbojet engines. However, it is necessary to limit the amount of cooling air from the compressor in order to minimize the loss of efficiency in the plant. [5-35]

On the other hand, transpiration cooling system is also known as one of the better cooling technologies. [35] Transpiration cooling system is combined of attached porous wall over the blade surface and film cooling process. The coolant may emerge from very small pores ( $\sim 10\text{--}100$   $\mu\text{m}$ ) of a porous surface. [5] The benefit of using this system is that it provides better cooling efficiency with less amount of coolant mass flux than conventional cooling systems. However, keeping the micropores unclogged is the main disadvantage of using transpiration system. Also, the practicality of transpiration cooling system is effected from other material characteristics (such as oxidation, resistance, material life mentioned before). Besides, the static pressure drop across porous foam is larger and coolant pressurized requirement is more compeller [5-35]

In addition to this, the material improvements, cooling effects of film cooling and TBC are shown in Figure 56 for different years. As seen in this figure, it is expected that the turbine entry temperature will be approximately 3780 R in 2025 depending upon material improvements. Besides, it is predicted that the usage of film cooling with TBC will increase.

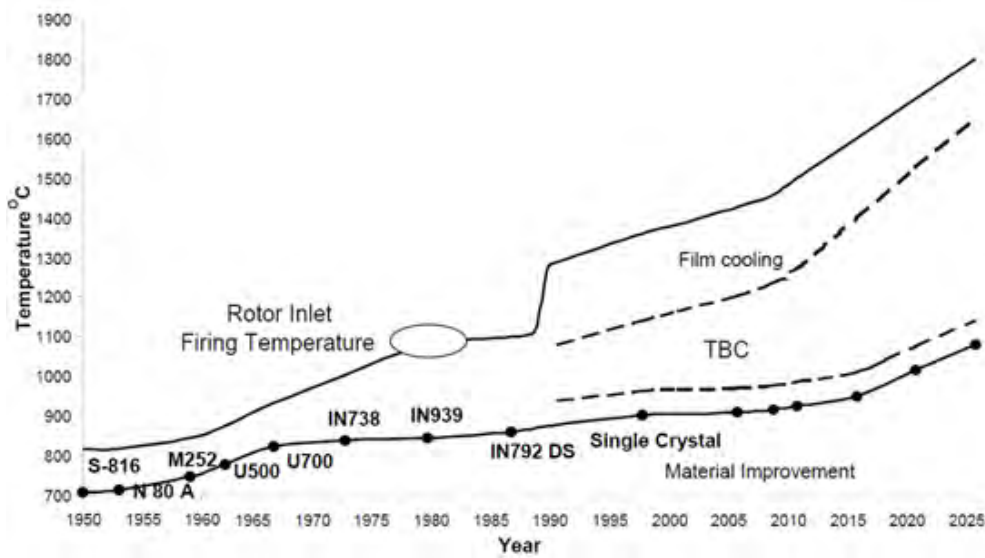


Figure 56: The material improvements and cooling effects of film cooling and TBC [34]

According to literature surveys, the combination of convection, impingement systems and film cooling methods was selected for TULPAR as a cooling method. Also, modern multi-pass turbine blade cooling technology was selected for more effective cooling.

In general, there are four different film cooling hole geometries. The typical types of shaped film holes are shown in Figure 57 [37].

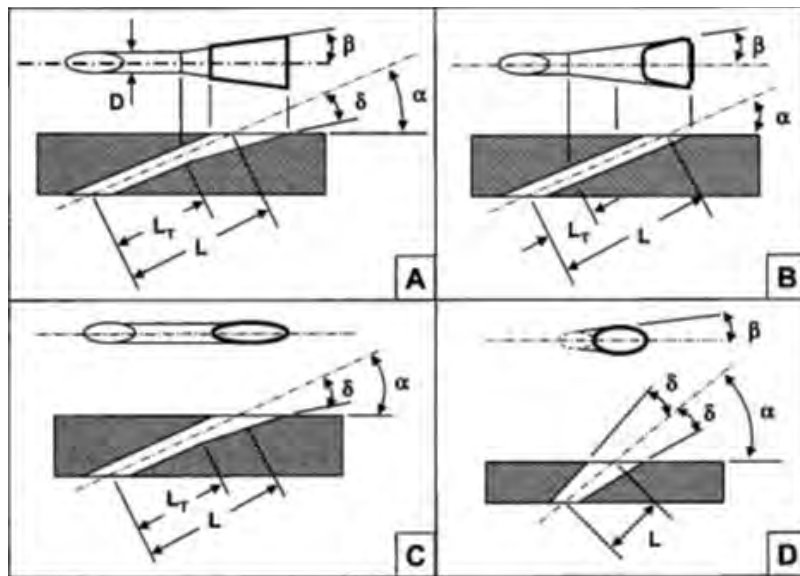


Figure 57: The types of shaped film holes [37]

In this types of shaped film holes, the type-A-shaped hole was selected for our design. Because there is no separation observed at the hole exit. Also, this type hole exhibits no vortex because of laidback diffusion which allows the diffused jet to fit on the surface better [37].

According to literature surveys, the blade cooling structure which was chosen in project is shown in Figure 58.

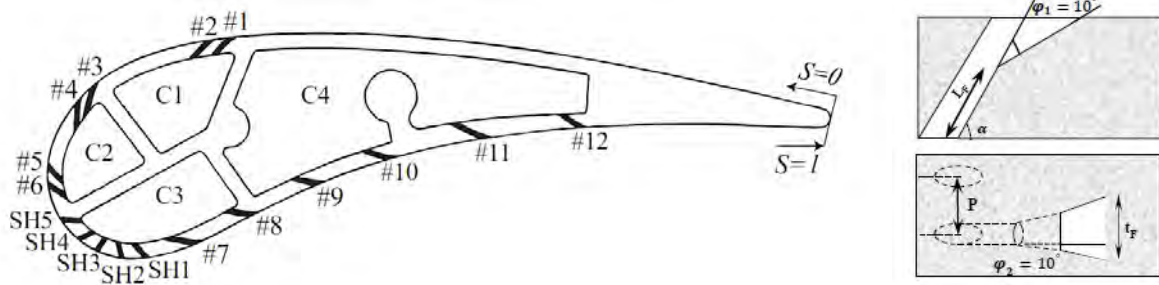


Figure 58: The nozzle guide vane geometry [36]

Also, the geometric dimensional rates and angle values of each cooling holes for this blade geometry are shown in Table 47.

Table 47: Cooling hole parameters for the suction and pressure side cooling rows. [36]

Hole number	T <sub>F</sub> /P	L <sub>F</sub> /D	α values
1	0.24	4.3	40
2	0.24	4.5	37
3	0.15	5.1	26.6
4	0.15	4.9	31.7
5	0.18	4.05	41.4
6	0.11	4.03	41.3
7	0.19	5.3	28.1
8	0.24	4.7	35.9
9	0.23	4.6	37.3
10	0.26	4.72	36.4
11	0.26	4.72	36.1
12	0.23	4.3	40.7

#### 4.7. MIXER DESIGN

A lobed mixer was used in TULPAR engine to mix the cold air from the bypass and hot exhaust gases from the core. Compared to other types of mixers, the lobed mixer can mix the primary and secondary streams with a higher effectiveness while inducing a lower pressure loss. Lobed mixers increase the mixing of the two streams with the vortices they create on both sides [38-42].

In addition, chevron nails and sword-like lobe channels placed in lobe peaks accelerate the mixing and effectively reduce the temperature of the mixing flow near the channel. With minimum pressure losses [40]. The nail length can be selected between 2,16 inches to 3,54 inches. The mixer with the nail angle ( $\alpha$ ) of 2.5 degrees and an area ratio between the channels of 2.64 improves the pumping ratio and the total pressure recovery coefficient [41].

As a result, in the TULPAR engine a lobed mixer which has chevron nails and sword like lobe channels was designed. While creating geometric dimensions, typical basic lobed mixer measurements which were adapted to the measurements of TULPAR engine dimensions were used. [38-39]. Schematic representations of the geometric dimensions are given in Figure 59 and the values used are given in Table 48.

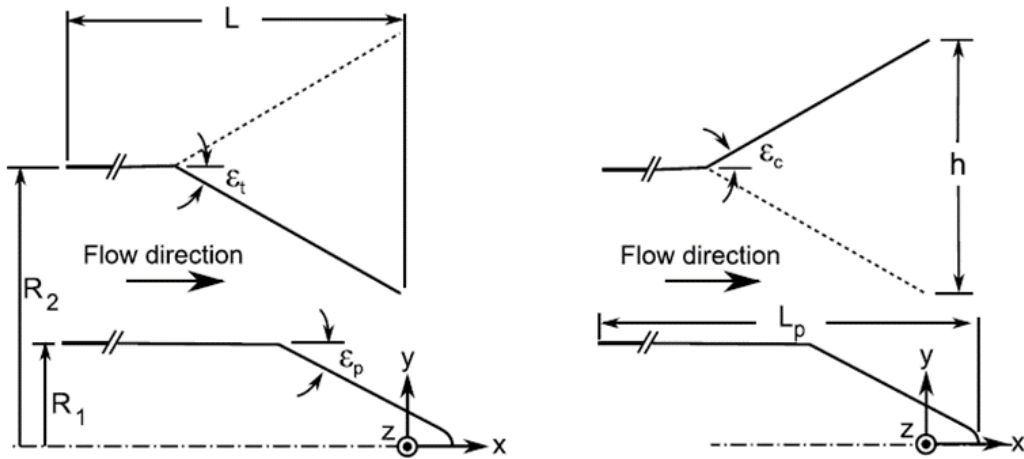


Figure 59: Schematic representation of geometrical dimensions [38]

Table 48: Geometric dimensions of the designed mixer

Parameter	Values
Inner radius R1	11,9 in
Outer radius R2	26 in
Lobe height h	10,21 in
Lobe angular spacing	30°
Number of lobes	12
Mixer axial length L	40,86 in
Plug axial length Lp	47,12 in
Lobe width b	5,37 in
Inner penetration angle $\epsilon_t$	12,5°
Outer penetration angle $\epsilon_c$	12,5°
Plug cone half-angle $\epsilon_p$	23°
Chevron nail angle $\alpha$	2,5°
Chevron nail length l	2,16-3,54 in

3D model of the TULPAR engine mixer which is designed with the Siemens NX software is given in the Figure 60 below. In addition to this, the cross-sectional view of mixer is given in Figure 61. The technical drawing of the mixer are given in detail Appendix A.

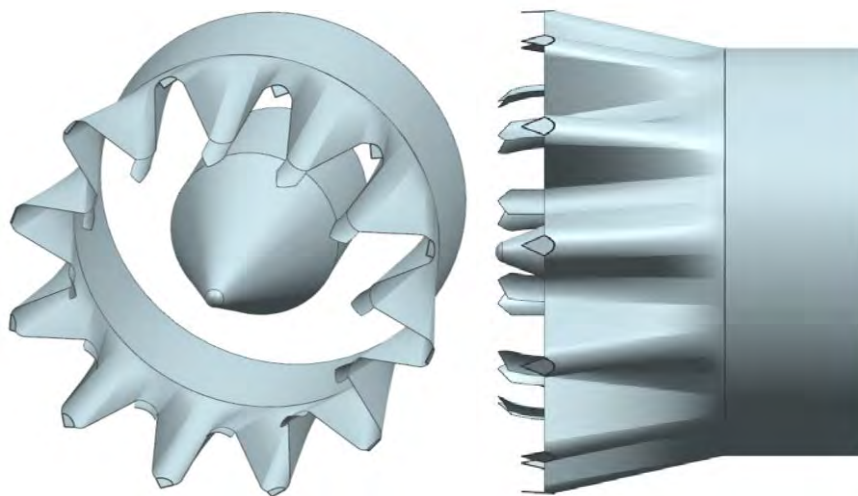


Figure 60: 3D model of the mixer

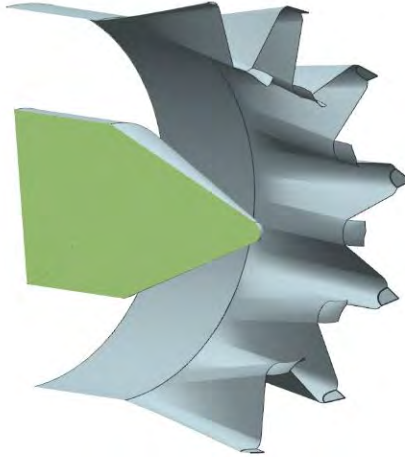


Figure 61: Cross sectional view of the mixer

#### 4.8. FULLY VARIABLE AREA NOZZLE

The exhaust nozzle is the component that provides the necessary thrust force. The aim of the nozzles is to increase the speed and correct the flow of the exhaust gas before leaving the engine. The most important criterion in nozzle design is to expand the exhaust gas so that it is equal to the atmospheric pressure before opening to the atmosphere. The maximum uninstalled thrust value can be obtained in this way.

To increase the speed of exhaust gas by keeping pressure loss at minimum, to be able to provide appropriate thrust for off design situations, to keep exit pressure value as close as possible to atmospheric pressure value, to suppress jet noise and having a long-life cycle, low cost and minimum weight when doing all these, constitute ETU V-TULPAR's design goals.

##### 4.8.1. Nozzle Type Selection

Among two nozzle types, Convergent and Convergent-Divergent (C-D), convergent-divergent nozzles are generally used under supersonic conditions. The choice of convergent-divergent nozzle, which has more complexity and weight, needs to be mathematically accounted. According to Saeid Farokhi [5], this choice should be made according to the following Equation 4.4 based on gross thrusts.

Adiabatic and isentropic assumptions are made in the following equation.

$$\frac{F_{g-condi}}{F_{g-conv}} = \sqrt{\frac{1 - (NPR)^{-\frac{\gamma-1}{\gamma}}}{\frac{\gamma-1}{\gamma+1}}} \times \frac{\gamma}{\gamma + \left(1 - \left(\frac{\gamma+1}{2}\right)^{\frac{\gamma}{\gamma-1}} \times \frac{1}{NPR}\right)} \quad (4.4)$$

Where;

- NPR, Nozzle pressure ratio ( $P_{07}/P_0$ ),
- $\gamma$ , Ratio of specific heats.

When the TULPAR nozzle pressure ratio is taken as 8.62 for the on-design condition, the gross thrust ratios are calculated as 1,075 and a nozzle thrust gain of 7.5% is observed. Convergent-divergent nozzle is recommended for more than 5.5% gross thrust gains [5]

A fully variable area nozzle is used to achieve sufficient performance for other off-design conditions from the convergent-divergent nozzle designed for the cruise design point. Nozzle throat area and divergent exit area are varied independently to achieve fully optimized thrust for all flight conditions [43]. At the same time, the use of fully variable area nozzle improves engine start-up. Increasing the nozzle throat area reduces the back-pressure on the turbine and increases the expansion ratio. In this way, the turbine power required to start the engine can be achieved with a lower turbine inlet temperature [4]

Noise reduction is achieved when flaps are used in the divergent part in the design of the fully variable nozzle. In take-off condition, the divergent area of the nozzle is minimum, and the divergent flaps are bent inwards. The hinge part between the flaps is folded inward so that the nozzle outlet become lob-like. Schematic representation of the nozzle is shown in Figure 62. This shape reduces the noise with negligible loss of the nozzle thrust [44]. Noise reduction is provided by deformation on the jet streams. The relationship between the nozzle geometry and the spectrum is similar to the chevron nozzle.

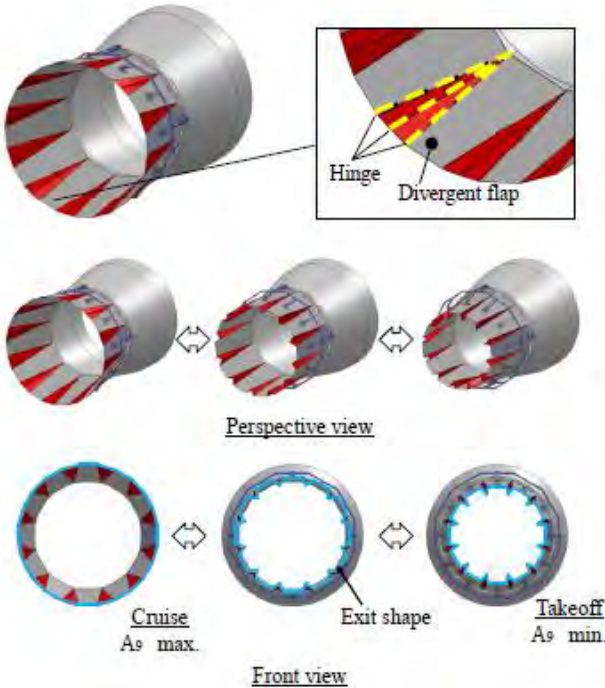


Figure 62: Schematic representation of the opening and closing mechanism of nozzle [44]

**4.8.2. Nozzle Geometry Calculations**

MATLAB code, which is prepared by TULPAR design team, is used to create the nozzle geometry. The code was derived from the isentropic nozzle relationships and the Mattingly Aircraft Engine Design source. To achieve the validation of the MATLAB code, the outputs obtained in the on-design case are compared to the outputs in the GasTurb program. The following Table 49 shows the validation results.

Table 49: Nozzle on design condition (Inputs and Outputs)

<b>Inputs</b>	Throat mass flowrate $\dot{m}_g$ (lb/s)	618,3
	Ambient Pressure $P_0$ (psi)	1,492
	Throat total temperature $T_{08}$ (R)	1074,8
	Throat total pressure $P_{08}$ (psi)	12,86
	Discharge coefficient $C_d$	0,963
	Area ratio $A_9/A_8$	1,7013

MATLAB Outputs		GasTurb Outputs		% dif
Throat area A8 (ft <sup>2</sup> )	21,46	Throat area A8 (ft <sup>2</sup> )	21,49	0,13
Throat radius R8 (ft)	2,614	Throat radius R8 (ft)	2,615	0,06
Nozzle exit area A9 (ft <sup>2</sup> )	36,51	Nozzle exit area A9 (ft <sup>2</sup> )	36,57	0,14
Nozzle exit Radius R9 (ft)	3,409	Nozzle exit Radius R9 (ft)	3,412	0,09
Nozzle gross thrust coefficient C <sub>fg</sub>	0,9566	Nozzle gross thrust coefficient C <sub>fg</sub>	0,9501	0,68
Nozzle exit static pressure P <sub>9</sub> (psi)	1,59	Nozzle exit static pressure P <sub>9</sub> (psi)	1,63	2,79
Nozzle exit Mach number M <sub>9</sub>	2,0005	Nozzle exit Mach number M <sub>9</sub>	2,002	0,07
Nozzle exit velocity V <sub>9</sub> (ft/s)	2404,3	Nozzle exit velocity V <sub>9</sub> (ft/s)	2409,3	0,21

As can be seen, the output of the MATLAB code and the data of the GasTurb program are quite similar. As a result, it is said that the generated code works as desired.

#### 4.8.3. Analysis and Configurations

Calculations have been made for on-design and off-design conditions. The input values used for each condition are given in Table 50 below. These values were obtained from the GasTurb.

Table 50: Input Parameters of Each Mission Profile

Inputs	Mission Profiles			
	Cruise	Hot Day Take-Off	SLS	Transonic Pinch
Throat mass flowrate $\dot{m}_g$ (lb/s)	618,3	1544	1533,5	626,9
Ambient Pressure P <sub>0</sub> (psi)	1,492	14,7	14,7	2,65
Throat total temperature T <sub>08</sub> (R)	1074,8	866,4	935,9	920
Throat total pressure P <sub>08</sub> (psi)	12,86	31,27	29,59	12,40
Discharge coefficient C <sub>d</sub>	0,963	0,963	0,963	0,961

Calculations were performed using the inputs above. By changing the area ratio, the best two possible options have been created for each mission profile. While choosing the best option, the nozzle design goals of the ETU V TULPAR engine have been considered. The selected nozzle parameters for each mission are given in Table 51 below. [45]

Table 51: Calculated Nozzle Parameters for Mission Profiles

Parameters	Cruise	Hot Day Take-Off	SLS	Transonic Pinch
Area Ratio A9A8	1,76	1,021	1	1,2880
Throat Area A8 (ft <sup>2</sup> )	20,67	20,80	20,78	20,07
Effective Throat Area A8e (ft <sup>2</sup> )	21,46	21,60	21,57	20,85
Nozzle Exit Area A9 (ft <sup>2</sup> )	37,77	22,05	21,57	26,85
Nozzle Gross Thrust Coefficient C <sub>fg</sub>	0,9568	0,9404	0,9391	0,9535
Velocity Coefficient C <sub>v</sub>	0,9885	0,9268	0,8489	0,9791
Actual Nozzle Gross Thrust F <sub>g</sub> (lbf)	46715	72795	66426	38384
Ideal Nozzle Gross Thrust F <sub>gi</sub> (lbf)	48824	77408	70734	40256
Actual Exit Mach Number M <sub>9</sub>	2,0401	1,1643	1	1,6422
Ideal Exit Mach Number M <sub>9i</sub>	2,0835	1,2838	1,2816	1,6965
Ambient Pressure P <sub>0</sub> (psi)	1,4920	14,70	14,70	2,649
Nozzle Exit Pressure P <sub>9</sub> (psi)	1,4918	13,09	15,11	2,650
Actual Exit Velocity V <sub>9</sub> (ft/s)	2431	1623	1366	1970
Ideal Exit Velocity V <sub>9i</sub> (ft/s)	2459	1751	1610	2012

The nozzle geometric parameters (Figure 63) for each mission profile are given in the Table 52. Mattingly Aircraft Engine Design resources were utilized when geometric calculations were carried out. In addition, CFD analyses were performed and the geometric boundaries were forced to obtain the nozzle in the most compact dimensions.



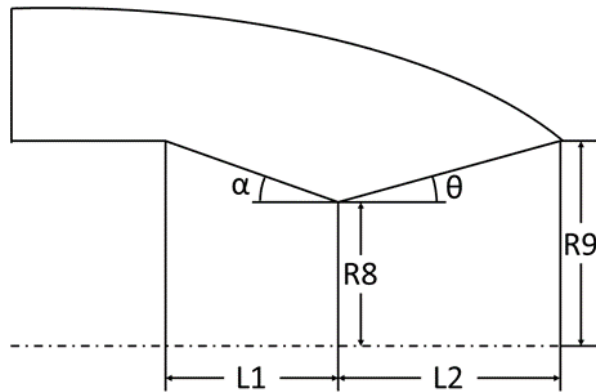


Figure 63: Geometric Parameters of the Nozzle

Table 52: Geometric dimensions for each mission profile

Variables	Cruise	Hot-Day Take Off	SLS	Transonic Pinch
Primary Half Angle $\theta$	20	19,81	19,84	20,87
Secondary Half Angle $\alpha$	10,5	0,34	0	4,313
Convergent Section Length L1 (in)	26,3	26,3	26,3	26,3
Divergent Section Length L2 (in)	55,3	55,3	55,3	55,3
Nozzle Throat Radius R8 (in)	31,37	31,46	31,45	30,91
Nozzle Exir Radius R9 (in)	41,61	31,79	31,45	35,08

3D model of the TULPAR engine cruise condition nozzle which is designed with the Siemens NX software is shown in the Figure 64.

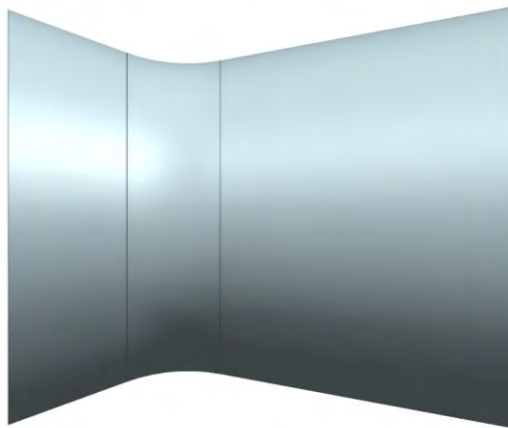


Figure 64: 3D model of the cruise condition convergent-divergent nozzle

#### 4.9. THRUST REVERSERS

Thrust reversers, which is also called reverse thrust, is the temporary diversion of an aircraft engine's exhaust gases for providing deceleration. The thrust reverser systems are designed for the use on ground only. This is the result of direction of the thrust produced by engine against the forward travel of the aircraft. During the initial stages of rejected take-off and landing on turbofan aircraft, thrust reversers provide an important way of increasing the rate of deceleration from high speed [46-5].

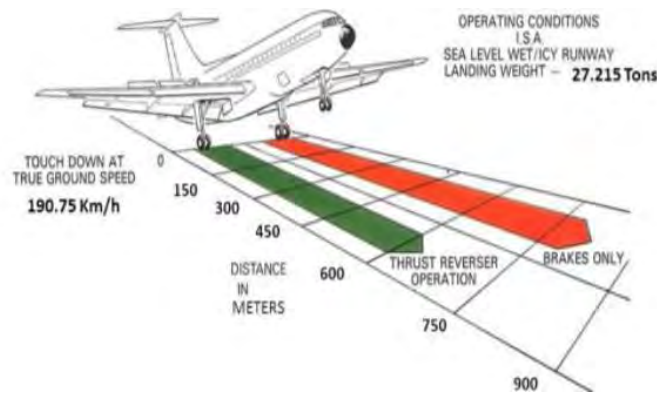


Figure 65: Comparative landing runs with and without thrust reversers [47]

Thrust reversers engine is an important component for an aircraft system. The advantages of using reverser are ensuring a good braking effect by reducing the maximum thrust force on the runway (wet, slushy and icy), reducing the brake wear, taxi distance and length of the certified landing field lengths, extending the working life of the brake discs and additional stopping force. In Figure 65, comparative landing runs with and without thrust reversers is showed [46-47-48].

The power of a engine is used as a deceleration force by the thrust reverser, which is done by reversing of the airflow direction. The reversers direct the exhaust gas flow at an angle of about 120 degrees and are usually placed in the engine nacelle. Thrust reversers must be open very soon after landing to obtain maximum efficiency. Because thrust reversers have higher efficiency values at higher speeds, this results in a faster deceleration of the aircraft (like 190 Km/h to 130 Km/h). Use of reverse thrust at low speeds can lead to engine damage through sand, stones and other foreign objects entering the intake. [5-47-48].

Thrust reversers have a significant impact on engine nacelle design, depending on their increasing weight, resulting in higher manufacturing and operating costs. So, mostly composite materials are used to reduce weight penalty. In addition, a design of the reverse thrust system may cause shock waves causing undesired severe noises during landing. Thrust reversers can be differentiated by the types of their subsystems. These subsystems are Airflow deflection systems, Actuation systems and Control systems [46].

In general, there are broadly two types of thrust reversers which are divided into sub-categories. These main types are;

- Using both core flow and fan flow,
  - Clamshell door reverser system (hot stream)
  - Bucket target reverser system (hot stream)
- Using fan flow only.
  - Cascade type reverser system (cold stream) [47]

According to researches, bucket target system (hot stream) was selected for ETU-V TULPAR. Bucket target reserver system is commonly used for turbojet and low bypass turbofan engine. Also, the maximum thrust value for low bypass engine is obtained at the exit of nozzle. So, bucket target system is more efficient than other types of thrust reverser for low bypass engine. Because maximum thrust is reversed by using deflector doors at the back of low bypass turbofan engine.

There are three types of bucket target reverser systems. These are;

- Pivot Fairing Thrust Reverser,
- Screw Jack Mechanism,
- Fishmouth Thrust Reverser Nozzle.

Fishmouth thrust reverser nozzle in bucket target systems was selected for ETU-V TULPAR. This type has been chosen to reduce the noise level that during the operation of the thrust reverser so that flow characteristics are not affected in the nozzle section where the hot and cold air mixes. The other reason is that the shape of the deflector doors outer surface which matches the existing aerodynamic contours of nacelle provides a lower boattail angle for improved drag characteristics. In Figure 66, The general structure of target type thrust reverser system is shown.

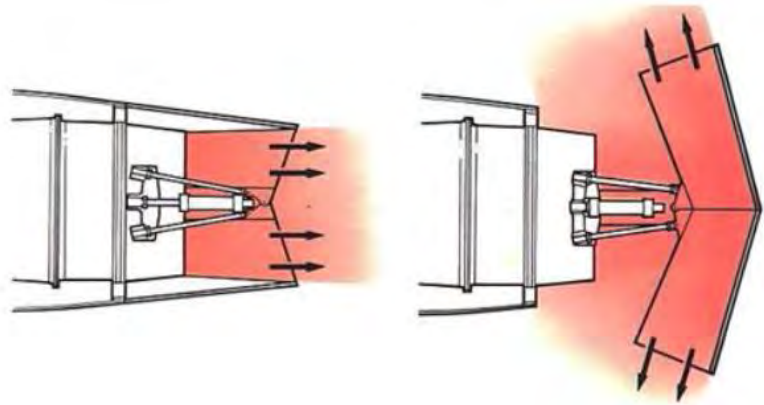


Figure 66: Bucket target type thrust reverser system using deflector doors [48]

Thrust reverser configurations are circular jet-axisymmetric deflector, plane jet-two dimensional deflector, cascade reverser and circular jet-curved deflector. Two dimensional deflector was selected for TULPAR. According to literature surveys, thrust reverser deflector angles are assumed between 15 and 75 degree depending on velocity field, pressure distribution on deflector surface and effectivity of deflector [50].

Thrust reverser calculations were completed by using newly developed MATLAB code. A control volume analysis was used in this code depending upon literature surveys. Thrust reverser control volume is shown in Figure 67 [49].

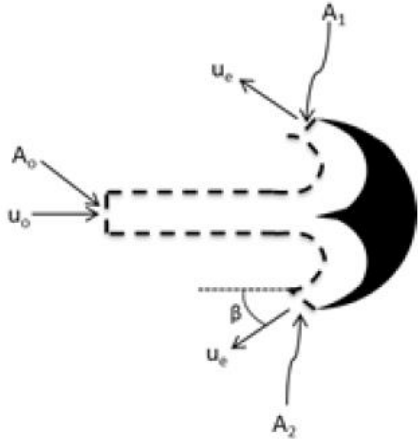


Figure 67: Thrust reverser control volume [49]

The exit velocity of the air at the end of the thrust reverser is calculated from Equation 4.5. The temperature and pressure values are calculated for each engine station by using GasTurb.

$$U_e = \sqrt{2 \times \eta \times \frac{\gamma}{\gamma - 1} \times R \times T_{05} \times \left[1 - \frac{P_7}{P_{05}}\right]^{\frac{\gamma - 1}{\gamma}}} \tag{4.5}$$

Where;

- $\eta$ , The nozzle efficiency,
- $U_e$ , Exit velocity (m/s),
- $\gamma$ , Specific heat ratio,
- $R$ , Gas constant (kJ/kg),
- $T_{05}$ , Total temperature at the end of mixer (K),
- $P_{05}$ , Total pressure at the end of mixer (bar),
- $P_7$ , Static pressure at the end of mixer (bar).

The derivation of the total thrust is shown below. The force shown in Equation 4.5 on the engine is found by integrating over the control surface; [51]

$$F_X = \frac{d}{dt} \left( \int_{cv} u \cdot \rho \cdot dV \right) + \int_{cs} u \cdot \rho \cdot \vec{V} \times \vec{n} \cdot dA \quad (4.6)$$

In Equation 4.6, differential term is zero because of the steady state condition at the first moment of landing. The equation gives;

$$-F_X = \rho U_0(-U_0)A_0 + \rho U_e(-U_e \cos\theta)A_1 + \rho U_e(-U_e \cos\theta)A_2 + \rho U_r(-U_r)A_r \quad (4.7)$$

which simplifies to:

$$F_X = \rho U_0^2 A_0 + \rho U_e^2 (\cos\theta) A_1 + \rho U_e^2 (\cos\theta) A_2 + \rho U_r^2 A_r \quad (4.8)$$

$$\dot{m}_0 = \rho U_0 A_0 = \rho U_e A_1 + \rho U_e A_2 + \rho U_r A_r \quad (4.9)$$

$$U_r = \frac{U_0 A_0}{A_r} \quad (4.10)$$

$$F_X = \dot{m}_0 U_0 + \dot{m}_{e1} U_e (\cos\theta) + \dot{m}_{e2} U_e (\cos\theta) + \dot{m}_r U_r \quad (4.11)$$

$$\dot{m}_{e1} = \dot{m}_{e2} \quad (4.12)$$

$$F_X = \dot{m}_0 U_0 + 2\dot{m}_e U_e (\cos\theta) + \dot{m}_r \times U_r \quad (4.13)$$

$$F_X = \dot{m}_0 (U_0 + U_e (\cos\theta)) \quad (4.14)$$

As a result of MATLAB calculations, reversed thrust value was determined as an approximately 9000 lbf. Furthermore, N115 was selected as a suitable material for thrust reverser system depending upon operational conditions. The selected material is described in Material Selection section in detail.

#### 4.10. SHAFT DESIGN

Depending on technological developments, increasing performance values in the aircraft engines causes the engines to have a more complex structure. This complexity introduces difficulties such as ensuring that components work together. The engine components (compressor, turbine) must be rotated at different speeds to ensure the compatibility of the parts with each other and the desired engine performance values. So, engines with different spool technologies have begun to be designed. The number and geometry of the shaft vary depending on the number of spools [52].

The most critical component in geometric sizing is a shaft design. Because the increasing performance values bring high engine temperatures and the shaft works at high rotational speeds. In addition, increased engine complexity causes the loading values on the shaft to increase [52-54]. The most important parameters in the shaft design is the

critical speed of the shaft. The critical velocity of the shaft can be defined as the speed at which the natural frequency of objects rotating around their axis is expanded and the axial deviations are increased [53].

Operating the shaft at speeds close to the critical speed value causes unbalanced loads in the engine. It is very important parameter for engine lifecycle. Thus, the shaft must be kept as far away from the critical speed as possible and operating conditions close to the critical speed should be kept as short as possible. Otherwise, this causes various problems within the engine. These are;

- Overloading of bearings and occurrence of failures,
- Wear and defects in compressor and turbine bleeds,
- Creation of vibrations and shear stresses in engine components,
- Decrease in engine performance and increase of engine running noise. [52]

There are two different calculation methods for shaft critical speed calculations. These calculation methods are Dunkerley’s Method and Rayleigh-Ritz Method. In this project, both Dunkerley’s and Rayleigh-Ritz methods were used for calculations. While, Dunkerley method was used to determine lower limit speed value of shaft, Rayleigh-Ritz method was used to determine upper limit speed value of shaft.

The material to be used for the shaft affects the critical speed of the shaft and hence the system. The shaft should be as light as possible, resistant to high temperatures and heavy loads. So, shaft material must be selected before starting calculations. Super CMV was selected as a material for TULPAR and described in detail in Material Selection section. The required material properties of Super CMV are shown in Table 53.

Table 53: The material properties of Super CMV [56-57]

Super CMV Material Properties	
Properties	Value
Elastic Modulus (psi)	$30 \times 10^6$
Density (lb/in <sup>3</sup> )	0.26
Poisson’s ratio	0.28
Yield strength (psi)	$180 \times 10^3$
Ultimate strength (psi)	$246 \times 10^3$

Depending on the literature surveys, the general shaft structure and bearing numbers for TULPAR engine were determined and the number, location and types of the bearings are shown in Figure 68. This shaft design is proposed for Energy Efficient Engines by Pratt & Whitney for next generation engines. This shaft structure is designed to reduce the effects of some inconveniences found in previous engines (like limited aerodynamic choices, noise considerations and mechanical complexity) [52].

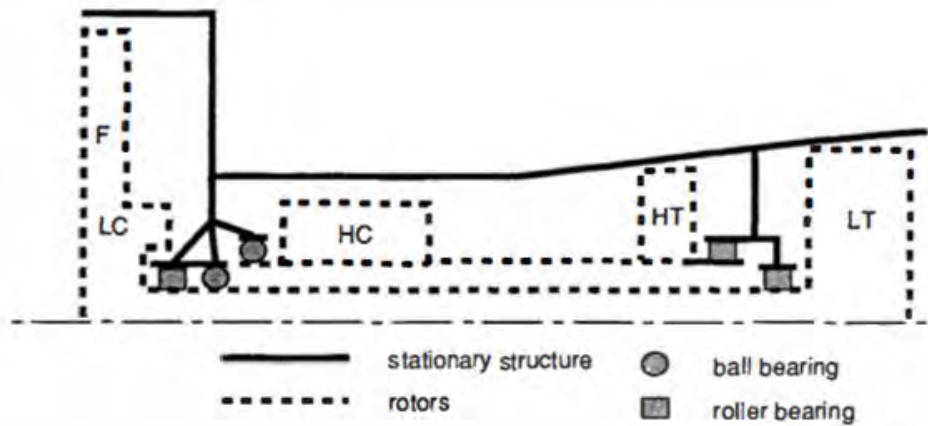


Figure 68: Shaft structure and bearing locations (two spool) [52]

In this design, each one of the rotating elements is supported by two or more bearings. These typical aircraft engine bearings (fluid-film bearings) are ball bearings which serve for axial positioning of the rotating element and absorption of radial loads at the shaft end and cylindrical roller bearings which allow unlimited differential thermal expansion between the rotating element and the supporting structure.

Besides, the use of magnetic bearings in future engine designs is contemplated and studies for this purpose are ongoing. There are several advantages of using magnetic bearing systems. These are low-wear in the bearings, lower friction losses, increased efficiency, reduced emissions, reduced fire hazard, longer maintenance intervals, lower direct operating and lifetime costs. There are also disadvantages, such as the required power support units are not light enough and there is not any applied example. In our design, classical roller bearing has been more appropriately chosen in terms of reliability and applicability. So, two ball bearings and three roller bearings were selected for TULPAR [55].

Shaft critical speed calculations were completed by using newly developed MATLAB code. Different MATLAB codes were written for each shaft by using superposition method. While the length and diameter values of each shaft are taken from the GasTurb, the properties of each component were determined with help of AxSTREAM. Verification of these codes was completed using sample cases from the literature surveys.

In this codes, ball and roller bearings which are on low spool shaft on the compressor side are considered as cantilever. The critical speeds of the shaft which the compressor is connected and the other shaft which turbine is connected are calculated separately. As a result, the lower critical speed value was selected.

The input parameters values which were used in developed code are shown in Table 54.

Table 54: Input values of MATLAB Code for each shaft

Fan - LPT Shaft		HPC – HPT Shaft	
Parameter	Value	Parameter	Value
Compressor Mass (lb)	4692,1	Compressor Mass (lb)	2014.01
Turbine Mass (lb)	1712.04	Turbine Mass (lb)	662.6
Shaft Mass (lb)	1102.3	Shaft Mass (lb)	840.6
Comp. -Bearing Length (inch)	47.87	Comp.-Bearing Length (inch)	20.07
Comp. - Shaft Tip Length (inch)	11.81	Turbine-Bearing Length (inch)	5.52
Mid Length (inch)	75.59	Shaft Length (inch)	74.8
Turbine-Bearing Length (inch)	14.17	Shaft Outer Radius (inch)	5.12
Shaft Radius (inch)	3.15	Shaft Inner Radius (inch)	3.386

The calculation results for each shaft are shown in Table 55 for two different calculation methods, respectively.

Table 55: The MATLAB critical speed results for each shaft

HP Spool Shaft		LP Spool Shaft	
Dunkerley's	Rayleigh's Energy	Dunkerley's	Rayleigh's Energy
4797.5 RPM	4911.5 RPM	2272.9 RPM	3506.8 RPM

The operating speed values of each shaft were calculated as 8850 RPM for HP Spool and 6525 RPM for LP Spool by using AxSTREAM and GasTurb. When compared MATLAB results to GasTurb results, it is clearly seen that the rotation speeds at the operating point of the shafts are far away from the critical speed values of each shaft. This situation indicates that the selected materials are suitable for the system and do not constitute a design problem. At the end of the studies, both HP Spool and LP Spool shaft geometries were modeled by using Siemens NX and the final shaft geometries are shown in Figure 69.

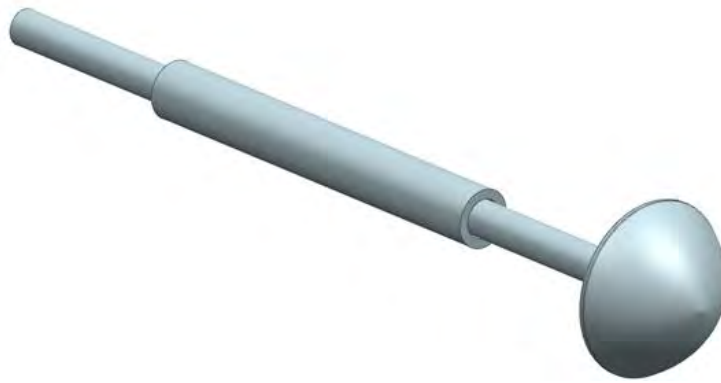


Figure 69: 3D model of HP Spool and LP Spool shafts

## 5. EMISSIONS

There are many compounds such as NO<sub>x</sub>, CO<sub>2</sub>, H<sub>2</sub>O, SO<sub>x</sub>, CO and unburned hydrocarbons in the exhaust gas released from aircraft engines. According to the Intergovernmental Panel on Climate Change [58], the results indicate that NO<sub>x</sub> gases released from aircraft engines increase the ozone which leads to warming and reduce the amount of methane which leads to cooling. The TULPAR engine uses RQL technology in the combustion chamber to reduce NO<sub>x</sub> emissions.

### 5.1. Rich Quick Quench Lean (RQL) Technology

Rich-Burn Quick-Quench Lean-Burn (RQL) combustor concept is widely used to reduce NO<sub>x</sub> emission from gas turbine engines. RQL combustor is divided mainly into three sections as shown in Figure 70.

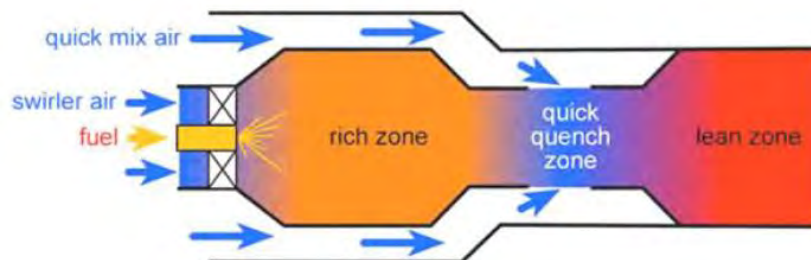


Figure 70: RQL Combustor Sections [59]

The first part is the rich zone, where fuel and air mix and burn in fuel rich conditions with the equivalence ratio normally in between 1.5 and 1.8. The second section is the quick-mix zone, where almost all the remaining compressor exit air mixes with the fuel-air effluent gases from the rich zone very quickly. The equivalence ratio is in the range of 0.6-0.8 for quick quenching. Third section is the lean zone, where all the mixture blends with the remaining air and the mixture itself is lean because of highest percentage of air. The equivalence ratio is in the range of 0.3-0.4 [60-61].

The emission of NO<sub>x</sub> during combustion in the fuel-rich region is reduced. At the same time, it not only reduces thermal NO<sub>x</sub> emissions but also reduces FBN (Fuel Bound Nitrogen) NO<sub>x</sub> emissions by converting them into N<sub>2</sub> form. In the Quick Quench section, the gas burned in the rich region is uniformly mixed and transferred to the lean region. In the Lean zone, CO, UHC and soot produced in the rich zone can be reduced by a suitable residence time. For this reason, the equivalence ratio and the temperature value should be carefully selected [62-63].

## 5.2. Emission Standards

Regulations on NOx emissions are made by the International Civil Aviation Organization's (ICAO) Committee on Aviation Environmental Protection (CAEP). The certification process is based on the Landing Take-off (LTO) Cycle. The NOx emission standards for turbojet and turbofan engines intended for propulsion at supersonic speeds were determined according to ICAO Annex 16 Volume 2 data as follows. [64]

$$Emission\ Standart\ (ES) = \frac{Dp}{F_{oo}} = 36 + 2.42 \times \pi_{oo} \quad (5.1)$$

Where;

- Dp, Pollutant mass in grams
- F<sub>oo</sub>, Rated Output in kN
- $\pi_{oo}$ , Engine Overall Pressure Ratio

The relationships between the emission index and sNOx (NOx severity parameter) used in the calculations are given below.

$$EsNO_x = \left( \frac{P3}{2965kPa} \right)^{0.4} * e^{\left( \frac{T_3-826K}{194K} + \frac{6.29-100war}{53.2} \right)} \quad (5.2)$$

$$Emission\ Index(EI) = \frac{Dp}{m_{fuel}} \left( \frac{gr}{kg} \right) = 32 * sNO_x \quad (5.3)$$

The inequality relation created by the obtained equations is also given below.

$$\frac{TSCF \left( \frac{gr}{kNh} \right)}{1000} * time(s) * 32 * sNO_x \leq 36 + 2.42 \times \pi_{oo} \quad (5.4)$$

Where;

- P3, Combustion chamber entry pressure
- T3, Combustion chamber entry temperature
- War, Water-Air Ratio
- Time(s), Flight condition time

As stated in the ICAO LTO Cycle, altitude conditions up to 3000ft in flight conditions are accepted as the standard for NOx emissions. For this reason, the calculations for NOx emissions are based on the flight conditions below this altitude. Table 56 gives the percent power and time in mode values for operating modes in the LTO cycle for supersonic engines and the comparison between NOx emission of ETU V-TULPAR and Emission Standards.

Table 56: LTO Cycle for supersonic engines and comparison between TULPAR engine NOx emission and emission standarts [2]

Missions	Power (%)	Time in Mode (minutes)	Dp/Foo NO <sub>x</sub> (gr/kN)	
			ETU V-TULPAR	Emission Standards
Takeoff	100	1.2	40,71	157,9
Climbout	65	2.0	48,8	
Descent	15	1.2	9,04	
Approach	34	2.3	32,2	
Taxi/Idle	5.8	26.0	27,12	
			Σ	169,1



As seen in Table 56, the emission value of the TULPAR engine meets the emission standards determined for the ICAO LTO cycle.

## 6. ENGINE SUBSYSTEMS

### 6.1. Lubrication Systems

Aircraft engines have a complex structure to produce more power. This complexity in aircraft engines brings about a number of design problems. One of the most important problems lubrication problem. There are many available types of lubrication systems and lubricants in order to overcome this problem.

The primary purpose of any lubricant is reducing friction caused by metal-to-metal contacts (between moving parts). The engines are exposed to many different friction types. These are sliding friction, rolling friction and wiping friction. [66-70-46]. The reduction of friction losses during the engine operations prevents unwanted friction effects between the moving parts of the aircraft engine (such as temperature increases and wear). Besides reducing the friction between the moving parts, there are many functions for reliable and safe operation of the engine as well. These functions are: [65-66]

- Lubrication of roller bearings, gearbox gears
- Cooling of bearings and removal of pollutants from lubricant,
- Supporting of the sealing of the carbon bearing seals,
- Supplying of a squeeze film between the bearing outer races and their housings for oil dampened bearings. This situation reduces the vibration levels and the fatigue loads for the casings [70-46].
- Also, lubricants can be used for operating the servo mechanism of some fuel controls, for controlling the position of the variable area exhaust-nozzle vanes and for operating the thrust reverser [65].

Another important parameter for the lubrication system is the oil type. These types can be classified according to their sources (animal, vegetables, petroleum, mineral or synthetic). The usage of oil types is restricted because of high performance increases. So, the development of synthetic lubricants that can withstand high temperatures has begun [70].

The main characteristics of oil types are viscosity, pour point, flash point, pressure resistance, oxidation resistance and thermal stability. Aircraft engines usually use low viscosity lubricants and non-mineral lubricants. Because these oils are more resistant to oxidation at high temperatures and have better characteristics in terms of thermal stability and viscosity. [46] Also, the oil types are required to operate over a wide range of temperatures. (from -40°C to 250°C+)

Reciprocating engine pressure lubrication systems are commonly used in aircraft industry and can be divided into two different lubrication systems. [67] These are Wet-sump and Dry-sump systems. However, there are three subsystems for each lubrication system in general so that the oil can be pumped to the required place and then sent back to the storage tanks. These are;

- Storage and supply system,
- Scavenge system,
- Venting system [65].

When wet-sump systems are compared to dry-sump systems, wet sump systems stores oil in a reservoir inside the engine and at the bottom of gears, dry sump systems stores oil in an external reservoir outside the engine. Besides, wet sump systems have some disadvantages. These are limited oil supply by the sump capacity, difficulty of cooling the oil due to the continuous exposure to high engine temperatures and the not being adaptable to unusual flight altitudes [68-69-70]. On the other hand, dry sump systems are the most common type of lubrication system. In this type systems, locating the tank near the engine provides extra oil capacity and makes the heat control easier. So, dry sump lubrication system was selected for TULPAR.

During operational process of engine, heat is transferred from components to oil. So, this oil which reached a limit temperature value must be removed from the system and must be cooled. For this reason, either an air-oil or a fuel-oil cooled heat exchangers is used in dry-sump systems. In addition to this, the streamlined design of the oil tank and oil cooler must keep the diameter of the engine as small as possible [68-69-70].

When fuel-cooled oil cooler is compared to air-cooled oil cooler, fuel-oil cooler system has many advantages. These advantages are less drag penalty because of smaller volume for the same cooling capacity, reduced fuel system icing, increased cycle thermal efficiency value, improved combustion process and easy mount. Typically, fuel-oil cooled heat exchangers are used in turbofan engines [70-46]. So, fuel-oil cooled heat exchanger were selected for TULPAR. The typical dry-sump lubrication system is shown in Figure 71.

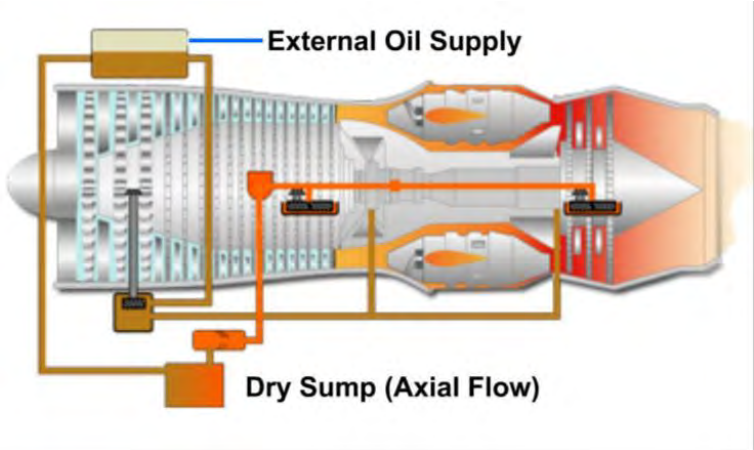


Figure 71: The typical dry-sump lubrication system [70]

As a result, synthetic oil lubricant with a dry-sump lubrication system was selected for TULPAR. As mentioned before, the fuel-oil cooler is used instead of air-oil cooler because of its advantages. As mentioned before, fuel-oil cooler is more suitable for very large reciprocating engines. Besides, additional air-cooled heat exchangers were used in TULPAR to control the temperatures of fuel and oil for low-fuel-flow operations.

Also, the typical lubrication system for an engine with three bearing compartments is shown in Figure 72.

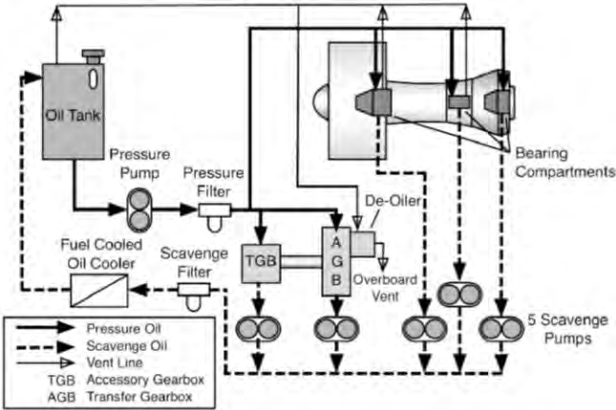


Figure 72: The typical lubrication system for an engine with three bearing compartments [46]

BP Turbo Oil 2197, latest generation 5 cSt High Thermal Stability (HTS) synthetic lubricant, was selected as a lubricant for TULPAR. It provides high performance for existing and next generation of turbines. The advantages of BPTO-2197 are thermal and oxidation stability, superior hydrolytic stability, less frequent oil filter replacement, less or no carbon deposits in oil supply and outstanding high temperature cleanliness. In addition, this lubricant

has been approved by Rolls-Royce, GE, Pratt & Whitney, Pratt & Whitney Canada, United Technologies Aerospace Systems, Honeywell, CFMI, IAE, MTU and used in Rolls-Royce Trent XWB series. The typical characteristics of oil are shown in Table 57.

Table 57: The typical characteristics of BP Turbo Oil 2197 [71]

Parameters	Value	Unit
Density @ 15°C	0.036	lb/in <sup>3</sup>
Kinematic Viscosity @ 100°C	0.008	in <sup>2</sup> /s
Kinematic Viscosity @ 40°C	0.041	in <sup>2</sup> /s
Kinematic Viscosity @ -40°C after 35 minutes	0.019	in <sup>2</sup> /s
Pour Point	389	°R
Flash Point	963.2	°R
Total acid Number	0.36	mg/KOH/g
Evaporation Loss (6.5 hrs @ 204°C)	2.30	%

**6.2. Engine Starter**

Two systems are essential to make an engine start. These are the starting system and the ignition system. They are always used together to run the engine on the ground. All the energy the engines deliver for the aircraft systems is electric energy. The engines are started with the two generators that are designed as starter generators. For the engine start system, the large generators offers the required supply without causing any additional weight [46].

The starter duct connects the starter with the pneumatic system of the aircraft. Depending on the size of the engine and the location of the start valve, the starter duct consists of two or more segments. The pneumatic starter consists of a turbine, a reduction gear and a clutch. The clutch connects the reduction gear with the starter output shaft during starter operation. The starter output shaft fits into the associated gear shaft of the gearbox. During further acceleration of the engine the claws are opened by centrifugal force and the starter gear is completely disconnected from the rotary shaft during engine operation. Figure 73 shows a pneumatic system driven by APU which is a little gas turbine that provides shaft power [46].

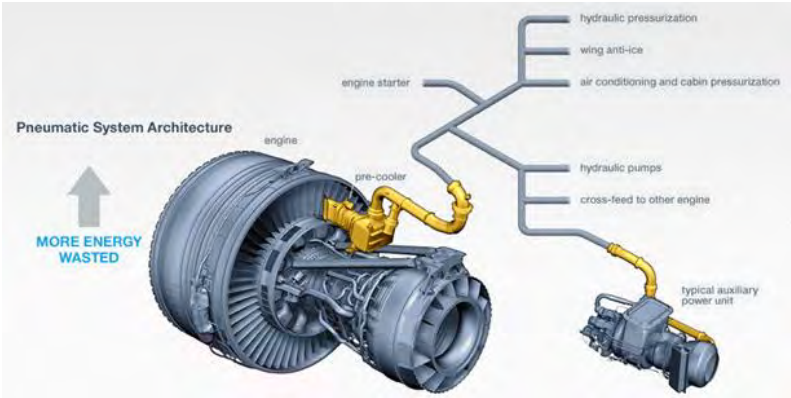


Figure 73: Pneumatic System Architecture [72]

An air-starter on a TULPAR would include axial flow turbine that is connected to the compressor mechanical device spool through the accessory gear, and the associated piping and valves. The starter is pneumatically powered and only sends air first to ensure the air is flowing in the right direction before fuel is added. The compressor should rotate fast enough to produce enough air to the combustor. A starter rotates the compressor until a sustained combustion occurs and the engine will operate on its own. Compressed air is provided to the system by bleed air from the aircraft's auxiliary power unit or from an compressor mounted on ground support equipment.

### 6.3. Anti-Icing System

When an aircraft flies through air with a high humidity and a temperature around the freezing point, moisture accumulates on the surfaces of the aircraft as ice. At the air inlet of a turbofan engine, there are two areas where ice can accumulate on the surfaces. These are the inlet lip of the air inlet and the fan rotor. In front of the compressor inlet, these vortices can lead to an unstable compressor operation. Ice on the fan blades additionally produces imbalance, which leads to vibration. The components located behind the fan rotor are normally in a warm environment. Here ice will accumulate only at low shaft speeds.

The compressor stage for bleed air supply is selected by the designer in such a way that the warm air has the optimum temperature level for the anti-ice system during engine operation. Upstream from the point where the duct is attached to the air inlet structure the shut-off-valve (usually pneumatically activated) is installed. They operate with the air pressure from anti-ice duct or with the air pressure from a more rearward HPC stage. The valve type can be selected either open/closed valves or valves with a pressure regulator. Within the air inlet structure, the anti-ice duct is connected to a spray tube that is installed circumferentially behind the skin of the inlet lip. The air exits in the spray tube through holes and impinges against the inner surface of the inlet lip skin. Hot air anti icing system is shown in Figure 74 [46].

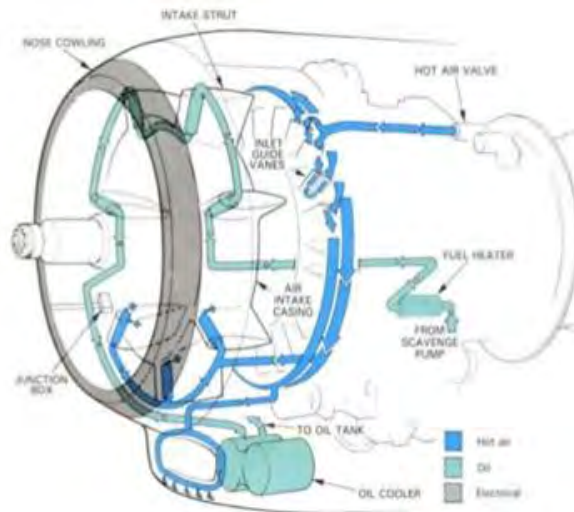


Figure 74: Hot air anti-icing system [73]

TULPAR will prevent icing by distributing the hot air to the heat pads on the outer skins taking bleed air from the appropriate stage of the HPC [46].

### 6.4. Fire Detection and Extinguishing System

The fluid lines installed on an engine contain flammable fluids. If a leak occurs at any point a risk of fire in the well vented space between the cowling and the engine case exists. This would endanger the structural integrity of the nacelle and the pylon.

Fire extinguishing system is shown in Figure 75. TULPAR Design Team decide to detect a fire, detectors should be used for the fire warning system are located the critical zones under the cowlings. The core engine/LPT zone are equipped with fire detectors which is pressurized containers to release gas into engine and can detect high temperature/fire. To protect passengers from the greatest danger, the engine nacelle can be covered with fire retardant materials [46].

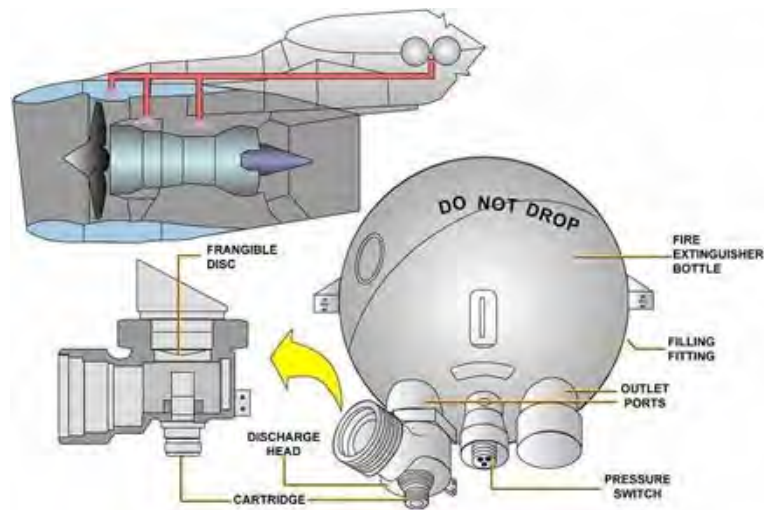


Figure 75: Fire Extinguishing System [74]

### 6.5. Cooling and Ventilation Systems

The cooling systems contains all the air systems for the cooling of engine parts and accessories. For the element cooling simple tubes and hoses deliver air from the fan air flow to the cooled elements. The cooling air flows through a spot between the ignition exciter housing and a cooling shroud. The air leaves the cooling shroud through the cooling passage of the high-tension lead. This cooling passage is found between the high-tension insulation and the outer steel braid of the high-tension lead. The ventilation systems are used to deliver the required ventilation air into the cavities between the cowlings and the engine case. This ventilation is critical to cool down the elements installed on the engine cases and to prevent the buildup of burnable vapors in case of fluid leaks. The cowlings installed around the engine two or a lot of cavities that require ventilation. TULPAR will provide component cooling by transferring the air taken by the fan, which is cold according to other component temperatures, and transmit it to the core using pressure difference.

## 7. MATERIAL SELECTION

Selection of material is one of the foremost vital processes to extend the turbine performance. Additionally, material choice is significant for the life cycle of the engine. Therefore, last supposed lifespan for every component of the engine should be acknowledged. Besides, a successful engine design should meet its aerodynamic, thermodynamic and structural requirement. Performance improvement of gas turbine engines is restricted with the development in the material science. For this reason, new materials are constantly being developed for more efficient, long-lasting and more strength -reliable gas turbines.

Technological developments over the past 60 years have made significant progress in the field of materials. Along with better mechanical and thermal properties provided by new materials, the fuel consumption of subsonic engines is reduced by about 40% and the maximum turbine entry temperature is increased from 800K to over 1900K.

The overall pressure ratio used in the engines was raised from 5 to 40. Later, stress fracture life and creep properties began to be investigated. All components on the engine are limited to specific variable loads due to their material properties and scientific studies are focused on possible faults in these components [75].

For ETU-V TULPAR design, the choice of materials for each component was based on all the research and historical experience. New materials that are thought to take their place by 2025 considered for material selection. The preferred materials, such as CMC, CFRP, Titanium and Aluminium are frequently used in nowadays as seen in Figure 76.

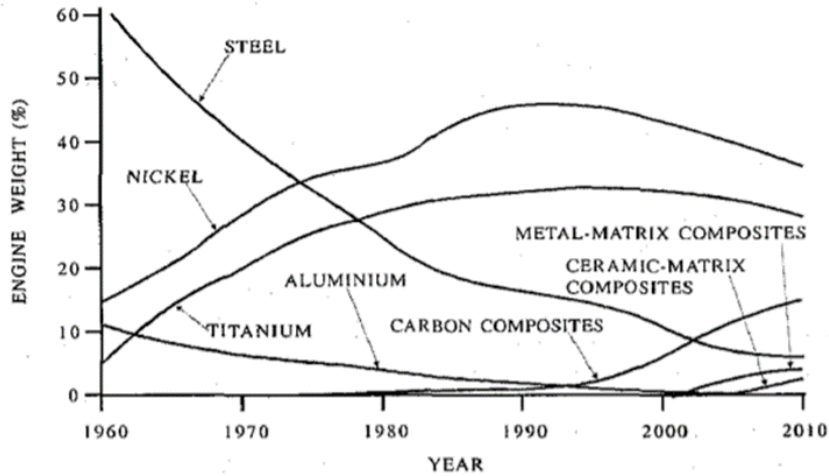


Figure 76: Common materials used in engine structure [77]

### 7.1. Inlet Materials

Air mass flow rate depends on the efficiency of air intake. Such efficiency is achieved with correct geometry design and accurate production. Especially for supersonic speeds, the materials utilized in the inlet should stand up to high temperatures [78].

Carbon fiber reinforced polymer is an extremely strong and light fiber-reinforced plastic which contains carbon fibers. Composite materials, reinforced with carbon fiber, are different from other FRP composites using traditional materials such as fiberglass or aramid fiber. CFRP materials bring great benefits to aircraft design in terms of saving weight and reducing fuel consumption, increasing payload, extending flight range, enhancing toughness and durability, optimizing design, reducing part count, decreasing maintenance cost and maximizing passenger comfort and safety. The improvement in fatigue performance with carbon fiber reinforced prepregs compared to aluminum is also a major benefit [78].

More than 50% of the Boeing 787 and the Airbus A350 XWB airframe (aerons, panels, flaps, floor beams for upper deck, wing ribs etc.) materials are carbon fiber composite. CFRP is a major material for programs and was awarded the contract by Airbus to supply the primary structure prepreg for the A350 XWB program [79]. CFRP materials completed both ground and flight tests with success. Also, CFRP materials are began to use Rolls-Royce Trent series.

As a result, TULPAR Team decided to use CFRP as an inlet material and its mechanical properties are shown in Table 58.

Table 58: Inlet Material Mechanical Properties [80]

Selected Material	CFRP
Density (lb/in <sup>3</sup> )	0.058
Max Service Temperature (R)	747
Cost (\$/lb)	27.2
Young Modulus (psi)	10.15 x 10 <sup>6</sup>
Elastic Modulus (psi)	19.14 x 10 <sup>6</sup>
Tensile Strength (psi)	0.17 x 10 <sup>6</sup>
Compress Strength (psi)	0.07 x 10 <sup>6</sup>

## 7.2. Fan (LPC) Materials

In today's technology, titanium alloys, steel-nickel alloys and composite materials are used in the production of fan blades. These materials have many advantages and disadvantages. Although titanium is expensive compared to other alloys, it is commonly used in terms of weight and strength. Nowadays, titanium is the most used material for fan blades. Along with the new technological development in material science, the use of composite materials with good strength values is improved. In addition, a lot of engine companies are planning to replace titanium with the new developed CFRPs which are durable up to 810-900R.

In addition, the silicon carbide (SiC) ceramic-matrix-composite material has been tested by GE Aviation for up to 3300 R without cooling. CMC materials are approximately 67% lighter than nickel-based alloys. When cost is considered (SiC/CMCs cost is \$230/Kg), the use of CFRP was ideal for TULPAR considering the fan outlet temperature (800 R). Also, these fan blades have titanium leading edge for extra protection. Ti-6Al-4V that has low density and used in implants and aviation was added to protect FOD.

In addition, it is important to use strong disks to holds the blades. The melting point of titanium is around 3420-3600 R and it is suitable for usage. In this design, a durable, lightweight fan disc should be used to attach the fan blades made of Ti-alloy which is more durable and suitable at high RPM. The mechanical properties of selected coating material are shown in Table 59.

Table 59: Fan Coating Material Mechanical Properties [81-82]

Selected Coating Material	Ti-6Al-4V
Density (lb/in <sup>3</sup> )	0.16
Max Service Temperature (R)	1170
Cost (\$/lb)	9.1-11.3
Young Modulus (psi)	16.53 x 10 <sup>6</sup>
Yield Stress (psi)	0.16 x 10 <sup>6</sup>

## 7.3. HP Compressor Materials

The compressor is the section where the air from the fan is compressed and the temperature increases. TULPAR also has an overall pressure ratio above 50 and temperature above 1000K. The compressor outlet temperature is around 1800 R. Under these conditions, materials with high strength must be used for high temperatures. In addition, the used material must have fatigue, crack, oxidation and creep resistance.

Titanium-beta-alloys may be recommended, because the temperature in the compressor is higher than the fan, for example Ti-15Mo-3Al-3Nb with a maximum service temperature of 1949.4 R. Ti-834 alloy compressor used in Rolls Royce's high compression level Trent series (OPR = 40 ~ 50) was selected as the compressor disc material. However, it is not suitable to use this material with maximum service temperature around 1530 R in compressor blades. High-strength SiC/CMC materials should not be used due to increasing the cost.

Table 60: Compressor Material Mechanical Properties [83-84]

Selected Disc Material	Ti-834
Density (lb/in <sup>3</sup> )	0.164
Max Service Temperature (R)	1550
Young Modulus (psi)	14.5 x 10 <sup>6</sup>
Selected Blade Material	Ti-45Al-8Nb
Density (lb/in <sup>3</sup> )	0.141-0.151
Max Service Temperature (R)	2340
Yield Strength (psi)	0.017 x 10 <sup>6</sup>

In this case the use of nickel-based alloys may be considered, but it is not feasible to use this material, which is heavier than titanium, in blades that rotate rapidly. The Ti-45Al-8Nb material, which is also titanium alloy and has a good strength up to 2340 R, has been selected for compressor blades. Also, chromium was added to improve the corrosion resistance. The mechanical properties of selected materials are shown in Table 60.

#### 7.4. Combustion Chamber Materials

In combustion chamber, temperature values increase high levels. So, the wall temperature of the combustion chamber should be lower than the melting point of the material. Nickel-based superalloys such as Hasteloy X, Nicomic 75, Nicomic 263, HA18(cobalt-based-superalloy) materials used in Pratt & Whitney F100 engines and Inconel625/718 are standard materials for combustion chambers for many years. In parallel with the developing technology, HA188 stands out from the others with higher temperature strength and good oxidation resistance up to 2460R. A cobalt-based superalloy such as HA188 could chosen as the base material, ultra-lightweight CMC tiles could be used to prevent the high temperatures at the start of burner liner. This method was applied in GE-9X, which was the first test flight in March 2018.

Nowadays, with the usage of CMC, increasing the operational temperatures becomes potential without incurring the penalties related to increased cooling air use. Si-C matrix composites are suitable materials for gas turbine engines due to their high thermal conductivity, wonderful thermal shock, creep and oxidation resistances. Thus, Sylramic-iBN developed by NASA for ultra-high temperature applications is chosen as combustion chamber material and C/SiC is preferred for both temperature resistance and weight. [77-85-86]. It can work under higher use temperature than silicon carbide in an oxidizing environment because a highly stable and protective hafnium silicate forms at the surface [87-88].

As a result of these search and evaluation, Layered Hafnium Carbide/Silicon Carbide with a coating of Yttrium-stabilized Zirconium was selected as a combustion chamber material. For this coating process, ceramic based Tantalum Carbide (it is known to be used in F-35 and GE-9X) was evaluated. However, this material is not suitable owing to its price. So, YSZ is able to resist high temperature up to 4200 R considering the adequate structural and thermal properties of SiC. Both materials are considered to be a good choice despite its price. Because maintenance costs will be reduced by this way.

Thermal barrier coating (based on ZrO<sub>2</sub> – Y<sub>2</sub>O<sub>3</sub> and produced by plasma spraying) which increases the temperature resistance of +200-300 K is also used to reduce the temperature in the insulation layer and to prevent high temperature streaking. The mechanical properties of selected materials are shown in Table 61.

Table 61: Combustion Chamber Materials Mechanical Properties [89-90]

<b>Selected Material</b>	<b>C/SiC CMC (hafnium layered)</b>
Density (lb/in <sup>3</sup> )	0.0722
Max Service Temperature (R)	4451.2
Cost (\$/lb)	104.3
Tensile Strength (psi)	0.79 x 10 <sup>6</sup>
<b>Selected Coating Material</b>	<b>Yttrium-stabilized Zirconium (YSZ)</b>
Density (lb/in <sup>3</sup> )	0.22
Max Service Temperature (R)	4239
Cost (\$/lb)	63.1

#### 7.5. Turbine Materials

The first set of turbine blades must have high temperature and pressure resistance. Because they are exposed to high temperature and high stress values. Therefore, the material for turbine elements should have sensible thermal and mechanical resistance. Powder metallurgy, common method to manufacture of super alloy elements, is employed usually for Nickel based super alloy. This methodology is usually used for production of high strength



alloys used in turbine discs. As a result, LC Astroloy (Nickel-base superalloy powder metallurgy route) route material was decided as a turbine disc material [77].

The 4th and 5th generation superalloys have very good temperature and creep strengths. Despite their good properties, their oxidation resistances are low due to refractory elements such as Mo, Re and Ru. 6th generation superalloys have high-temperature creep strength and improved oxidation resistance, has been developed [91]. Some different generation superalloy materials are chosen to compare suitable materials such as CMSX-10, TMS-138, TMS-196 and TMS 238 for TULPAR. The necessary investigations were carried out on these materials. Selection criteria under high temperature and pressure such as oxidation resistance, creep rate, temperature strength and mechanical strength were determined. In following figures, mass change according to one-hour cycles, metal loss in hot corrosion test and creep rupture life vs oxidation resistance graphs for different materials are presented. (Figure 77, 78).

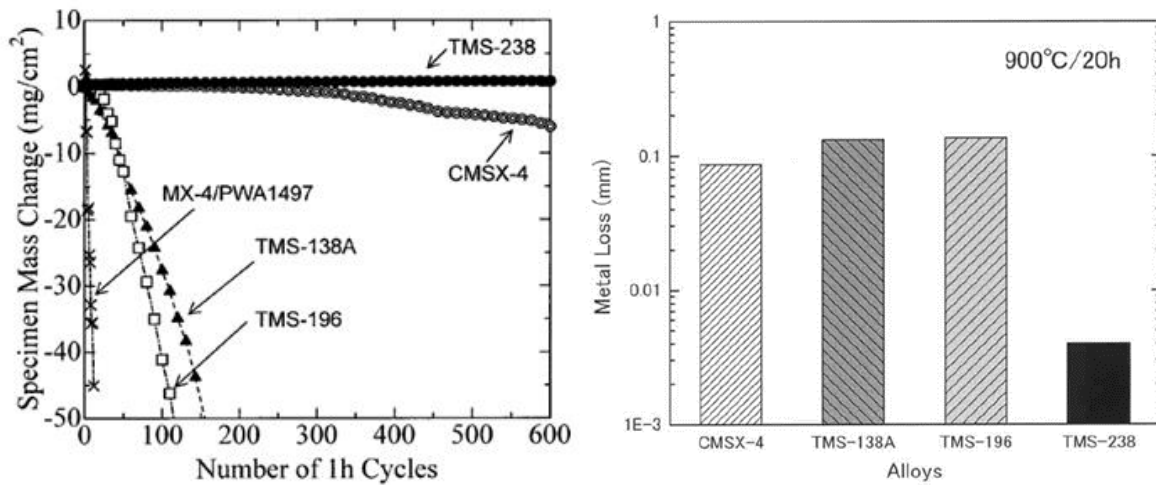


Figure 77: Cyclic Oxidation Tests (left) and Results of Hot-Corrosion Tests (right)

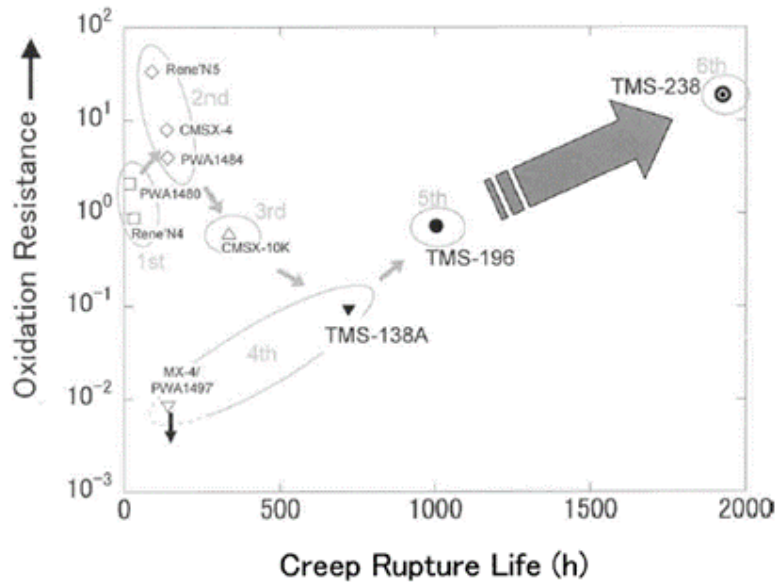


Figure 78: Comparisons among alloys in terms of a combination of creep and oxidation [46]

As a result of these studies, 5th generation single crystal super alloy TMS-238 was selected as a high and intermediate pressure turbine blade material [77-91-92-93].

## 7.6. Mixer-Nozzle Materials

The nozzles are exposed to different temperatures throughout the flight. Generally, inconel, stainless steel alloys, Hastelloy X and CFRPs are suitable for nozzle and exhaust. The Inconel (nickel-chromium-iron) alloys are frequently used in turbine engines because of their ability to resist corrosion and extremely high temperature conditions. The alloy has considerably higher creep strength compared to FSX414. N155, an iron-based superalloy, has good weldability and is used for later stage nozzles of some GE engines. Table 62 gives the main points of materials used for nozzles in nowadays. [77]. ETU-V TULPAR design team decided to use an N155 as a mixer nozzle material.

Table 62: Frequently used nozzle materials by GE, P&W, RR [77]

Grade	Chemical Composition	Remarks
X40	Co-25Cr10Ni8W1Fe0.5C0.01B	Cobalt-base s.all.
X45	Co-25Cr10Ni8W1Fe0.25C0.01B	Cobalt-base s.all.
FSX414	Co-28Cr10Ni7W1Fe0.25C0.01B	Cobalt-base s.all.
N155	Fe-21Cr20Ni20Co2.5W3Mo0.20C	Iron-base s.all.
GTD-222	Ni-22.5Cr19Co2.0W2.3Mo1.2Ti0.8Al0.10V0.008C1.0B	Nickel-base s.all.

## 7.7. Shaft Materials

TULPAR uses two shafts to connect the LPT to the fan and the other to connect HPT to compressor section. A wide range of engine shafts constructed from conventional and maraging steel to titanium and nickel-based super-alloys. [94] Steel is one among the most useful materials as a result of its good strength and heat treated for specific characteristics. Weight is also a problem when selecting a shaft material. Therefore, new materials need to tolerate this weight problem. TULPAR shaft specially designed and made of heat-treated steel like Super CMV(Chrome-Molybdenum-Vanadium). The next generation engine design is trying to switch the primary shaft with F1E which is not steel, however an iron-based superalloy that looks like becoming a part of future Rolls Royce engines until 2025.

Bearings are used to support shafts and their type, material and quality are very important to ensure that all designed components are efficient and stable. Generally, for rings and rolling elements, high speed steel such as molybdenum-based AISI M50 or tungsten-based T1 is used. M50 has hardness of around 58HRC at 300°C and high dimensional stability. Rotating components and shafts generate the centrifugal force on the inner ring and that leads to tensile stress. In order to overcome this problem, M50NiL which is resistant to high temperatures and has good fracture-corrosion and mechanical shock resistance, has been chosen as a bearing material for TULPAR [95-96]. Selected materials for designed components are shown in Table 63.

Table 63: Selected materials for designed components

Components	Design Temperature Pt.	Selected Material	Maximum Service Temperature
Inlet		Carbon fiber reinforced polymer (CFRP)	~720-900R
Fan	~ 800R	Carbon fiber reinforced polymer (CFRP) Ti-6Al-4V coating	~720-900R ~1170-1260R
Compressor	~ 2000R	Disc: Ti-834 Blade: Ti-45Al-8Nb	~1575R-2160R
Combustion Chamber	~ 3600R	C/SiC CMC Yttrium-stabilized Zirconium coating Thermal Barrier Coating: $ZrO_2 - Y_2O_3$	~4320R-4500R
Turbine	~3600R	Disc: LC Astroloy Blade: TMS – 238 MCrAlY Coating	-
Mixer-Nozzle	~ 1600R	N115	-
Shaft	-	Super CMV	-
Bearing	-	M50NiL	-

## 8. CONCLUSION

Within the scope of this project, a supersonic mixed flow turbofan engine, planned to enter service in 2025, is designed. Nowadays, supersonic speed transport has become a necessity. Therefore, ETU-V TULPAR engine was designed in this report

In the first stage of the project, the base engine given in RFP (Request for Proposal) has been replicated in GasTurb software in terms of thermodynamic conditions and engine cycle. The replicated engine, which gives values very close to the base engine data, has been used in the optimization process. Today's engines and the characteristics of these engines are examined with detailed literature surveys and used as a guide in the optimization process.

Four main design parameters, turbine entry temperature (TET), overall pressure ratio (OPR), fan pressure ratio (FPR) and bypass ratio (BPR), are optimized to reduce the thrust specific fuel consumption (TSFC) value within the consideration of the technologies and materials which will be developed until 2025. At the same time, various constraints are included in the optimization process, such as providing engine thrust values for all flight conditions (on-design and off-design), less engine weight than the base engine, lower NO<sub>x</sub> emission values than standard values, and minimizing noise levels. At the end of the optimization process, the TULPAR, which is decided on the engine cycle characteristics, provides all these constraints and improved TSFC by %10.4 for the on-design condition.

At another stage of the Project, each component of the TULPAR engine is detailly designed. When designing components such as intake, combustion chamber, nozzle and shaft, MATLAB codes which were developed and validated. The design of turbomachinery components such as fans, compressors and turbines were implemented in AxSTREAM software and supported by 1-dimensional CFD analyses. All components with geometric dimensions are modelled in 3D with the Siemens NX program.

The materials of the completed engine components have been determined by a comprehensive literature surveys, taking into consideration the 2025 technology. All subsystems were also highlighted, including lubrication, engine starter, anti-icing, fire detection and cooling systems.

The aviation sector grows day by day and hosts many technologies. ETU V TULPAR, designed in detail in this project, is the turbofan motive planned to be a pioneer in the field of new generation supersonic transport of the aviation industry.

## REFERENCES

- [1]How does a jet engine work, National Aeronautics and Space Administration, <<https://www.grc.nasa.gov/www/k-12/UEET/StudentSite/engines.html>>, (Accessed on: 2018, February 22)
- [2]AIAA, "Undergraduate Engine Design Competition - Candidate Engines for a Next Generation Supersonic Transport RFP",2018.
- [3]Supersonic Transport, Wikipedia, <[https://en.wikipedia.org/wiki/Supersonic\\_transport](https://en.wikipedia.org/wiki/Supersonic_transport)>, (Accessed on: 2018, February 20)
- [4]Mattingly Jack D., Heiser William. H., Pratt David T., Aircraft Engine Design, AIAA Education Series, Reston, Virginia, 2nd Edition, 2002
- [5]Farokhi, Saeed, Aircraft Propulsion, Wiley, 2nd Edition, 2014
- [6]Rolls Royce, The Jet Engine, Rolls Royce PLC., Derby, England, 5th Edition, 1996
- [7]Cohen H., Rogers GFC, Saravanamutto HHH, Gas Turbine Theory, Longman Group Limited, England, 4<sup>th</sup> Edition, 1996.
- [8]2-Spool vs. 3-Spool, D.J. Airways, <<http://www.dj-airways.com/2-spool-vs-3-spool/>>, (Accessed on: 2018, February 27)
- [9]California Institute of Technology, Course Ae107, Case Studies in Engineering: The Lockheed SR-71 Blackbird, Spring 1991. Published by Cal Tech for course students and presenters only.
- [10]Whitford, R., "Design for Air Combat", Jane's, London, 1987
- [11]Dankanich Andrew, Peters David," Turbofan Engine Bypass Ratio as a Function of Thrust and Fuel Flow", Washington University Open Scholarship, MEMS 500 Independent Study at Washington University in St. Louis, Washington, USA, March 2017
- [12]Law Peter, SR-71 Propulsion System P&W J58 Engine (JT11D-20)
- [13]Davide Boiani, "Finite Element Structural and Thermal Analysis of JT9D Turbofan Engine First Stage Turbine Blade", Bachelor Thesis, Alma Mater Studiorum, Bologna, Italy
- [14]Walsh Philip P., Fletcher Paul, Gas Turbine Performance, Blackwell Science Ltd a Blackwell Publishing Company, India, 2th Edition, 2004
- [15]Slater John W.," SUPIN: A Computational Tool for Supersonic Inlet Design", NASA John H. Glenn Research Center, Cleveland, Ohio 44135, January 2018
- [16]Mavris Dimitri, Ran Hongjun, "Preliminary Design Of A 2d Supersonic Inlet To Maximize Total Pressure Recovery", AIAA 5th Aviation, Technology, Integration, and Operations Conference, Arlington, Virginia, September 2005
- [17]Aziz Mohammed A., Elbanna H.M., Abdelrahman M.M., "High Fidelity Design Optimization of a Three Dimension Supersonic Intake", 43rd Fluid Dynamics Conference, San Diego, CA, June 24-27, 2013
- [18]Prasad J. K., Das S., "Cowl Deflection Angle in a Supersonic Air Intake", Defence Science Journal, Vol. 59, No. 2, March 2009, pp. 99-105
- [19]Barnhart Paul J., "IPAC - Inlet Performance Analysis Code", NYMA, Inc. 2001 Aerospace Parkway Brook Park, Ohio 44142, July 1997
- [20]Bravo P.D., Ceron H.D., Catalano F., "Analytical And Numerical Design Of A Mixed-Compression Air Intake For A Supersonic Fighter Aircraft" Escola de Engenharia de São Carlos – Universidade de São Paulo, 12-13 September, 2016
- [21]Axial-Flow Compressors
- [22]Nagpurwala Q. H., "Design of Gas Turbine Combustors", M.S. Ramaiah School of Advanced Studies, Bengaluru
- [23]Lefebvre Arthur H., Ballal Dilip R., Gas Turbine Combustion Alternative Fuels and Emissions, CRC Press Taylor & Francis Group, England, 3rd Edition, 2010
- [24]Mark C. Priyant, Selwyn A., "Design And Analysis Of Annular Combustion Chamber Of A Low Bypass Turbofan Engine In A Jet Trainer Aircraft" a Department of Aerospace Engineering, Karunya University, Coimbatore ,T.N., India
- [25]Tacina Robert R., "Low NO<sub>x</sub> Potential of Gas Turbine Engines", American Institute of Aeronautics and Astronautics, 28th Aerospace Sciences Meeting, Reno, Nevada, January 1990
- [26]Mohammed B. S., Jeng S. M., "Design procedures and a Developed Computer Code for Preliminary Single Annular Combustor Design", 45th AIAA/ASME/SAE/ASEE Joint Propulsion Conference & Exhibit, Denver, Colorado, August 2009
- [27]Conrado Ana Costa et al., "Basic Design Principles For Gas Turbine Combustor",

Proceedings of the 10o Brazilian Congress of Thermal Sciences and Engineering, ABCM, Rio de Janeiro, Brazil, Nov. 29-Dec. 03, 2004

[28]Çelik Ender, “On-Film Oluşumlu, Hava Parçalamalı Atomizere Sahip Bir Yanma Odasının Sprey Ve Yanma Karakteristiklerinin Hesaplamalı Akışkanlar Dinamiği İle İncelenmesi”, TOBB University of Economics and Technology, Faculty of Mechanical Engineering, MSc Thesis, Ankara, 2013

[29]Cumpsty Nicholas, Jet Propulsion: Aerodynamic and Thermodynamic Design and Performance of Jet Engines, Cambridge University Press, New York, USA, 7th Edition, 2009

[30]Mattingly Jack D., Ohain Hans Von, Elements of Propulsion: Gas Turbines and Rockets, AIAA Education Series, Reston, Virginia, 2<sup>nd</sup> Edition, 2006

[31]Oates Gordon C., Aerothermodynamics of Aircraft Engine Components, American Institute of Aeronautics and Astronautics, Broadway, New York, 3<sup>rd</sup> Edition, 1989

[32]Jakubowski, “Modeling And Analysis Of Jet Engine With Cooling Turbine”, Journal of KONES Powertrain and Transport, Rzeszow, Poland, Vol. 19, 2012

[33]Bunker Ron S., “Cooling Design Analysis Ron S. Bunker”, GE Global Research, Niskayuna, New York

[34]Cerri Giovanni, “Preliminary Turbine Cooling Requirement”, ROMA TRE Mechanical and Industrial Engineering Department, Rome, 2013

[35]Fransen Remy, “LES based aerothermal modeling of turbine blade cooling systems”, Institut National Polytechnique de Toulouse, France, 2013

[36]Najafabadi Hossein Nadali, “On Film Cooling of Turbine Guide Vanes”, Department of Management and Engineering Linköping University, Linköping, Sweden

[37]Bunker Ron S., “A Review of Shaped Hole Turbine Film-Cooling Technology”, General Electric Global Research Center, Niskayuna, New York

[38]Mengle Vinod G., Dalton William N., “Lobed Mixer Design for Noise Suppression Acoustic and Aerodynamic Test Data Analysis”, Rolls Royce Allison, Indianapolis, Indiana, 2002

[39]McCormick, D. C., Bennett, J. C., “Vortical and Turbulent Structure of a Lobed Mixer Free Shear Layer,” AIAA Journal, Vol. 32, No. 9, 1994

[40]Sheng Zhi-qiang, Huang Pei-lin, Ji Jin-zu, “Configurations of Lobed Nozzles For High Mixing Effectiveness”, School of Aeronautic Science and Engineering, Beijing University of Aeronautics and Astronautics, Beijing 100191, China

[41]Sheng Zhi-qiang, Huang Pei-lin, Ji Jin-zu, “Chevron Spoiler To Improve The Performance Of Lobed Ejector/Mixer”, School of Aeronautic Science and Engineering, Beijing University of Aeronautics and Astronautics, Beijing 100191, China

[42]Brinkerhoff Joshua R., Oria Harun, Yaras Metin I., “Experimental and Computational Study of Mixing Mechanisms in an Axisymmetric Lobed Mixer”, Journal Of Propulsion And Power, Vol. 29, Carleton University, Ottawa, Canada, No. 5, September–October 2013

[43]Gamble Eric, Terrell Dwain, DeFrancesco Rich, “Nozzle Selection and Design Criteria”, American Institute of Aeronautics and Astronautics, SPIRITECH Advanced Products, Inc., 2004

[44]Akatsuka Junichi, Watanabe Yasushi, Ishii Tatsuya, “Simple Jet Noise Reduction Technique for Variable Nozzle”, 22nd AIAA/CEAS Aeroacoustics Conference, Lyon, France, 30 May - 1 June, 2016,

[45]Flack Ronald D., Fundamentals of Jet Propulsion with Applications, Cambridge University Press, New York, USA, 1<sup>st</sup> Edition, 2005

[46]Linke Andreas, Diesinger, Systems of Commercial Turbofan Engines an Introduction to Systems Functions, Springer-Verlag Berlin Heidelberg, 1<sup>st</sup> Edition, 2008

[47]Siddiqui Mohd Anees, Haq Md Shakibul, “Review of Thrust Reverser Mechanism used in Turbofan Jet Engine Aircraft” International Journal of Engineering Research and Technology, Volume 6, Number 5, pp. 717-726, 2013

[48]Siddiqui Mohd Anees, “Utilization of Thrust Reverser Mechanism in Turbofan Engines – A Review”, Department of Mechanical Engineering, Lucknow Institute of Technology, Lucknow, INDIA

[49]Campbell Angle, Cheng Andrew, “Uncertainty Analysis for Calculating Reverse Thrust Using In Situ Data”, 16th AIAA Aviation Technology, Integration, and Operations Conference, Washington, D.C., 13-17 June 2016

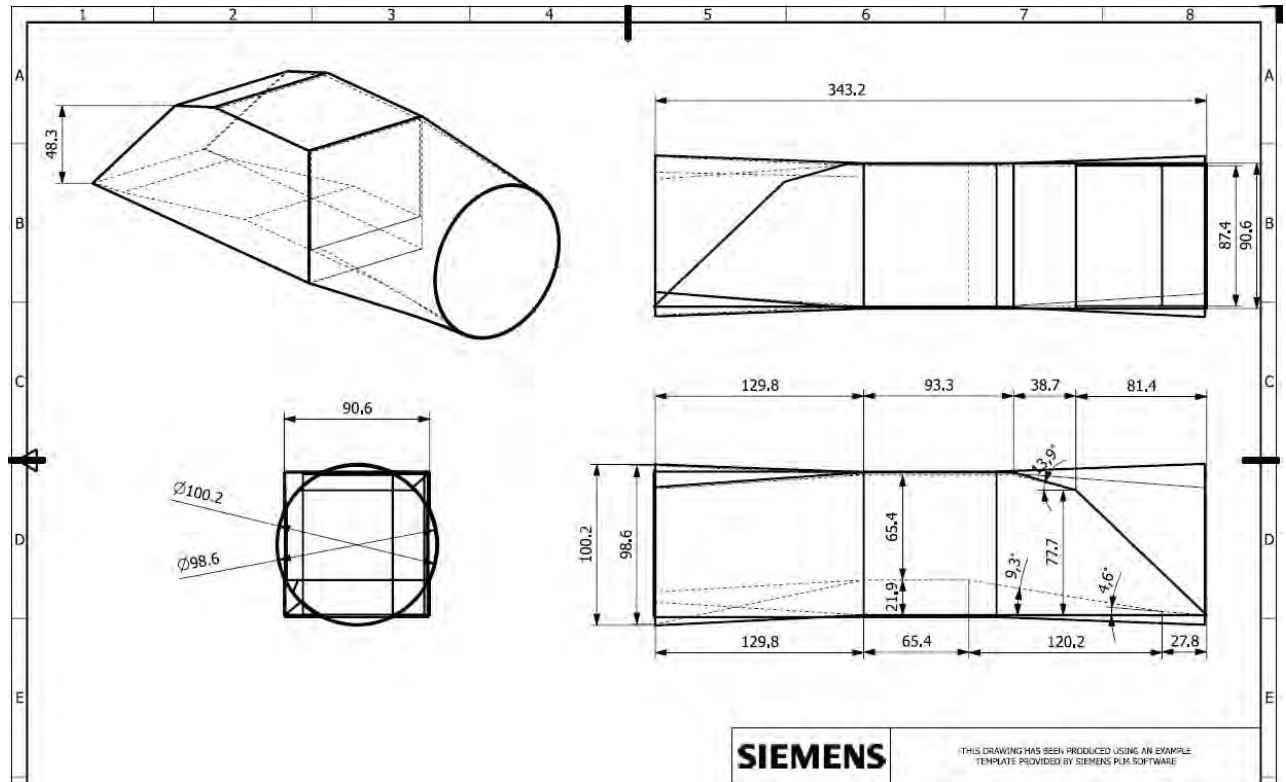
[50]Schnurr N.M., Williamson J.W., Tatom J.W., “An Analytical Investigation of the Impingement of Jets on Curved Deflectors” Vanderbilt University, Nashville; Tennessee, 1972

- [51]Munson Bruce R., Young Donal F., Okiishi T. H., Huebsch Wade W., Fundamentals of Fluid Mechanics, John Wiley & Sons, , Hoboken, NJ, 6th Edition, 2009
- [52]Kerrebrock Jack L., Aircraft Engines and Gas Turbines, The MIT Press, London, England, 2<sup>nd</sup> Edition, 1992
- [53]Budynas Richard G., Nisbett J. Keith, “Shigley’s Mechanical Engineering Design”, Mc Graw Hill, New York, 9th Edition, 2010
- [54]Hibbeler R.C., ”Mechanics of Materials”, Pearson, USA, 8<sup>th</sup> Edition, 2011
- [55]Eğik Rulmanlar, Ardmak, < <http://www.ardmakina.com/urun-35-Egik-Rulmanlar.html>>, (Accessed on: 2018, February 15)
- [56]Li R., Hyde T.H., Sun W., Williams E.J., ”Fatigue crack growth testing of the Super CMV hollow shafts under combined torsional and axial loading”, Department of Mechanical, Materials and Manufacturing Engineering, University of Nottingham, Nottingham NG7 2RD, UK, 2014
- [57]Siswanto W.A., Nagentrau M., Tobi A.L. Mohd, ”Prediction of residual stress using explicit finite element method”, Journal of Mechanical Engineering and Sciences (JMES), Malaysia, Volume 9, pp. 1556-1570, December 2015
- [58]Penner, J.E. et al., ”IPCC Special Report on Aviation And The Global Atmosphere”, Cambridge University Press, England, 1999
- [59]Hossaini, M. Khosravy, "Review of the New Combustion Technologies in Modern Gas Turbines", 2014
- [60]Prakash Atma, ”Prediction of NO<sub>x</sub> Emissions for an RQL aero-engine combustor using a stirred reactor modelling approach”, 52nd AIAA/SAE/ASME Joint Propulsion Conference, July 2016 Salt Palace Convention Center, Salt Lake City, Utah, 2015
- [61]Rizk N. K., Mongia H. C., “Low NO<sub>x</sub> Rich-Lean Combustion Concept Application” AIAA/SAE/ASME 27th Joint Propulsion Conference, Sacramento, CA, June 1991
- [62]Lefebvre Arthur H., Ballal Dilip R., Gas Turbine Combustion Alternative Fuels and Emissions, CRC Press Taylor & Francis Group, England, 3rd Edition, 2010
- [63]Elbir Tolga, “Estimation of Engine Emissions from Commercial Aircraft at a Midsized Turkish Airport”, Journal Of Environmental Engineering ASCE, March 2008
- [64]ICAO Meeting Presentation, Kenya, 2014
- [65]Lubrication Systems, <<http://www.waybuilder.net/sweethaven/MechTech/Aviation/default.asp?iNum=5>>, (Accessed on: 2018, March 12)
- [66]Aircraft and engine fuel system and engine lubrication system, <<https://www.slideshare.net/sansiaf20011972/aircraft-and-engine-fuel-system-and-engine-lubrication-system>>, (Accessed on: 2018, March 12)
- [67]Reciprocating Engine Lubrication Systems, Flight Mechanic, <<http://www.flight-mechanic.com/reciprocating-engine-lubrication-systems/>>, (Accessed on: 2018, February 18)
- [68]Lubrication, <<http://www.cfnotebook.net/notes/ebook/operation-of-aircraft-systems/lubrication>>, (Accessed on: 2018, March 12)
- [69]Function Of The Lubrication System, <<https://www.aircraftspruce.ca/catalog/pdf/13-08714.pdf>>, (Accessed on: 2018, March 18)
- [70]Jet Aircraft Engine Lubrication Systems, <[http://navybmr.com/study%20material/14008a/14008A\\_ch5.pdf](http://navybmr.com/study%20material/14008a/14008A_ch5.pdf)>, (Accessed on: 2018, March 16)
- [71]BP Production Data, BP Turbo Oil 2197
- [72]Pneumatic System Architecture, Available in: <https://leehamnews.com/wp-content/uploads/2016/02/Bleed-architecture.png>
- [73]Aerospace Propulsion Study For Shenyang Aerospace University, < <https://www.slideshare.net/SAU420/aerospace-propulsion-study-for-shenyang-aerospace-university-by-lale420-finalex4>>, (Accessed on: 2018, March 18)
- [74]Aviation Maintenance Technician Powerplant Handbook, <http://content.aviation-safety-bureau.com/allmembers/faa-h-8083-32-amtpowerplant/sections/chapter-9.php>, (Accessed on: 2018, March 20)
- [75]Long term performance of polymers, <[www.mech.umn.edu/labs/composites/Project s/P olymer%20Heat%20Exchanger/Creep%20description.pdf](http://www.mech.umn.edu/labs/composites/Project%20polymer%20Heat%20Exchanger/Creep%20description.pdf)>, (Accessed on: 2018, March 20)
- [76]Kazymyrovych Vitaliy, “Very High Cycle Fatigue of Engineering Materials”, Karlstad University Studies, Faculty of Technology and Science, Karlstad 2009
- [77]Muktinutalapati Nageswara Rao, ” Materials for Gas Turbines – An Overview”, VIT University, India

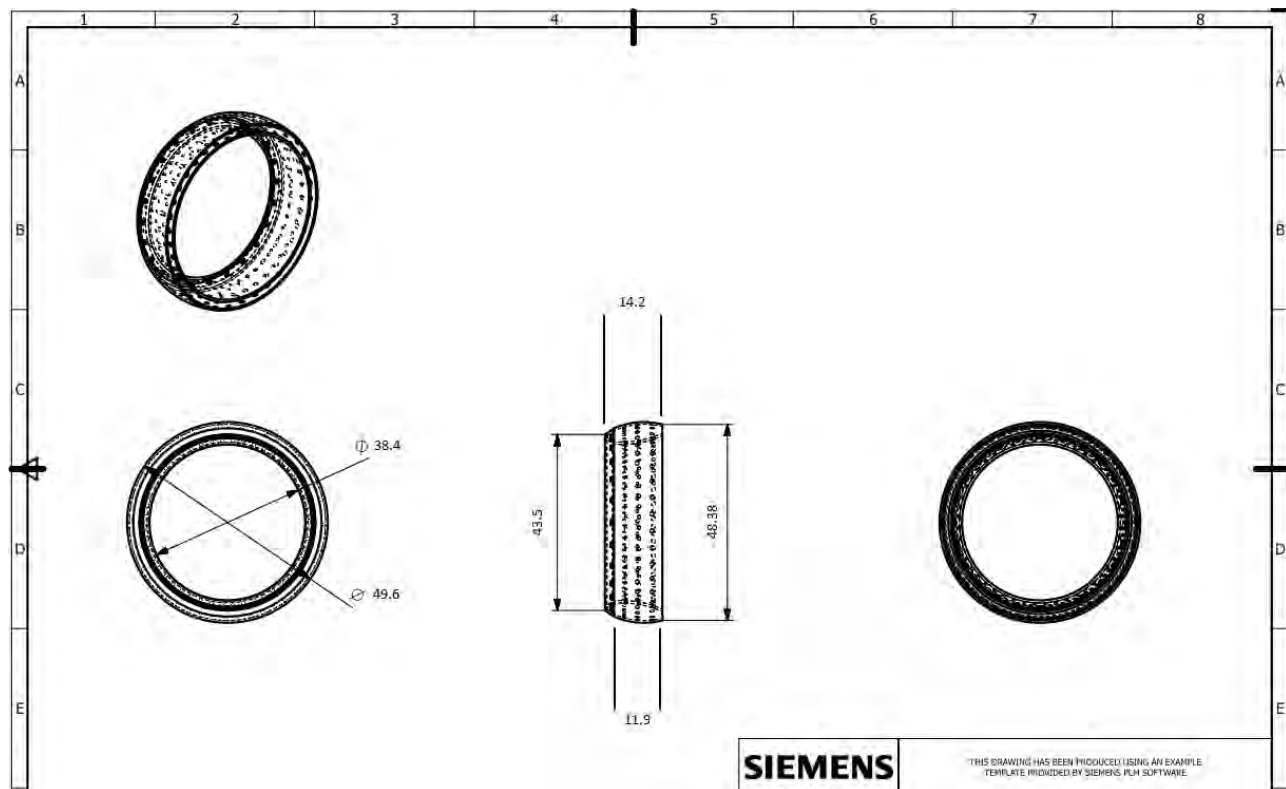
- [78]El-Sayed Ahmed, Emeara Mohamed S, “Aero-Engines Intake: A Review and Case Study”, The International Conference of Engineering Sciences and applications, Aswan, Egypt, January 2016.
- [79]Carbon Fiber Reinforcements, Hexcel, <<http://www.hexcel.com/Products/Fabrics-Reinforcements/Carbon-Fiber-Reinforcements>>, (Accessed on: 2018, February 25)
- [80]Lin Jinbao, Jin Yanjuan, Zhang Zhu, Cui Xiaochao, “Strength Analysis of the Carbon-Fiber Reinforced Polymer Impeller Based on Fluid Solid Coupling Method”, Mathematical Problems in Engineering, Volume 2014 (2014), Article ID 803261, April 2014
- [81]Titanium Alloys - Ti6Al4V Grade 5, Azo Materials, <<https://www.azom.com/properties.aspx?ArticleID=1547>>, (Accessed on: 2018, February 22)
- [82]Titanium Ti-6Al-4V (Grade 5), ASM Aerospace Specifications Metals Inc, <http://asm.matweb.com/search/SpecificMaterial.asp?bassnum=mtp642>,(Accessed on: 2018, March 22)
- [83]Du Zhihao, Zhang Kaifeng, Jiang Shaosong, Zhu Ruican, U Shuguang,” High Temperature Mechanical Behavior of Ti-45Al-8Nb and Its Cavity Evolution in Deformation”, Journal of Materials Engineering and Performance, ASM International, August 2015
- [84]Gogia A.K., “High-temperature Titanium Alloys”, Defence Science Journal, Vol. 55, No 2, April 2005
- [85]DiCarlo J, Jacobson N, Lizcano M., Bhatt R., “Ultra High Temperature (UHT) SiC Fiber”, NASA Aeronautics Mission Directorate FY11 Seedling Phase I Technical Seminar, June 2012
- [86]Bertrand J. D., “Ceramic Matrix Composite Characterization Under a Gas Turbine Combustion and Loading Environment”, Wright-Patterson Air Force Base, Ohio, March 2014
- [87]Ultramet, <<http://www.ultramet.com>>, (Accessed on: 2018, February 15)
- [88]NASA-Small Business Innovation Research,<[http://sbir.gsfc.nasa.gov/.](http://sbir.gsfc.nasa.gov/)>, (Accessed on: 2018, February 20)
- [89]Petko Jeanne F., Kiser Douglas, McCue Terry, “Characterization of C/SiC Ceramic Matrix Composites (CMCs) with Novel Interface Fiber Coatings”, QSS Group, Inc., Cleveland, Ohio, USA, 2002
- [90]Shirooyeh Mahmood R., “Mechanical Properties Of Yttria-Stabilized Zirconia Ceramics”, Faculty Of The Usc Graduate School, December 2011
- [91]Kawagishi Kyoko, Yeh An-Chou, Yokokawa Tadaharu, Koyashi Toshiharu, Koizumi Yutaka, Harada Hirsohi, "Development of an Oxidation Resistant High Strength Sixth Generation Single-Crystal Superalloy TMS-238", 12th International Symposium on Superalloys, 2012.
- [92]Pollock T. M., Tin Sammy, “Nickel-Based Superalloys for Advanced Turbine Engines: Chemistry, Microstructure, and Properties”, Journal Of Propulsion And Power, Vol. 22, No. 2, March–April 2006
- [93]Sato Akihiro, Harada Hiroshi, Yeh An-Chau et al., ”A 5th Generation Sc Superalloy With Balanced High Temperature Properties and Processability”, TMS (The Minerals, Metals and Materials Society), 2008
- [94]Shaft & Structural, < <https://ismswansea.com/home/jet-engine/shaft-structural>>, (Accessed on: 2018, February 22)
- [95]Materials of Rolling Bearing Technology, IINAA FAG, Schaeffler
- [96]Nishikawa Takashi, Hayashi Nao, Hayakawa Akiko, “Technical Trend of Aircraft Bearings”, Ntn Technical Review, 2014

## APPENDIX A

### A.1. Technical Drawing of Supersonic Intake (All dimensions in inch)

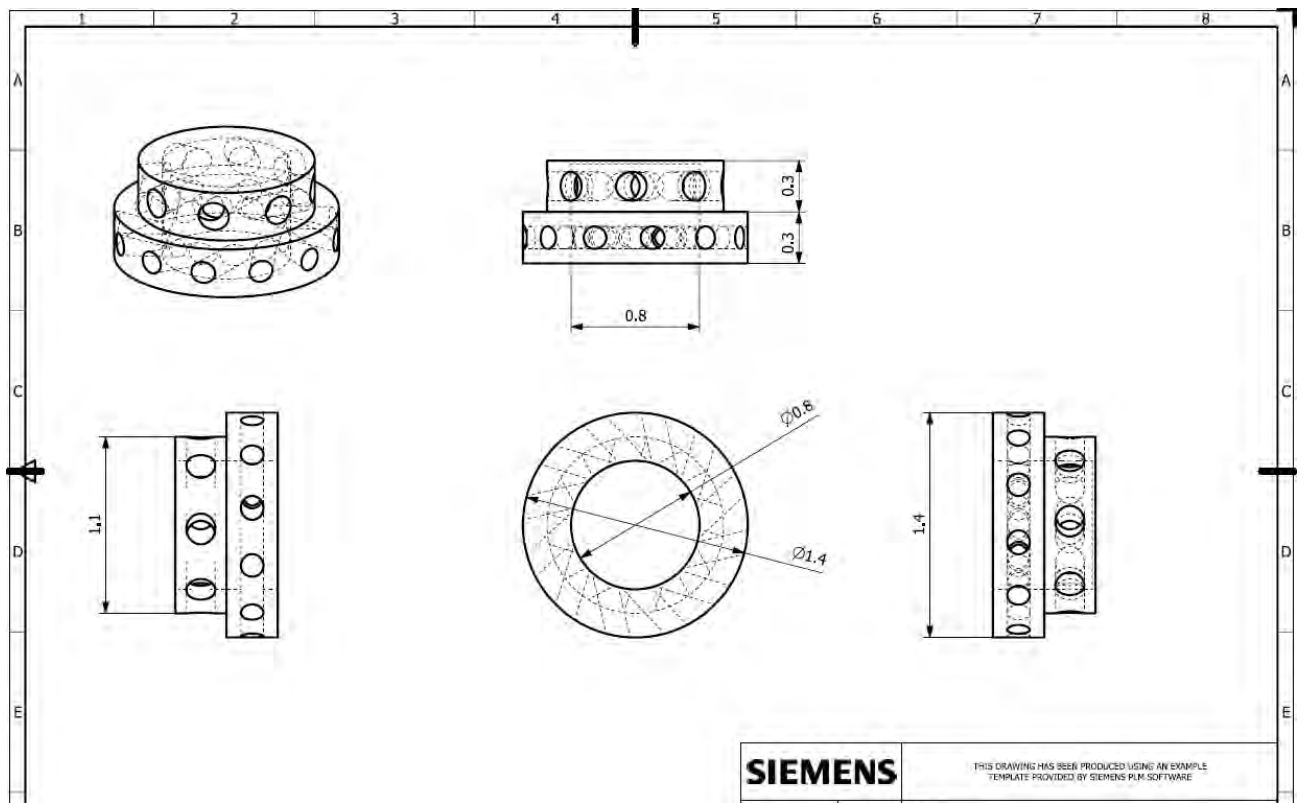


### A.2. Technical Drawing of Combustion Chamber (All dimensions in inch)

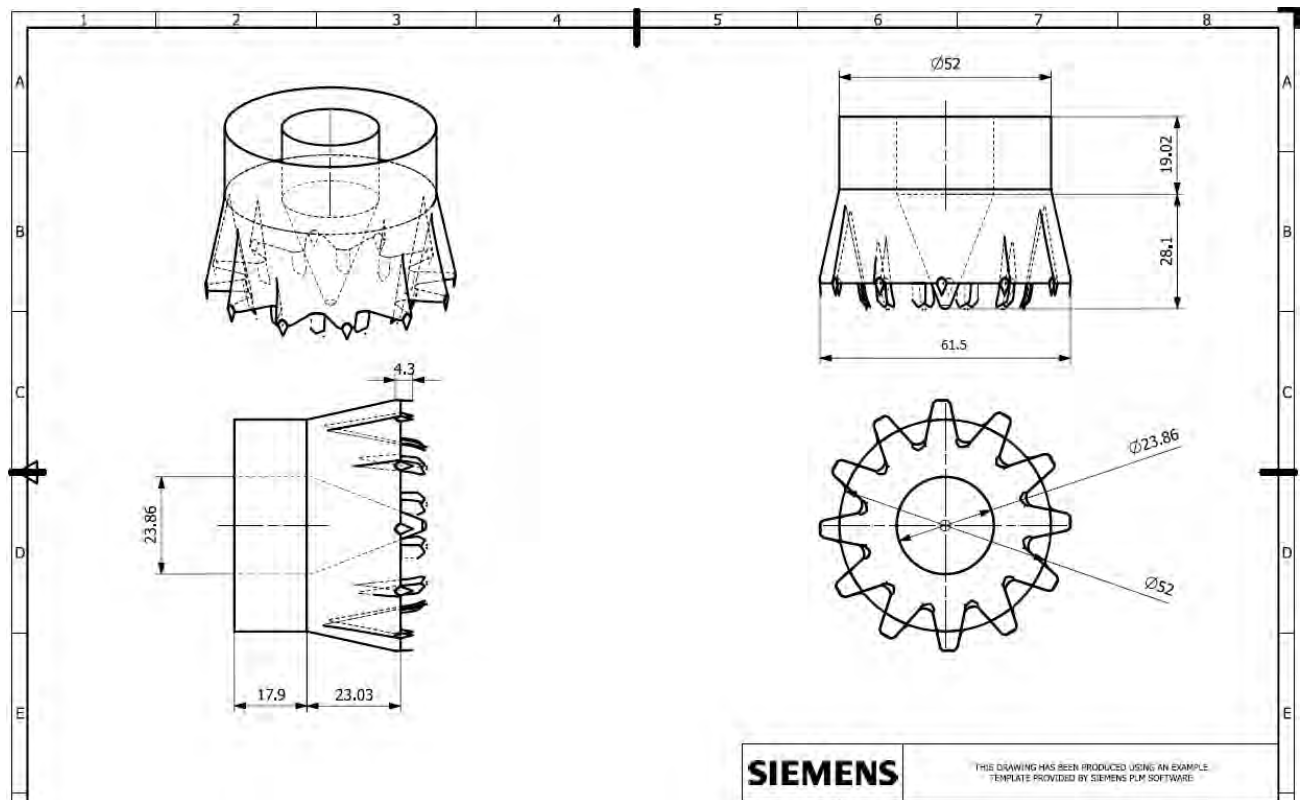




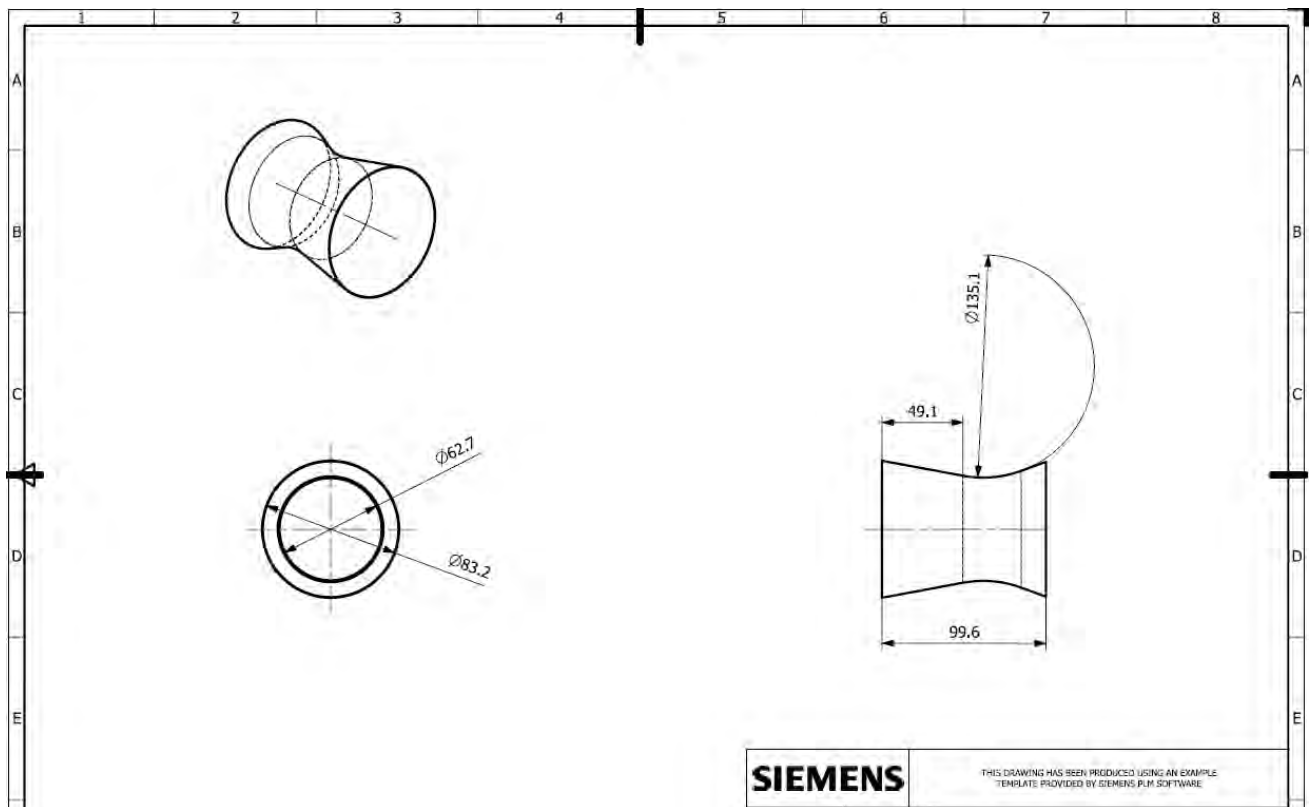
**A.3. Technical Drawing of Radial Airblast Swirler (All dimensions in inch)**



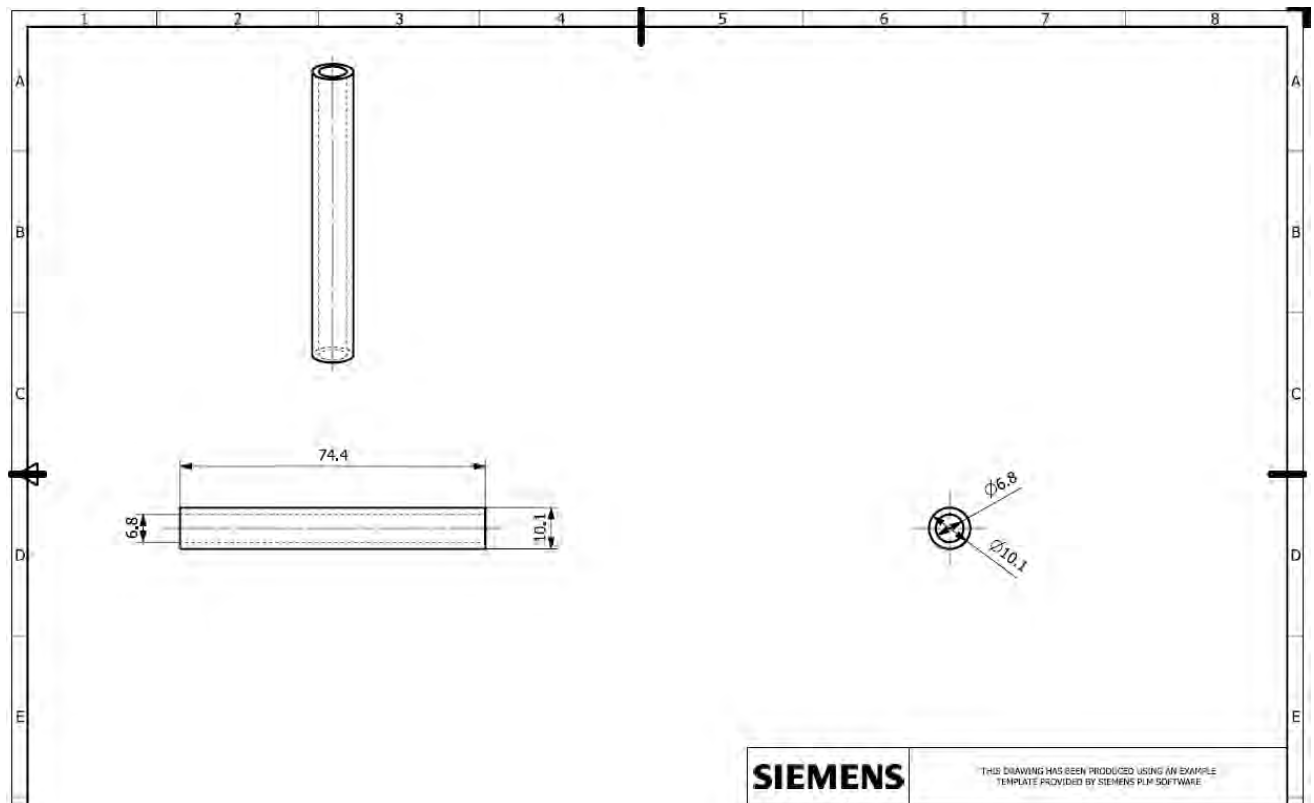
**A.4. Technical Drawing of Lobed Mixer with Chevron Nails (All dimensions in inch)**



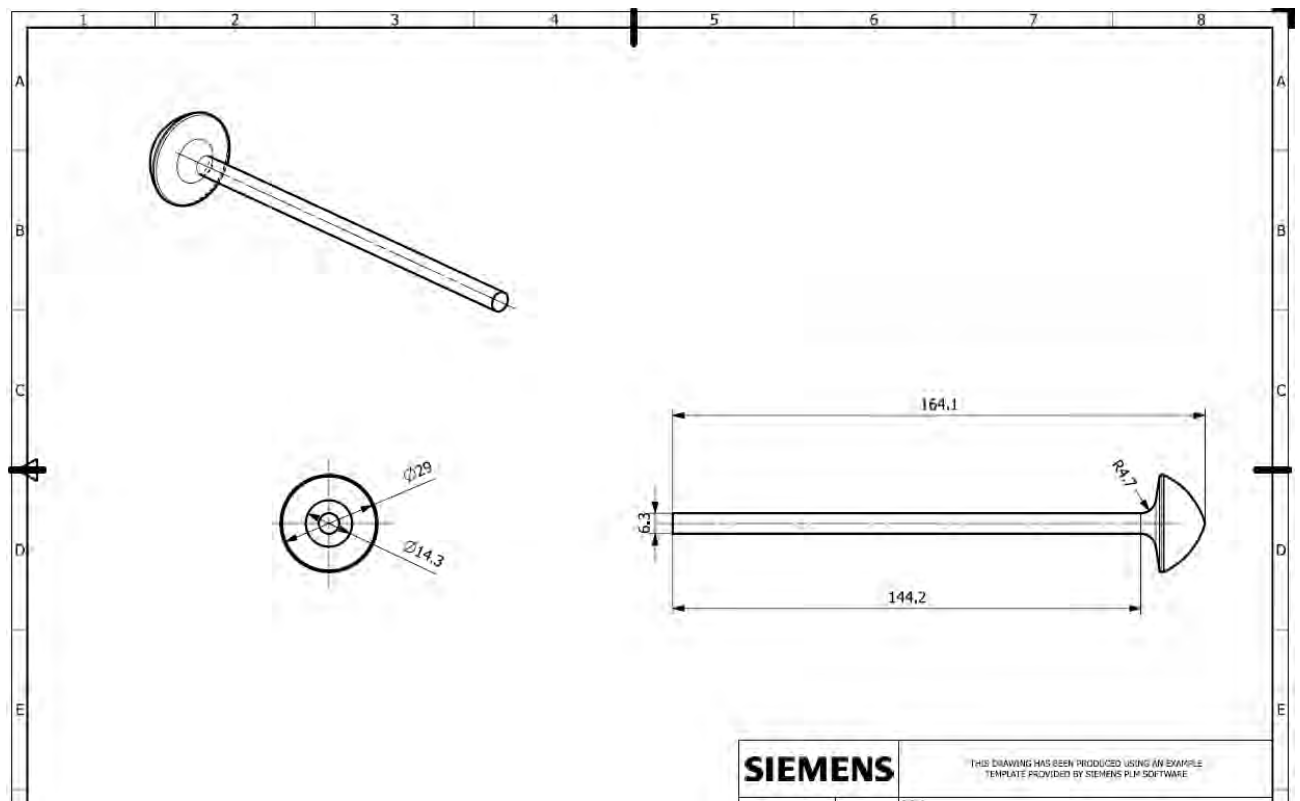
**A.5. Technical Drawing of Fully Variable Nozzle at Cruise Condition (All dimensions in inch)**



**A.6. Technical Drawing of HP Spool (All dimensions in inch)**



**A.7. Technical Drawing of LP Spool (All dimensions in inch)**



## APPENDIX B

### B.1. Turbofan Engines Comprehensive Literature Survey

Engines	Thrust (kN)	SFC	BPR	OPR	FPR	TET (C)	TET (K)	Weight (kg)	Size (cm)
GTRE GTX-35VS Kaveri	81,0-52,0		0,16	21,50		1427,00	1700,00	1236kg	L = 349cm / Dia = 91cm
Rolls-Royce Conway RB80 MK201	91,00	0,87 lbm/hr/lbf	0,25					2000kg	L = 341cm / Dia = 96 cm
Pratt & Whitney F119 (F22)	160,00	2,17 lbm/hr/lbf	0,30	26,80				1800kg	L = 516cm / Dia = 120cm
General Electric YF120 (Northrop YF23)	160,00		1,00					1840kg	L = 424cm / Dia = 106,7cm
General Electric F404-402 (F18)	80,00	1,74 lbm/hr/lbf	0,34	26,00	4,30			1036kg	L = 391cm / Dia = 89cm
RR&Snecma M53(MK610)	95,0- 64,0	0,88 lbm/hr/lbf 2,06 lbm/hr/lbf	0,36	9,80		1576,00	1849,00	1515kg	L = 507cm / Dia = 80cm
Pratt & Whitney F100-229 (F15-F16)	129,7-79,2	2,05 lb/hr/lbf	0,36	32,00	3,80	1350,00	1623,00	1737 kg	L = 490cm / Dia = 118cm
Klimov RD-33	81,3-50,0	0,77 lbm/hr/lbf 1,85 bm/hr/lbf	0,49	21,00		1407,00	1680,00	1055kg	L = 422cm / Dia = 104cm
NPO Saturn AL-55	17,26	0,69 kg/kgf.h	0,52	17,50		1445,00	1718,00	315kg	L = 195cm / Dia = 59cm
NK-144A Turbofan	178,0-47,0	0,92 kg/hr 1,81 kg/hr	0,53	14,20					L = 520cm / Dia = 150cm
Soloviev D-30	93,00	0,790 kg/kN/h	0,57	17				2305kg	L = 483cm / Dia = 145cm
Pratt & Whitney F135	191,3-28,1	0,7 lbm/hr/lbf 2,0 lbm/hr/lbf	0,57	28,00					L = 559cm / Dia = 117cm
Guizhou WS-13	86,0-51,0		0,57						
NK-8	93,20	21,53 mg/Ns	1,00	10,80		870,00	1143,00	2100kg	L = 476cm/Dia = 144cm
Pratt & Whitney JT8D-219	93,40	0,585 lbm/hr/lbf	1,00	16-9- 19,4		580,00	853,00	2150kg	L = 391cm/Dia = 125cm
Kobchyenko / Tumansky R- 79-300	153,0-107,0	1,66 kg/kp.h	0,81			1357	1630,00	2750 kg	L = 523cm/Dia = 172cm

B.1. Turbofan Engines Comprehensive Literature Survey (continued)

Engines	Thrust (kN)	SFC	BPR	OPR	FPR	TET (C)	TET (K)	Weight (kg)	Size (cm)
Saturn Lyulka AL-31f	123,0 74,5	24,6 g/kN.s 54,3 g/kN.s	0,59	23,00		1412,00	1685,00	1570kg	L = 499cm/Dia = 90cm
Saturn Lyulka AL-41f-1s	134,6 85,0	22,4 g/kN.s 51,5 g/kN.s	0,59					1636kg	L = 495cm/Dia = 90cm
NK-144	378,4 281,0	1,81 lbm/hr/lbf	0,60	14,20					L = 520cm/Dia = 150cm
TU-144	171,6 127,5	2,23 kg/hr sfc	0,60						L = 520cm/Dia = 150cm
Pratt & Whitney F100-220	105.7 64.9	0,73 lb/lbf.h	0,63	25,00				1467kg	L = 490cm/Dia = 118cm
Rolls-Royce Spey	91,2 54,0	0,63 lbm/hr/lbf 1,95 lbm/hr/lbf	0,64						L = 520cm/Dia = 109cm
General Electric F110 (F14)	80,0 142,0	1,47 lbm/hr/lbf	0,76	30,70	2,98	1510,00	1783,00	1900kg	L = 462,3cm/Dia = 116cm
General Electric F118-GE-100 (B2)	84,00	0,67 lbm/hr/lbff	0,81	32,2-35	3,41			1452kg	L = 255cm/Dia = 118cm
Pratt & Whitney TF30	111,6 64,8		0,87	19,80		1176,00	1449,00	1807kg	L = 614cm/Dia = 124cm
Williams FJ44-1A	8,50		3,28						
Rolls-Royce BR710	68,00		4,20						
Rolls-Royce BR725	75,00		4,20						
Aviadvigatel PS-90	171,00	0,595 kg/kgf.h	4,40					2950kg	L = 496cm
Honeywell HTF700	33,9 30,8		4,40	28,20					
PowerJet SaM146	79,2 71,6	0,629 lbm/hr/lbf	4,40	28,00					Dia = 122cm
Rolls-Royce AE 3007	40,00		5,00	23,00				740kg	L = 292cm Dia = 98cm

B.1. Turbofan Engines Comprehensive Literature Survey (continued)

Engines	Thrust (kN)	SFC	BPR	OPR	FPR	TET (C)	TET (K)	Weight (kg)	Size (cm)
Pratt & Whitney JT9D	249,0 213,0		5,00	23,4-26,7	1,60				L = 337cm
General Electric CF6	275,0 231,0		5,00	27,8-31,1					
Pratt & Whitney PW4000-112	436,0 329,0		5,00	34,2-42,8					
Lotarev D-36	29,00		5,60	20,00					
Honeywell Lycoming ALF502/507	31,00		5,70						
Lotarev/Progress D-18T	229,85		5,70	27,50		1327	1600,00		
Rolls-Royce Trent 800-895	422,60	15,86 g/kN.s (TSFC)	6,00	41,60					
CFM International CFM56	150,0 87,0		6						
General Electric TF34	40,30		6,22	21		812	1085		L= 254 cm/Dia=123cm
General Electric TF39 (Lockheed C5 Galaxy)	75,00	0,315 lbm/hr/lbf	8,0	0,00	1,56				
Aviadvigatel PD-14 (Next engine for MS-21)	151,0 125,0		8,00	38-46					
Rolls-Royce Trent 900	340,0 310,0		8,50	37-39					
General Electric GE90/Genx	388,80	8,3 g/kN.s	9,00	50,00					
General Electric GE90-94B	416,80		9,00	40,00					
Pratt & Whitney W1000G Series	160,0 67,0		9,00						
Rolls-Royce Trent XWB	430,0 374,0	18 g/kN.s	9,60	50,00	1,43			7277kg	L=581 cm
General Electric 9X	470,0		10,00	60,00	2,22				Dia = 335 cm

B.1. Turbofan Engines Comprehensive Literature Survey (continued)

Engines	Thrust (kN)	SFC	BPR	OPR	FPR	TET (C)	TET (K)	Weight (kg)	Size (cm)
Turbo-Union RB199	40-73		1,10	23,50				976 kg	L = 360cm / Dia = 72cm
Kuznetsov NK-86	127,00		1,15				1260,00	1540kg	L = 623cm / Dia = 160cm
Ivchenko-Progress AI-222	41,0 25,0		1,19						
Rolls-Royce Pegasus 11	106,00	0,76 lbm/hr/lbf	1,2	16,3				1796kg	L = 348cm / Dia = 121cm
Pratt&Whitney TF33-PW-7	93,00		1,21						
Kuznetsov NK-25	245,00		1,40						
Kuznetsov NK-321	245,00 137,00	0,73 kg/kgf/h 1,7 kg/kgf/h	1,40	28,40		1357,00	1630,00	3400kg	L = 600cm / Dia = 146cm
TU-144LL	245 137,5	0,72 kg/hr 1,7 kg/hr	1,40						L = 600cm / Dia = 146cm
PW JT3D	76,00		1,41						
General Electric CJ805-23	71,00		1,46						
Pratt & Whitney Canada PW600	13,00		1,83						
F101-GE-102	136,0 77,0		1,91	26,8	2,31			1996kg	L = 459cm / Dia = 140cm
General Electric F414	116,0 98,0			30,00					L=139 cm/Dia=89 cm
General Electric CF700	18,00	0,67 lbm/hr/lbf	2,00						
Rolls-Royce Trent 1000	330,0 240,0		10,00	52,00					
General Electric RR F136	180,0 100,0								L=560 cm/Dia=120 cm

